CRACK2. Modelling calcium carbonate deposition from bicarbonate solutions in cracks in concrete

Brodersen, Knud Erik

Publication date:
2003

Document Version
Publisher's PDF, also known as Version of record

Risø-R-1143(EN)

CRACK2 - Modelling Calcium Carbonate Deposition from Bicarbonate Solution in Cracks in Concrete

Knud Brodersen

Risø Decommissioning
Risø National Laboratory, Roskilde
March 2003

Abstract:

The numerical CRACK2 model simulates precipitation of calcite from calcium bicarbo-nate solution (e.g. groundwater) passing through cracks in concrete or other cementitious materials. A summary of experimental work is followed by a detailed description of the model.

Hydroxyl ions are transported by diffusion in pore systems in columns of cementitious materials. The hydroxyl is precipitating calcite from a flow of bicarbonate solution in a crack connecting the ends of a row of such columns. The cementitious material is simulated as calcium hydroxide mixed with inert material but with sodium hydroxide dissolved in the pore solution. Diffusive migration of cesium as radioactive isotope is also considered. Electrical interaction of the migrating ions is taken into account.

Example calculations demonstrate effects of parameter variations on distribution of precipitated calcite in the crack and on the composition of the outflowing solution, which can be compared directly with experimental results. Leaching behavior of sodium can be used to tune the model to experimental observations.

The calcite is mostly precipitated on top of the original crack surface and may under certain circumstances fill the crack. The produced thin layers of low porosity calcite act as a diffusion barrier limiting contact between cement and solution. Pore closure mechanisms in such layers are discussed.

Implications for safety assessment of radioactive waste disposal are shortly mentioned.

The model is also relevant for conventional uses of concrete.

Acknowledgements:

Part of the CRACK2 model development and most of the supporting experimental work were carried out under the EU Research Programs 1988-2000 on Management and Disposal of Radioactive Waste.

ISBN 87-550-2612-5
Internet 87-550-2613-3
ISSN 0106-2840

Print: Pitney Bowes Management Services Denmark A/S, 2003

Contents:

Page:

1. Introduction

Transport properties of cracks and other defects in concrete barriers are important for ordinary use of concrete in dams, water reservoirs, tunnels, roofs etc. Present knowledge in the field has been reviewed by a RILEM committee [1]. Formation of cracks and flow of water or other liquids through interconnected crack or pore systems have been extensively studied. The chemical changes caused by the flow of solution are less well established, although it is generally agreed that presence of dissolved carbonate species are important. For a general discussion of carbonate behaviour in cement systems see [2]. An example of experimental work and theoretical interpretation is available in [3].

When groundwater, tap-water, rainwater or seawater flow through cracks in defect concrete barriers dissolved calcium bicarbonate and other carbonate species react with hydroxyl ions from the hydrated cement resulting in precipitation of nearly insoluble calcium carbonate as a covering layer on the inner surface of the crack. Other components from the water may also precipitate, primarily magnesium hydroxide.

Under certain circumstances the precipitate may block the flow of water, but for coarse cracks this is not necessarily the case, because the growing calcite layer prevents efficient contact between the bicarbonate solution and the alkaline materials in the concrete. The result is slower formation of additional precipitate and inefficient buffering of the solution, which then leave the crack nearly unchanged by the passage.

These phenomena are also of considerable interest for safety assessments of the use of concrete in engineered barriers in disposal facilities for radioactive waste. A two-dimensional model of a repository taking calcite deposition and other dissolution/ precipitation reactions into account is presented in [4]. However, in this case porosity is regarded as distributed homogeneously inside individual grid elements. This will not permit evaluation of the crack-covering mechanism described above and in the following.

Crack healing - or crack filling - in concrete has been studied experimentally at Risø National Laboratory from 1988 to 2000 as part of CEC shared cost contracts FI1W-0089-DK, FI2W-CT90-0040 and FI4W-CT96-0030 under the EC Research Program on Management and Disposal of Radioactive Waste.

In connection with contract FI1W-0089-DK a primitive model - CRACK1 - of the crack filling process was presented. Examples of the results are given in [5]. The model describes the formation of the precipitate and the eventual changes in pressure loss and flow rate. However, the release of OH^- from the inner surfaces of the crack was modelled using an analytical expression for simple diffusive leaching disregarding formation of a covering layer and the chemical reactions taking place in and near the layer. One result of this simplification is that all cracks - thin as well as coarse - eventually will be closed and this is not realistic.

As support for the experimental work carried out under contract FI2W-CT90-40 a more advanced model - CRACK2 - was developed as described in [6,7] and in more detail in the present report. In this case the diffusive release of ions from the concrete and out in the flowing solution is calculated using finite difference technique. The numerical approach is flexible and permits the introduction of various more realistic features into the model. However, the cost is a considerable increase in complexity and rather long calculation times.

The CRACK2 model is restricted to simulation of the behaviour of the following dissolved major species: Ca^{2+}, Na^{+}, OH^{-}, CO_3^{2-}, HCO_3^{-} and H_2CO_3. The precipitate and the cement matrix are represented by $CaCO_3$ and $Ca(OH)_2$, respectively. Leaching of hydrated calcium silicate and other cement paste minerals is disregarded. Behaviour of ionic species present in low concentration as typical for radioisotopes can also be simulated provided no interaction with solids takes place.

Introduction of a more realistic cement chemistry and possibilities for handling interacting radioisotopes are desirable, but the present version of the model is already able to simulate many aspects of actual crack filling experiments.

Transport of the dissolved species is by advection in the solution flowing through the crack and by diffusion perpendicular to the flow direction. In the pore structure of the cementitious material and in the layer of precipitated calcite all transport is by diffusion. Diffusivities for the relevant species are obtained from the diffusivities in water modified with suitable form factors accounting for transport delay in the porous materials. Correction for diffusion potential is carried out to compensate for interaction between the migrating ionic species.

Assumptions about the porosity of the materials and especially the tendency to nearly complete blockage of the transport pores in the calcite layer are found to be very important for the behaviour of the system.

The modelled systems are fully saturated and exposed to relatively slow water flow. This will be typical for most underground repositories where the hydraulic gradient normally is slight and the flow rates determined by the surrounding formations. For ordinary applications – water reservoirs etc. - the hydraulic gradients may be much higher and the flow rate primarily determined by the pressure loss over the cracked barrier. This will create other circumstances probably with less tendency to crack closure but such cases should in principle also be covered by the model.

The report presents the structure of the model, gives some calculation examples and indicates some areas for desirable improvements.

A summary of modelling and results was presented in [8].

Experimental results for comparison with the modelling are available in [6,7]. A few examples are given in the following section together with a summary of typical observations from the experiments.

2. Examples from crack filling experiments

Precipitation of calcite and other minerals from simulated groundwater flowing through cracks in cementitious materials has been studied at Risø National Laboratory using experimental methods described in the following and in more detail in [6,7]. Cylindrical specimens with diameter 4.3 cm and length up to 9 cm were cast from various types of cement mortar in form of two half cylinders. After hardening the two parts were mounted together using suitable spacers to give at flat artificial crack with well-defined dimensions (breadth = 3.5 cm and width between 0.01 and 0.04 cm). The specimen was sealed on the outside by rubber tubing and fitted with conical end-pieces connected to reservoirs through a peristaltic pump supplying feed solution at a constant rate (often about 4 ml/h). The feed was normally entering the crack in the specimen from below and overflowed through glass pipes permitting measurement of pressure loss over the specimen and collection of the out-flowing solution.

A so-called type b mortar was used in many of the experiments. It is made from Danish SRPC (sulphate resistant Portland cement), sand (particle size 0.3 to 1 mm) and water, in the proportions 100:140:38, i.e. a mortar with water cement ratio 0.38. The water-saturated density is 2.32 g/cm^3 and the porosity about 20 %. The examples included here are mostly for this type of mortar. High porosity materials of interest as backfill material in repositories were also investigated [7].

The configuration of the specimens are shown in Fig. 1 and the cylindrical cross section is compared with the rectangular 4×3.5 cm approximation used in the model, see Section 3. The cross-sectional areas are 14.5 and 14.0 cm^2 and therefore in reasonable agreement.

A photo of Specimen 8-4$_1$ after the experiment is shown in Fig 2. The spacers remain in position along the rim of the left half cylinder. A light grey layer of precipitated calcite covers both sides and is partially bridging a side crack in the right half-cylinder, a special feature investigated in this experiment. At the top of the specimen the calcite is seen to extend outside the crack. Fig. 3a shows the tube-like extensions of the crack seen from above before the specimen was opened. Similar tubes or mounts were seen in many other experiments and indicate that the solution is over-saturated in calcite when leaving the crack. In early experiments with flow in downward direction, long and thin needle-like formations were formed in the solution-filled conical outlet space as shown in Fig. 3b.

The employed feed solution was either a synthetic 0.002 M $Ca(HCO_3)_2$ solution equilibrated with $CaCO_3$, or local tap water with approximately the same amount of calcium bicarbonate but in addition containing some Mg, K and Na as sulphates and chlorides.

Fig. 1

Typical dimensions of specimens used in the crack-filling experiments.

The rectangle below the cross-section represents the configuration used in the modelling, see Section 3.

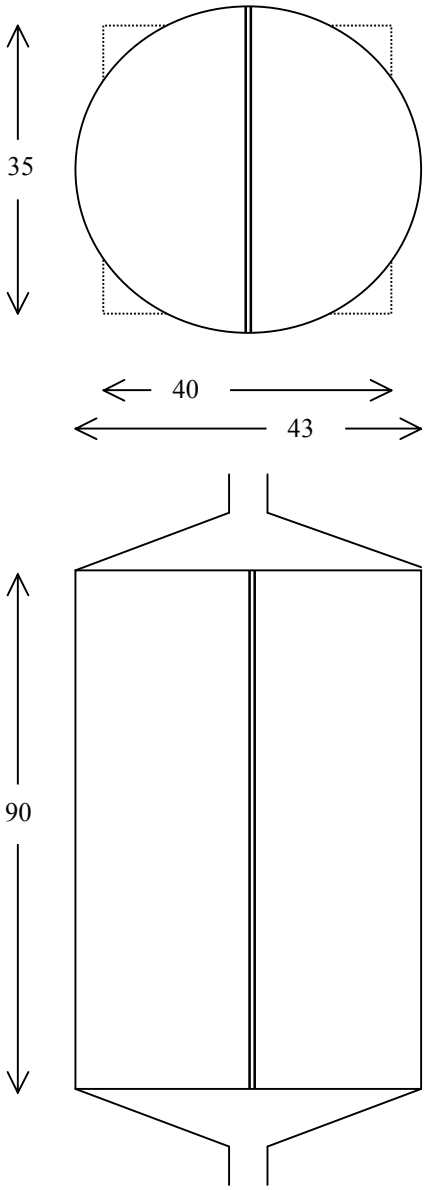

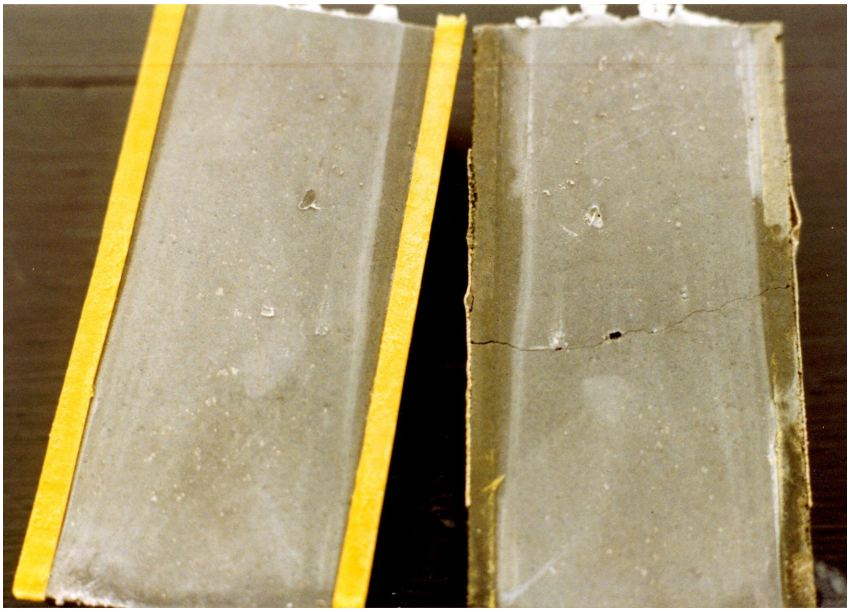

Fig. 2 Specimen 8-4_1 opened after the experiment

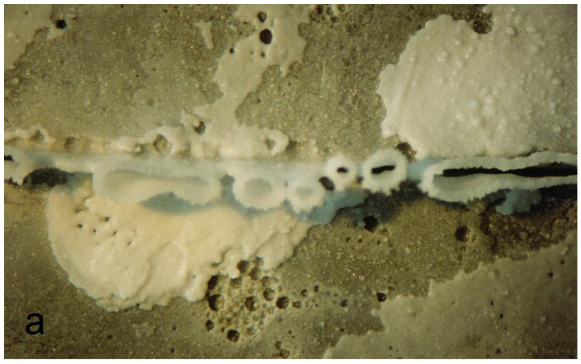

Fig. 3a Top of specimen 8-4_1 with calcite tubes formed from outflowing oversaturated solution.

Fig. 3b Calcite needles formed along the crack in the conical outlet space at the bottom of specimen 3-4 with downward flow.

The morphology of the calcite precipitate is quite different with the two types of feed solution:

The synthetic solution gives rise to well-developed rhomboedric calcite crystals. On even surfaces they are typically 2-5 μm large (Fig. 4c) but near the rim or where the flow rate for other reasons is diminished (e.g. around air bubbles trapped in the crack, Fig. 4b) the crystal size can be up to 100 μm. Hollows after air bubbles trapped in the surface of the cast mortar may be covered on the inside by calcite crystals (Fig. 4a) but are more often closed-over by a 'lid' of calcite crystals. The liquid behind such lids is strongly alkaline while the feed solution on the other side is near neutral.

When tap water was used the crystals are uneven and more plate-like (Fig. 5a,b). Analyses shows that the precipitate in addition to calcite also contains 1 to 2 % magnesium as brucite, $Mg(OH)_2$ or maybe dolomite.

A certain amount of silicate was found in both types of precipitate and may indicate a slight precipitation of C-S-H in between the calcite crystals.

The layers of precipitated material were typically 20 –50 μm thick. The material could be evenly distributed along the crack but the thickness could be largest at the feed entrance or at the exit. While wet the material could be easily scraped away without damaging the underlying mortar surface.

Thin cracks (~0.1 mm) were often closed while wider cracks (> 0.2 mm) normally remained open. During crack closure the experimental set-up permitted development of a pressure loss corresponding to up to two meter water before the flow decreased. A slight flow was normally attained through nearly closed cracks. Initially formed precipitate giving rise to a slight pressure drop over the crack could be unstable so that low-pressure flow was re-established. Indications of preferential flow over part of the crack surface were often seen.

The out-flowing solution was collected in batches and analysed for Ca, Mg, K, Na, OH and the carbonate species. Analyses for ^{45}Ca, ^{134}Cs, ^{85}Sr, ^{154}Eu or uranium were carried out when the radioisotopes were used as additives in the mortar or the feed solution.

Some typical results are shown in Figs. 6, 7 and 8. Further examples covering a wide variety of conditions are available in [6,7]. Curves of similar types generated by the model are shown in Section 7.

Figs. 6a and b presents the analyses for out-flowing solution from specimen 8.1 with a 0.3 mm crack exposed to a ~4.5 m/h flow of synthetic 0.002 M calcium bicarbonate solution. The mortar was in this case prepared from activated cement powder and the hydrated cement paste therefore contained ^{45}Ca as a tracer.

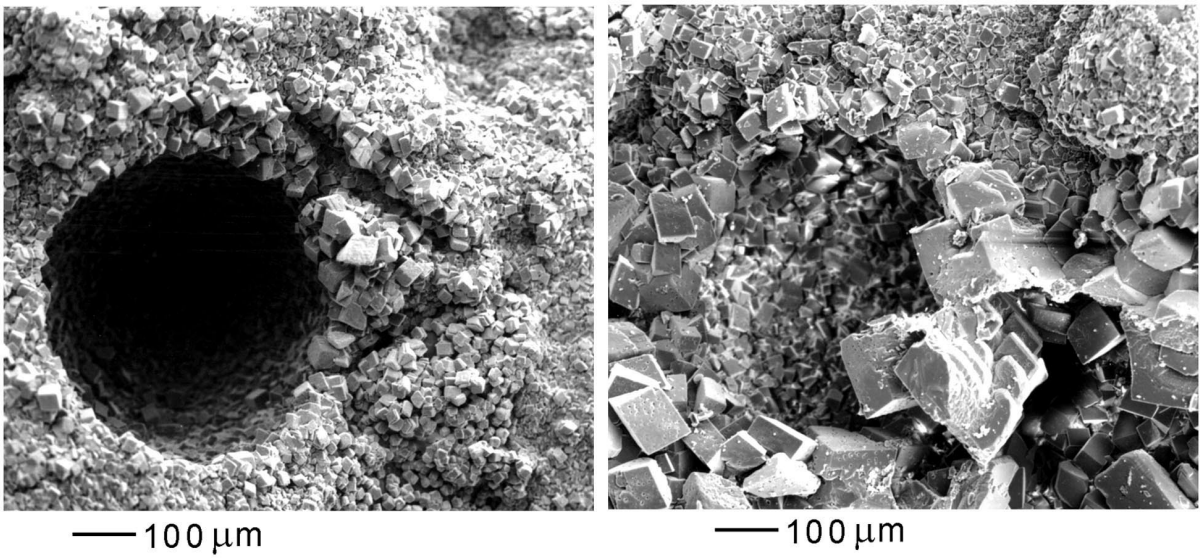

Fig. 4abc
SEM (Scanning electron microscopy) of surface of calcite layers precipitated from synthetic $Ca(HCO_3)_2$ solution in cracks in cement mortar.

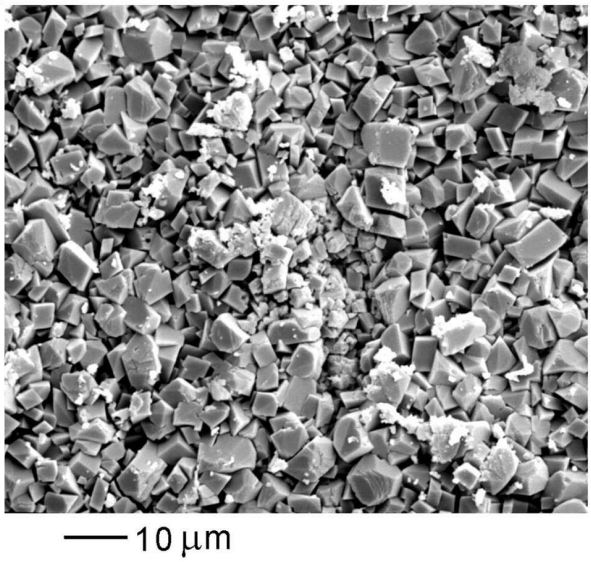

Fig. 5ab (below)
SEM of surface of calcite layers precipitated from tap-water in cracks in cement mortar.

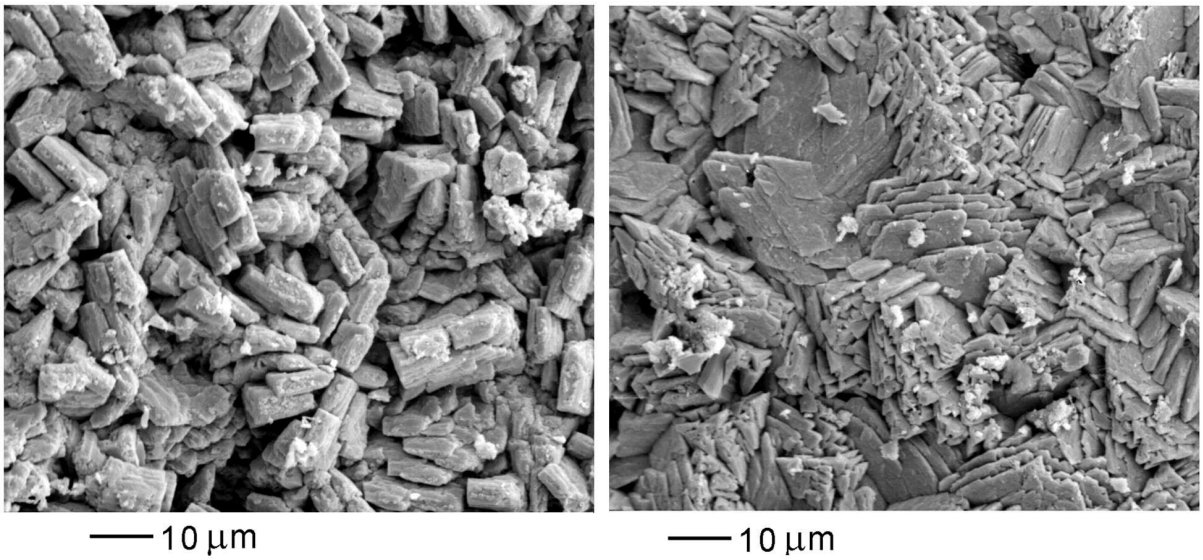

The shape of the obtained curves are typical, with the calcium concentration starting high due to initial leaching of $Ca(OH)_2$ from the freshly exposed crack surface. Then follows an about 10 days long period with decreased concentration because Ca in the feed is precipitated by calcium an alkali metal hydroxide from the mortar. The resulting $CaCO_3$ layer eventually prevents contact with the interior of the mortar and the composition of the solution approaches the concentration in the feed solution as represented by the horizontal line. The ^{45}Ca curve initially follows the Ca curve but after formation of the covering calcite layer the concentration of the tracer drops to low values, actually one to two orders of magnitude lower than the concentration of the alkali metals.

The concentration curves for the OH, CO_3 and HCO_3 are shown in Fig. 6b. As for calcium it is characteristic that the OH and HCO_3 concentrations do not quite reach the composition in the feed. This indicates a slight continuing leakage of OH^- mainly associated with out-diffusion of sodium and potassium hydroxide through defects in the calcite layer and resulting in the Na and K found in the out-flowing solution. See also the discussion in Section 9.

Fig. 6c presents the time development of mass-balances over the system. The amount of precipitated calcium carbonate is obtained as the difference between carbonate species entering with the feed and leaving with the out-flowing solution. The amounts of K and Na leached from the mortar are shown as negative. The OH-curve represents hydroxyl removed with the outflowing solution, additional OH^- has been consumed in calcite precipitation in the covering layer. The Ca_{leach} curve is obtained as $Ca_{feed} - Ca_{out} - Ca_{calcite}$, and the Ca curve represents calcium removed from the system with the flow, i.e. $Ca_{feed} - Ca_{out}$ The Ca-45 curve represents calcium which has leached out and removed with the solution flow. The difference to the Ca_{leach} curve then represents calcium originating from the mortar and precipitated in the calcite layer.

Fig. 6d shows the leach curve for potassium presented as the equivalent leached thickness, i.e. the summated amounts of the alkali metals found in the out-flowing solution divided by the original concentration in the mortar and the area of the crack surface (for theory see also Section 6.3). The initial slope of the curve corresponds to a K-diffusivity of $0.37\ 10^{-7}$ cm^2/s. After about two weeks – when a covering calcite layer has been established on the whole inner surface of the crack – the slope decreases and the apparent K-diffusivity is now $0.30\ 10^{-7}$ cm^2/day.

Fig. 7 shows a comparison between leach curves for ^{134}Cs introduced as an additive to the mortar used for Specimens 6-1 and 6-2. The two cracks were exposed to synthetic ~0.002 M $Ca(HCO_3)_2$ and deionised CO_2-free water, respectively. The 6-2 specimen shows the expected linear form of a leach curve for diffusive leaching from a 'semi-infinitely' thick specimen of porous material. The Cs-diffusivity corresponding to the slope of the curve is $6.8\ 10^{-8}$ cm^2/s. In case of Specimen 6-1 the slope of the curve decreases after about two weeks and formation of the covering calcite layer. The new slope corresponds to an apparent Cs-diffusivity of $2.6\ 10^{-8}$ cm^2/s.

Table 2 in Section 6.2 shows further values for leach diffusivities obtained from conventional leaching of various types of cement mortar including especially porous backfill material: the above $0.37\ 10^{-7}$ cm^2/s for potassium leaching from type b mortar is probably too low. More likely values are $0.9\ 10^{-7}$ cm^2/s for K^+ and $1.2\ 10^{-7}$ for Na^+.

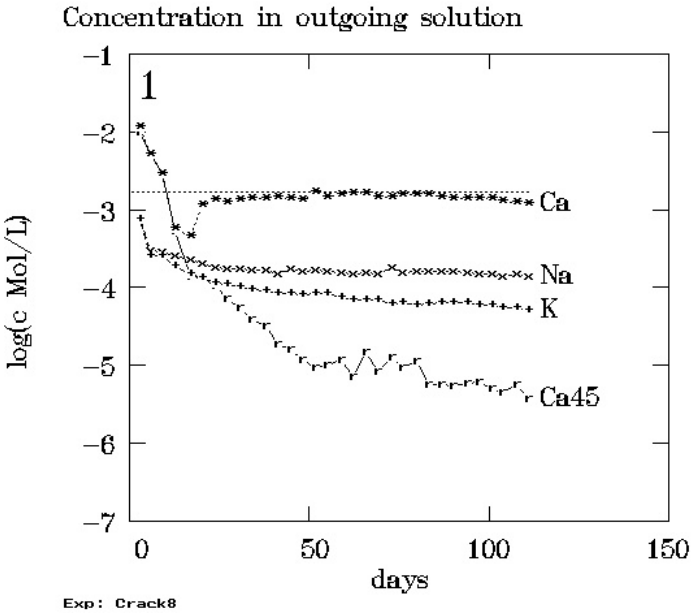

Fig. 6a Specimen **8-4$_1$**

Concentrations versus time for Ca, Na and K in solution leaving the crack compared with the Ca-concentration in the synthetic $Ca(HCO_3)_2$ feed solution (the horizontal line).
Ca-concentrations corresponding to ^{45}Ca in the cement mortar are also shown.

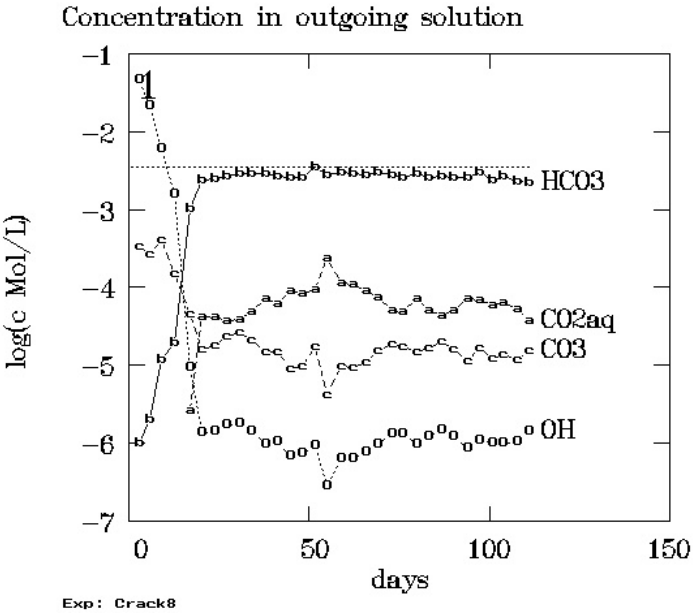

Fig. 6b Specimen **8-4$_1$**

Concentration versus time for H_2CO_3, HCO_3 CO_3 and OH in solution leaving the crack.
and HCO_3-concentration in the synthetic $Ca(HCO_3)_2$ feed solution (horizontal line).

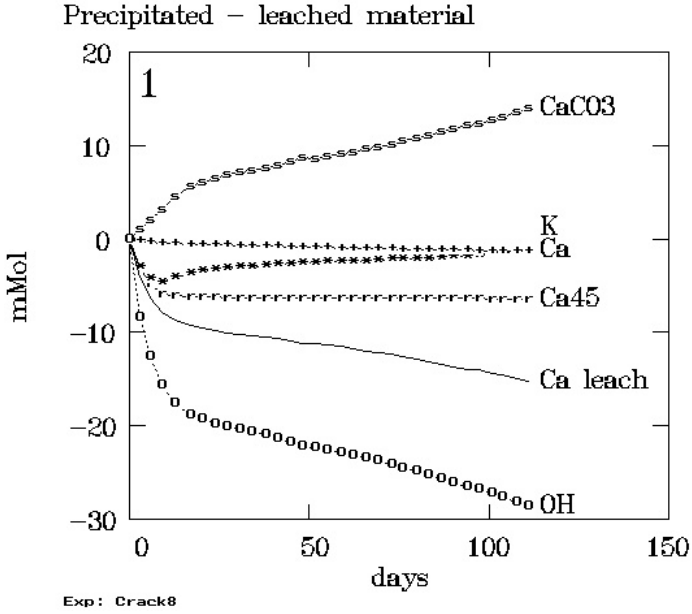

Fig. 6c Specimen **8-4$_1$**

Cumulative amounts of precipitated calcite, and
(shown negative) Ca and ^{45}Ca removed from the system with outflowing solution, and calcium, potassium and hydroxide leached from the mortar as given by analyses and mass balance considerations.

Fig. 6d Specimen **8-4$_1$**

Leach curve for potassium. The equivalent leached thickness is plotted versus the square root of time. After about two week the slope of the curve decreases slightly. Diffusivities corresponding to the two slopes are 3.7 10^{-8} and 3.0 10^{-8} cm^2/s, respectively.
(Somewhat higher diffusivities and a more pronounced decrease were found in other cases).

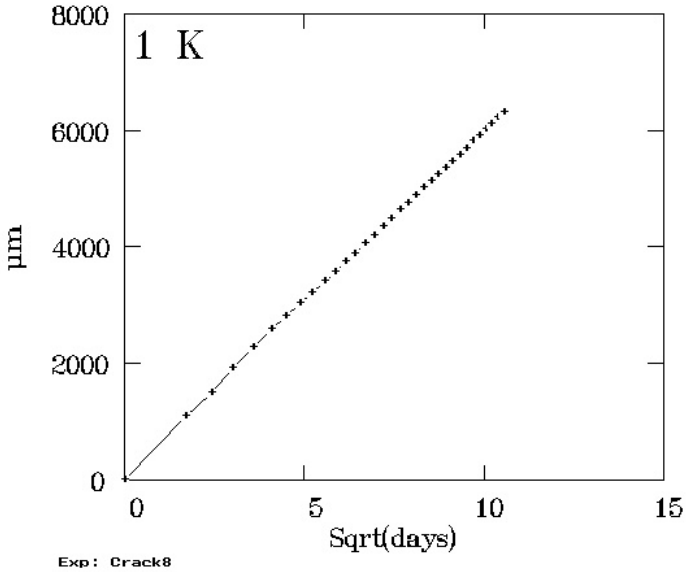

Fig. 7 Specimens **6-1** and **6-2**

Leach curve for cesium as ^{134}Cs in the mortar. The equivalent leached thickness is plotted versus the square root of time. Specimen 6-2 was leached in pure CO_2-free water while 6-1 was exposed to synthetic bicarbonate solution.
After about two weeks the slope of the curve for Specimen 6-1 decreases considerably. The corresponding diffusivities are 6.8 10^{-8} and 2.6 10^{-8} cm^2/s, respectively

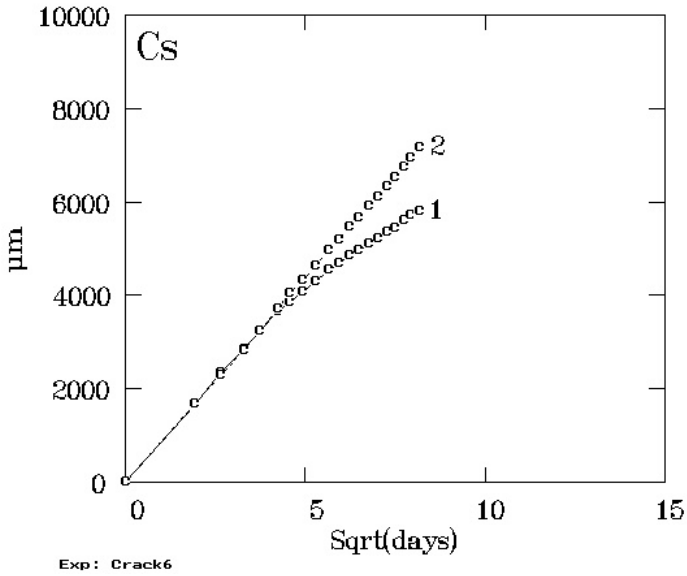

Fig. 8 Specimen **11a**

Concentrations versus time for Ca, Mg and Sr (calculated from ^{85}Sr measurements) in solution leaving the crack. The strontium was entering with the feed solution. The Ca-concentration in the tap water feed solution was somewhat low and variable, with higher values towards the end. The shown horizontal lines represent mean values. Both Ca and Mg remained slightly below the actual feed concentrations.

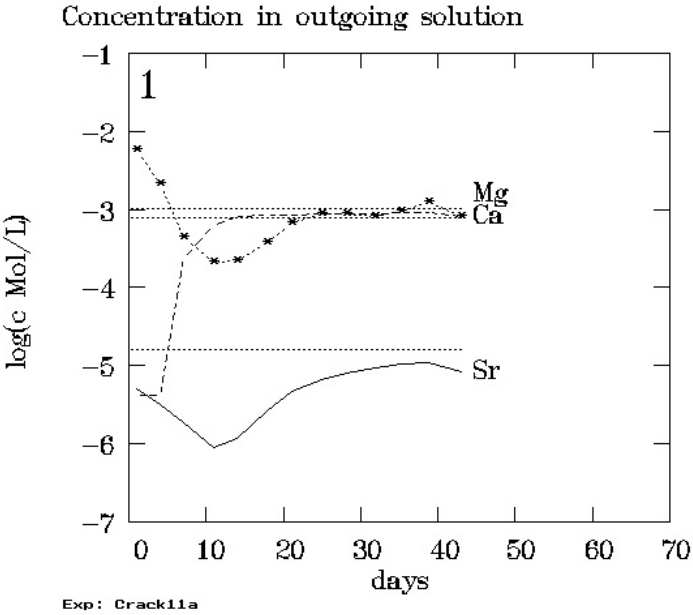

Finally Fig. 8 presents another example of the development of concentrations in out-flowing solution, in this case for Specimen 11a-1 exposed to tap water. Curves for Ca, Mg and Sr are presented. The calcium curve shows similar behaviour as in Fig. 6a. The magnesium curve show efficient removal before formation of the covering layer, while the concentration approaching the content in the feed solution after the formation.

About 1.4 ppm strontium was present naturally in the tap water with some ^{85}Sr added as tracer. It is seen that the strontium mimics the behaviour of calcium at a lower concentration level. Initially some Sr is removed as strontianite, $SrCO_3$ or – maybe more likely – by co-precipitation with the calcite. After formation of the covering calcite layer the solution is passing through the crack practically without removal of the radioisotope.

Behaviour of this type is of interest in safety assessment of the use of concrete in barriers around radioactive waste: If strontium in some manner has been dissolved and passed into a flowing solution it may be released through calcite-covered cracks if such have been formed. On the other hand if strontium isotopes are present as a component in cementitious materials they are expected to show low leachability in a solution containing carbonate species because they cannot pass through but are precipitated in the surface calcite layer formed under such conditions.

In other experiments it was shown that uranium (under oxidising conditions and probably as an UO_2^{2+}-carbonate complex) is also able to pas through calcite covered cracks. Results for europium (which as Eu^{3+} can be used as stand in for the actinides under reducing condition) were uncertain due to experimental difficulties.

Overall the experiments demonstrate that preferential flow of dissolved radioisotopes is possible through concrete barriers in form of containers or constituting the outer shell around a repository for radioactive waste. The importance of such phenomena will to a large extend depend on availability of carbonate ions either from groundwater or generated internally by degradation of organics in the waste.

The experiments also demonstrate that actual conditions may be very far from the homogeneous behaviour often assumed in formulating source term expressions for release of radioisotopes from buried radioactive waste.

3. Sample geometry and grid structure

The system which is to be modelled for simulation of the experiments consists of a block of concrete (or cement mortar or paste) with dimensions b · (2C+a) · L cm as indicated in Fig. 9. The outer surfaces of the block are supposed to be impermeable (i.e. all fluxes = 0). In actual experiments as described in Section 2 a system consisting of two half-cylinders are used in stead of the box-like arrangement in the figure. However, the difference is of minor importance except in case of extreme leaching.

The block is cut through the middle by an (idealised) crack with plane-parallel surfaces with distance or crack width a cm.

Typical dimensions used in the experiments and as parameter values in most of the example calculations are:

-	length of sample and crack	L	= 9	cm
-	breath of crack	b	= 3.5	cm
-	thickness of the cement walls	C	= 2	cm
-	crack width	a	= 0.02	cm

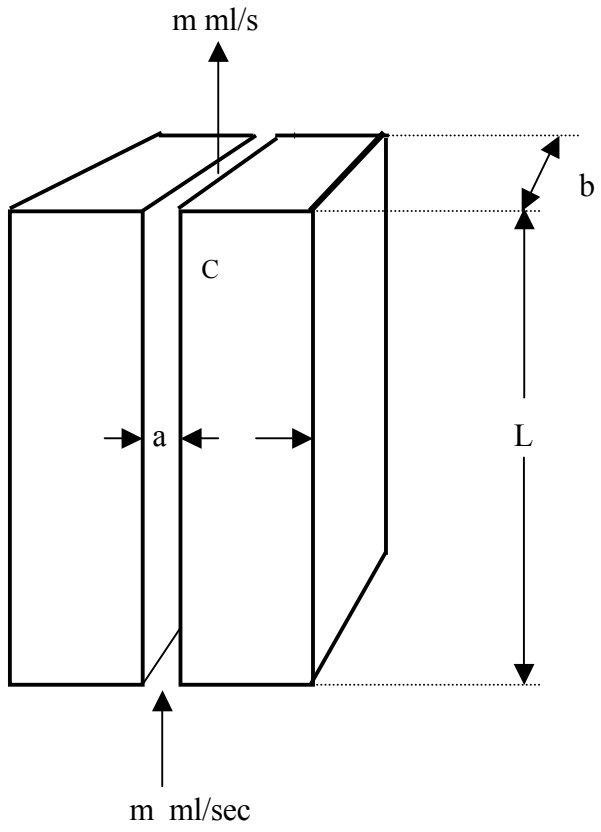

Fig. 9. Basic geometry of the modelled cracked block of cementitious material.

Feed solution at a normally constant flow of m ml/s enter at the bottom and leave at the top. This flow direction corresponds to typical experimental conditions but is unimportant for the modelling.

The solution is supposed to move by laminar flow distributed over the crack cross-section so that the initial mean flow velocity is: $v = m/(a \cdot b)$ cm/sec and the residence time inside the crack is $(a \cdot b \cdot L)/m$ sec. Eventually, as the crack is partly filled by precipitates, the mean flow velocity increases and the residence time decreases correspondingly. Due to friction the flow velocity will be highest at the middle of the crack diminishing towards zero at the crack surfaces. For laminar flow the velocity distribution over the crack follows a parabolic expression:

$$v_y = k\left((a/2)^2 - y^2\right) \tag{1}$$

where y is the distance from the mid-plane of the crack and the constant k is obtained by integration and comparison with the total flow m.

The pressure loss Δh cm water pressure over the crack regarded as a flat box is then given as a special case of Poiseuille's law according to the following expression available in standard reference books on hydraulics:

$$\Delta h = \frac{12 \cdot m \cdot L \cdot \eta}{b \cdot a^3 \cdot g \cdot \rho_w} \tag{2}$$

where g is the acceleration due to gravity, η the viscosity and ρ_w the density of water at 20 ^oC.

In most of the experiments [2] the flow rate was about 4.3 ml/hour equal to $m = 1.2\ 10^{-3}$ ml/sec corresponding to an initial mean water velocity 0.17 mm/sec and a residence time in the crack of about 530 sec for the sample dimensions given above.

The initial pressure loss obtained from (2) for a crack with dimensions as indicated is only 0.0048 cm H_2O, but this is for an ideal smooth gab. In reality the pressure loss will be somewhat higher especially for cracks with rough surfaces as it is typical for actual defects in concrete. This is discussed extensively in [1,3]. The formula shows that the pressure loss will increase rapidly with decreasing width of the crack.

The total surface of the crack in contact with the solution is $A = 2 \cdot b \cdot L$ cm^2, but the system is symmetrical about the mid-plane of the crack and therefore only half of the block needs to be modelled. Figure 10 shows a cut through the block in the flow direction and perpendicular to the plane of the crack. The block is seen to be subdivided into n individual concrete sections or collums with thickness L/n. Presently the number of columns are limited to n = 5.

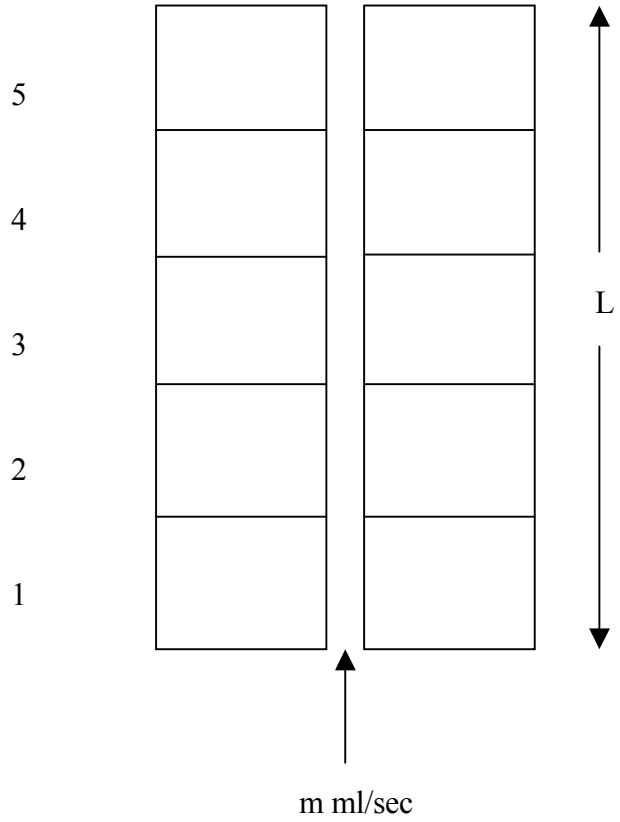

Fig. 10. Cut through the block of cementitious material perpendicular to the plane of symmetry through the crack and showing the subdivision into n (here n = 5) individual columns.

Transport of substances from the concrete out in the solution occurs by diffusion in the pore system, and is supposed to take place only in the direction perpendicular to the crack, i.e. the individual layers or columns are treated as one-dimensional systems separated by impermeable barriers. This is a simplification, but the fluxes inside the cementitious material and parallel to the crack will be small compared with the fluxes perpendicular to the crack. The present version of the model must be classified as pseudo two-dimensional, taking account of flow in the crack and perpendicular to that transport by diffusion in a number n of independently modelled columns interacting with the flowing solution through individual surface fractions with areas $(2 \cdot b \cdot L)/n$ cm^2.

The system can be converted to a true two-dimensional model and this may be needed if cracks in very porous materials such as backfills have to be modelled.

The system can be further simplified by omitting the subdivision into individual columns, i.e. n = 1. This version of the model can (with reservations) be regarded as simulating the leaching of a slap of cementitious material by a flowing solution under simultaneous precipitation of a partly protective layer of calcium carbonate. It is less time consuming to run and has been used for the development of the diffusion and chemistry modelling described in the following.

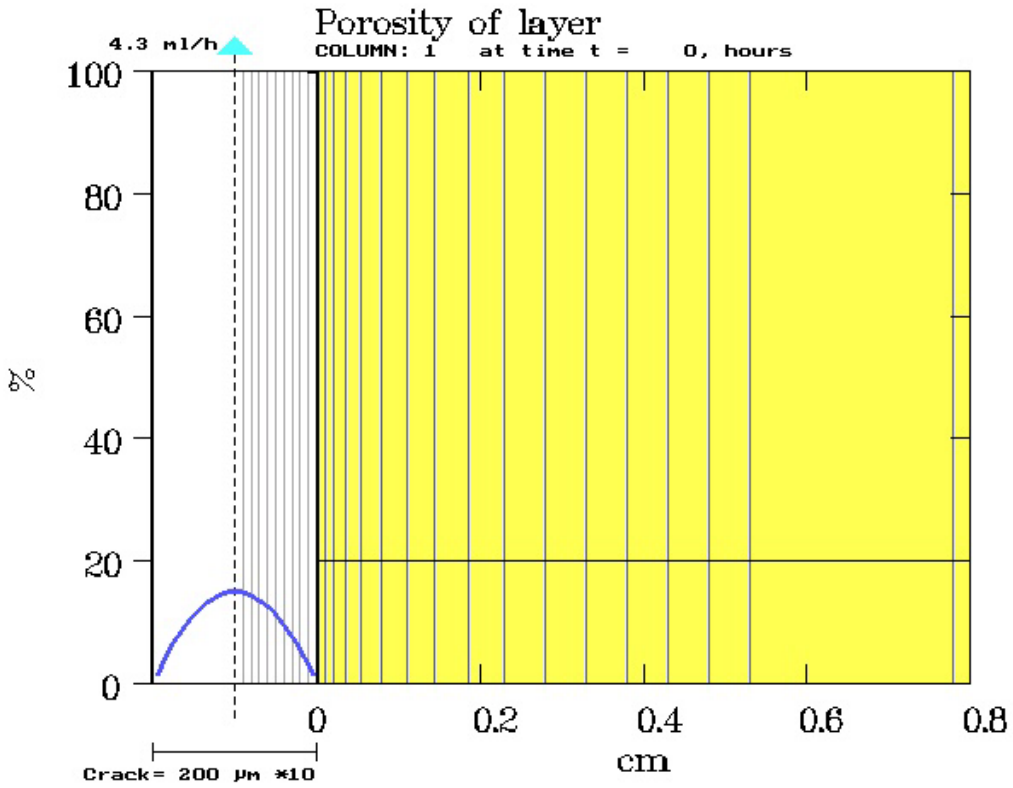

Fig. 11. Example of grid structure in the crack and the cementitious material. The whole crack but only the right-hand side of 0.8 cm of a section through the cementitious part of the specimen is shown in the figure. The linear scale inside the crack is multiplied by a factor 10.

For use in the numerical calculations the individual one-dimensional columns must be subdivided into layers of thickness Δx. The structure employed in the example calculations is shown in Fig. 11.

Due to steep concentration gradients near the crack surface it is necessary to use small Δx values in the vicinity of the crack, in the layer of precipitate and in the solution filled part of the crack which is treated as part of the columns.

Within the half-thickness of the crack the grid consists of 10 layers with thickness $\Delta x = a/20$ (or 0.010 mm for the 0.2 mm crack in most of the examples). These layers will be filled successively by precipitate as described in Section 4.4. Within the cementitious material Δx is selected to increase from 0.1 mm nearest the crack surface to 4.7 mm at the outside of the two 2-cm thick slabs of the symmetrical sample. A total of 30 grid layers are employed, with 10 (number -9 to 0) in the crack and the rest (number 1 to 20) in the cementitious material. The grid system must be changed as needed if other systems are to be simulated.

In the figure the thin layers inside the crack are presented on a larger scale than for the grid system in the cementitious material. Here the initial solution filled porosity is 0.20 as indicated by the horizontal line in Fig. 11. The calculated development of concentration profiles, amounts of precipitated $CaCO_3$ and remaining undissolved $Ca(OH)_2$, etc. are presented in similar manners, see the examples in Section 7.

4. Materials

Concrete and other cementitious materials are typically prepared from Portland cement, various additives and aggregates and water. The chemical constitution of the reacted product can be estimated approximately from the composition of the cement and the added amounts of other components. The main constituents of hardened Portland cement paste are hydrated calcium silicate C-S-H, and calcium hydroxide. The aggregates – such as sand particles in cement mortar - remain mostly unchanged while the water is partly used in the reactions and partly retained as pore solution inside the porous product.

The cementitious material in the two slabs constituting the solid part of the cracked system is here simplified to a porous solid consisting of $Ca(OH)_2$ crystals mixed with inert material. The presence of $CaCO_3$ (as calcite) may also be specified as an potentially reactive additive in the original mixture but C-S-H, forming the major part of a hardened cement paste, is disregarded i.e. it is included in the inert material. This simplification is permissible as long as the free calcium hydroxide is not leached completely from the material, but it is obviously not correct at higher Ca-leaching.

Cements contain small amounts of alkali metals which tend to be more or less dissolved as hydroxides in the pore solution of cementitious materials. This gives rise to high pH values and will via the common ion effect suppress the solubilisation of $Ca(OH)_2$. In the model potassium and sodium are treated together as dissolved NaOH.

Minor hydrated minerals containing Al, Fe, Mg, SO_4 etc. are disregarded.

4.1. Chemical equilibria

With the above composition simplifications the concentrations in the pore solution are regulated by the dissolution equilibria for calcium carbonate (as calcite) and calcium hydroxide:

$$CaCO_3 \leftrightarrow Ca^{2+} + CO_3^{2-}$$

$$g_2 \cdot cCa \cdot g_2 \cdot cCO_3 = L_{CaCO3} = 3.53\ 10^{-9}$$

or rearranged

$$cCa = \frac{L_{CaCO3} / g_2^{\,2}}{cCO_3} = \frac{R_3}{z} \qquad (3)$$

and

$$Ca(OH)_2 \leftrightarrow Ca^{2+} + 2\ OH^-$$

$$g_2 \cdot cCa \cdot g_1^{\,2} \cdot cOH^2 = L_{Ca(OH)2} = 6.0\ 10^{-6}$$

or rearranged

$$cCa = \frac{L_{Ca(OH)2} / (g_2 \cdot g_1^{\,2})}{cOH^2} = \frac{R_4}{x^2} \tag{4}$$

Carbonate is primarily introduced into the system with the flow of calcium bicarbonate solution entering the crack. The equilibria for the dissolved carbonate species are given by:

$$CO_2 + H_2O \leftrightarrow H_2CO_3 \leftrightarrow HCO_3^- + H^+$$

$$\frac{g_1 \cdot cHCO_3 \cdot g_1 \cdot cH}{p_{CO2} \cdot K_{CO2}} = \frac{g_1 \cdot cHCO_3 \cdot g_1 \cdot cH}{cH_2CO_3} = K_1 = 4.14\,10^{-7} \tag{5}$$

where $K_{CO2} = 0.0395$

and $HCO_3^- \leftrightarrow CO_3^{2-} + H^+$

$$\frac{g_2 \cdot cCO_3 \cdot g_1 \cdot CH}{g_1 \cdot cHCO_3} = K_2 = 4.19\,10^{-11} \tag{6}$$

Introducing the dissociation of water

$$g_1 \cdot cOH \cdot g_1 \cdot cH = K_w = 1\,10^{-14} \tag{7}$$

and rearranging equation (6) and (5) gives:

$$cHCO_3 = \frac{K_w \cdot g_2}{K_1 \cdot g_1^2} \cdot \frac{cCO_3}{cOH} = R_1 \frac{cCO_3}{cOH} = R_1 \frac{z}{x} \tag{8}$$

$$p_{CO2} \cdot K_{CO2} = cH_2CO_3 = \frac{K_w^2 \cdot g_2 \cdot cCO_3}{K_1 \cdot K_2 \cdot g_1^2 \cdot cOH} = R_2 \frac{cCO_3}{cOH^2} = R_2 \frac{z}{x^2} \tag{9}$$

from which $cHCO_3$, cH_2CO_3, p_{CO2} (and cH and therefore pH) can be calculated when cOH and cCO_3 are known.

In the equations cCa, cNa, cH, x = cOH, z = cCO_3, $cHCO_3$ and cH_2CO_3 represent the concentrations of Ca^{2+}, Na^+, OH^-, CO_3^{2-}, HCO_3^- and dissolved CO_2. The partial pressure of CO_2 in equilibrium with the solution is p_{CO2}, and the chemical activity coefficients for one- and two-valent ions are g_1 and g_2, respectively. The same notation is used in the computer code.

The numerical values for the equilibrium constants are given for 20°C. They are taken from a review in [9]. In most cases temperature dependence is also available and can if needed be introduced into the program. Partial dissociation of dissolved calcium is disregarded.

4.2. Activity coefficients

The values of the chemical activity coefficients g_1 and g_2 are obtained from the general Deby-Hückel theory in the simplest possible manner:

For a cat- or anion i with charge z_i and concentration c_i mol/L the chemical activity is:

$$a_i = g_i \cdot c_i \tag{10}$$

where the activity coefficient g_i is given by:

$$\log(g_i) = \frac{z_i^2 \cdot 0.511 \cdot \sqrt{Is}}{1 + \sqrt{Is}} \tag{11}$$

and the ionic strength Is by:

$$Is = 0.5 \sum_i (z_i^2 \cdot c_i) \tag{12}$$

or for the considered 5 major ionic species:

$$Is = 0.5 \, (4 \, cCa + cNa + cOH + cHCO_3 + 4 \, cCO_3)$$

Corrections taking interaction between an- and cations into account can be introduced into equation (11) but are unnecessary in the weak solutions typical for the crack. In the stronger pore solution inside the cementitious material this is more questionable but hardly significant compared with effects of other simplifications.

Using these expressions the coefficients are only dependent on the charges and the same g_1 and g_2 values may be used for all one- or divalent ions, respectively. As a further simplification the concentrations from the previous time steps are used to calculate the ionic strength of the solution in individual cells. Since the time steps are short and the concentration changes relatively slight, this is considered of no significance.

4.3. Mass balances

The numerical calculation of diffusive transport of dissolved species in the porous material and in the solution in the crack is carried out on a system subdivided into n columns which again are split into a number of individual grid cells as specified in Section 3. The diffusive processes are described in Section 5. For the present purpose of deriving the general mass balance for a single cell it is sufficient to specify that there is a certain diffusive transport into the cell through the surface nearest the crack mid-plane corresponding to a flux q_n. In the same way there is a flux q_f out of the cell through the surface away from the crack, see Fig. 12.

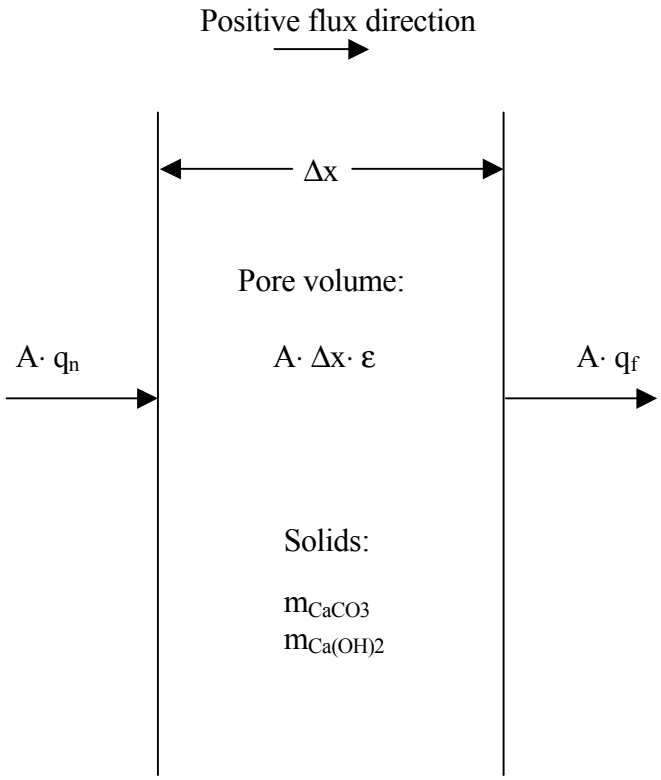

Fig. 12. Schematic presentation of a diffusion cell in a porous material with porosity ε. The cell has thickness Δx and area A, and contains m_{CaCO3} mol calcium carbonate and $m_{Ca(OH)2}$ mol calcium hydroxide as undissolved crystals mixed with inert materials.

The equilibrium concentrations inside each cell is determined by equations (3), (4), (8) and (9) in combination with the mass balances for the cell, which for the 6 major species may be written:

$$\Delta m_{CaCO3} + \Delta m_{Ca(OH)2} + A(qCa_n - qCa_f) - A\,\Delta x\,\varepsilon\,(cCa^* - cCa) = 0 \quad (13)$$

$$\Delta m_{CaCO3} + \Delta HCO_3 + A(qCO3_n - qCO3_f) - A\,\Delta x\,\varepsilon\,(cCO_3^* - cCO_3) = 0 \quad (14)$$

$$-\Delta HCO_3 + \Delta H_2CO_3 + A(qHCO3_n - qHCO3_f) - A\,\Delta x\,\varepsilon\,(cHCO_3^* - cHCO_3) = 0 \quad (15)$$

$$-\Delta H_2CO_3 + A(qH2CO3_n - qH2CO3_f) - A\,\Delta x\,\varepsilon\,(cH_2CO_3^* - cH_2CO_3) = 0 \quad (16)$$

$$2\Delta m_{Ca(OH)2} - \Delta HCO_3 - \Delta H_2CO_3 + A(qOH_n - qOH_f) - A\,\Delta x\varepsilon\,(cOH^* - cOH) = 0 \quad (17)$$

$$A(qNa_n - qNa_f) - A\,\Delta x\,\varepsilon\,(cNa^* - cNa) = 0 \quad (18)$$

where during a time step Δt:

Δm_{CaCO3} and $\Delta m_{Ca(OH)2}$ are mol $CaCO_3$ and $Ca(OH)_2$ dissolved,

ΔHCO_3 is the amount of HCO_3^- converted to CO_3^{2-} according to $HCO_3^- + OH^- \rightarrow CO_3^{2-} + H_2O$,

ΔH_2CO_3 is the amount of $H_2CO_3^-$ converted to HCO_3^-
according to $H_2CO_3^- + OH^- \rightarrow HCO_3^- + H_2O$.

For calcium

$A \cdot \Delta qCa = A \cdot (qCa_n - qCa_f)$ is the increase in Ca content in the cell due to diffusion

and

$A \cdot \Delta x \cdot \varepsilon \cdot (cCa^* - cCa)$ is the increase in the amount of dissolved Ca present in the pore solution,

i.e. cCa^* is the concentration in the solution after and cCa before the time step.

The notation for the other species is similar.

Rearranging and eliminating ΔHCO_3 and ΔH_2CO_3 gives the following set of equations:

$$cCa^* = cCa + (\Delta m_{CaCO3} + \Delta m_{Ca(OH)2} + A\,\Delta qCa)/(A\,\Delta x\,\varepsilon) \quad (19)$$

$$cNa^* = cNa + A\,\Delta qNa/(A\,\Delta x\,\varepsilon) \quad (20)$$

$$cCO_3^* = cCO_3 - (cHCO_3^* - cHCO_3 + cH_2CO_3^* - cH_2CO_3) + (\Delta m_{CaCO3} + A\,(\Delta qCO3 + \Delta qHCO3 + \Delta qH2CO3))/(A\,\Delta x\,\varepsilon) \quad (21)$$

$$cOH^* = cOH + (cHCO_3^* - cHCO_3 + 2\,cH_2CO_3^* - 2\,cH_2CO_3) + (2\Delta m_{Ca(OH)2} + A\,(\Delta qOH - \Delta qHCO3 - 2\Delta qH2CO3))/(A\,\Delta x\,\varepsilon) \quad (22)$$

Inserting (8) and (9) in the forms:

$$cHCO_3^* = \frac{K_w \cdot g_2}{K_1 \cdot g_1} \cdot \frac{cCO_3^*}{cOH^*} = R_1 \frac{z}{x} \quad (23)$$

$$cH_2CO_3^* = \frac{K_w^2 \cdot g_2 \cdot cCO_3^*}{K_1 \cdot K_2 \cdot g_1 \cdot cOH^*} = R_2 \frac{z}{x^2} \quad (24)$$

in (21) and (22) eliminates $cHCO_3^*$ and $cH_2CO_3^*$ and gives:

$$z = cCO_3^* = -R_1\,z/x - R_2\,z/x^2 + cCO_3 + cHCO_3 + cH_2CO_3 + (\Delta m_{CaCO3} + A\,(\Delta qCO3 + \Delta qHCO3 + \Delta qH2CO3))/(A\,\Delta x\,\varepsilon) \quad (25)$$

$$x = cOH^* = R_1\,z/x + 2\,R_2\,z/x^2 + cOH - cHCO_3 - 2 \cdot cH_2CO_3 + (2\Delta m_{Ca(OH)2} + A\,(\Delta qOH - \Delta qHCO3 - 2\Delta qH2CO3))/(A\,\Delta x\,\varepsilon) \quad (26)$$

Equations (19), (20), (23), (24) together with (3) and (4) are sufficient to determine the 6 unknown: cCa^*, cNa^*, $cCO_3^* = z$, $cOH^* = x$, Δm_{CaCO3} and $\Delta m_{Ca(OH)2}$.

Equation (20) alone is sufficient to determine cNa^* because only diffusion and no chemical reactions are involved.

For practical reasons computation of the change in concentrations due to diffusion is carried out separately and before the chemical equilibration for all the species. The procedure is described in Section 5 and results in a new set of concentrations: cCa', cOH', cCO_3', $cHCO_3'$ and cH_2CO_3' where

$$cCa' = cCa + \Delta qCa/(\Delta x\, \varepsilon)$$

and similar for the other species. Inserting cCa' etc. in equations (19) to (26) results in the removal of the Δq terms.

Four different cases must be distinguished:

Case 4: Neither $Ca(OH)_2$ nor $CaCO_3$ are present, i.e. $m_{CaCO3} = 0$ and $m_{Ca(OH)2}=0$ and equations (3) and (4) are therefore irrelevant.

This case is applicable on the grid cells with solution flow in the middle part of the crack, for further discussion see Section 4.4.

Inserting Δm_{CaCO3} and $\Delta m_{Ca(OH)2} = 0$ (or a small known value r_{CaCO3} or $r_{Ca(OH)2}$ corresponding to dissolution of the last amount of calcium carbonate or hydroxide within the time step) and solving the remaining four equations gives:

$$x^3 + (R_1-S1)x^2 + (R_2-R_1(S1+S0))x - R_2(2\cdot S0+S1) = 0 \qquad (27)$$

where the 'constants' defined by the Δq's and the concentrations from the previous time step are

$$S0 = cCO_3'+cHCO_3' + cH_2CO_3' + r_{CaCO3}'/(A\, \Delta x\, \varepsilon) \qquad (28)$$

and

$$S1 = cOH' - cHCO_3' - 2\, cH_2CO_3' + 2\, r_{Ca(OH)2}/(A\, \Delta x\, \varepsilon) \qquad (29)$$

$x = cOH^*$ can be obtained from (27) using Newton iteration and $z = cCO_3^*$ from a combination of (25) and (26):

$$z = S0/(1 + R_1/x + R_2/x^2) \qquad (30)$$

The calcium concentration is given directly by (19) because both solid phases are absent at the end of the time step:

$$cCa^* = cCa' + (r_{CaCO3} + r_{Ca(OH)2})/(A\, \Delta x\, \varepsilon) \qquad (31)$$

Case 1: Only $Ca(OH)_2$ is present, as might be the case initially for the inner layers of the cementitious material. It follows that $m_{CaCO3} = 0$ and equation (3) is irrelevant.

Inserting $\Delta m_{CaCO3} = 0$ or a small known value r_{CaCO3} corresponding to dissolution of the last amount of calcium carbonate within the time step and combining the calcium concentration as given by (4) in the form: $cCa^* = R4/x^2$ with equations (19), (20), (23), (24) gives an equation in $x = cOH^*$ which may be solved by Newton iteration:

$$x^5 + (R_1\text{-}S2)x^4 + (R_2 - R_1(S0+S2))x^3 - (R_2(S2+2\,S0) + 2R_4)x^2 - 2R_1R_4x - 2R_2R_4 = 0 \quad (32)$$

Here S0 is given by equation (23) and

$$S2 = cOH' - cHCO_3' - 2\cdot cH_2CO_3' - 2\cdot cCa' - 2\cdot r_{CaCO3}/(A\cdot\Delta x\cdot\varepsilon) \quad (33)$$

when x is known $z = cCO_3^*$ is given by (25), $cCa^* = R4/x^2$ and the amount of dissolved $Ca(OH)_2$ is obtained from (13):

$$\Delta m_{Ca(OH)2} = - r_{CaCO3} + A\,\Delta x\,\varepsilon\,(R4/x^2 - cCa') \quad (34)$$

Case 2: Only $CaCO_3$ is present as is the case for the layer of precipitated material, see also Section 4.4. The situation may also occur in strongly leached layers of the (simplified) cementitious material. It follows that $m_{Ca(OH)2} = 0$ and equation (4) is irrelevant.

Inserting $\Delta m_{Ca(OH)2} = 0$ or a small known value $r_{Ca(OH)2}$ corresponding to dissolution of the last amount of calcium hydroxide within the time step and combining the calcium concentration as given by (3) in the form: $cCa^* = R3/z$ with equations (19), (20), (23), (24) gives:

$$z = (x\text{-}S1)x^2/(R_1x + 2\,R_2) \quad (35)$$

$$x^6 + (R_1\text{-}2\,S1)x^5 + (R_2+S1(S1\text{-}R_1)\text{-}R_1(S1+S3))x^4 + (S1+S3)(S1\,R_1\text{-}2R_2)x^3 + (S1\,R_2(S1+2\,S3)\text{-}R_1^2\,R_3)x^2 - 4R_1R_2R_3x - 4R_2^2R_3 = 0 \quad (36)$$

where S1 is given by equation (29) and

$$S3 = cCO_3' + cHCO_3' + cH_2CO_3' - cCa' - r_{Ca(OH)2}/(A\,\Delta x\,\varepsilon) \quad (37)$$

$x = cOH^*$ is then obtained from (36) by Newton iteration whereafter $z = cCO_3^*$ is given by (35), $cCa^* = R3/z$ and the amount of dissolved $CaCO_3$ is calculated from (13) in the form:

$$\Delta m_{CaCO3} = - r_{Ca(OH)2} + A\,\Delta x\,\varepsilon\,(R_3/z - cCa') \quad (38)$$

Case 3: Both $CaCO_3$ and $Ca(OH)_2$ are present as will be the case in the cementitious material after contact with the bicarbonate containing solution.

Equations (3) and (4) must both be followed which give the identity:

$$cCa^* = \frac{R_4}{x^2} = \frac{R_3}{z} \qquad \text{and therefore} \qquad z = \frac{R_3}{R_4} x^2 \tag{39}$$

Introducing this into equations (19), (20), (23), (24) and rearranging gives:

$$2R_3 x^4 + (R_4 + R_1R_3)x^3 - S4\, R_4 x^2 - 2R_4^2 = 0 \tag{40}$$

where

$$S4 = cOH' + 2\, cCO_3' + cHCO_3' - 2\, cCa' \tag{41}$$

$x = cOH^*$ is then obtained from (40) by Newton iteration whereafter $z = cCO_3^*$ is given by (39), $cCa^* = R_3/z$, and the amounts of dissolved $CaCO_3$ and $Ca(OH)_2$ are calculated from a combination of (25) and (13) in the form:

$$\Delta m_{Ca(OH)2} = - A\, \Delta x\, \varepsilon(z\,(1 + R_1/x + R1/x^2) - R_3/z - cCO_3' - cHCO_3' - cH_2CO_3' + cCa') \tag{42}$$

$$\Delta m_{CaCO3} = - \Delta m_{Ca(OH)2} + A\, \Delta x\, \varepsilon\, (R_3/z - cCa') \tag{43}$$

All cases:

In all four cases $cHCO_3^* = R_1\, z/x$ and $cH_2CO_3^* = R_2\, z/x^2$ as given by equations (23) and (24), respectively. In case 3 it follows from equation (39) that $cH_2CO_3^* = R_2 \cdot R_3/R_4 \approx 2.5 \cdot 10^{-14}$ corresponding to a constant CO_2 pressure of only about $5 \cdot 10^{-12}$ atm.

The dissolution of $Ca(OH)_2$ or precipitation of $CaCO_3$ influences the porosity of the material, see for example equation (83). The employed mineral densities are $\rho_{CaOH2} = 2.24$ and $\rho_{CaCO3} = 2.71$ g/cm^3.

The sum of the cat- and anions present in the pore solution must fulfil the requirement about electro neutrality:

$$2\, cCa^* + cNa^* = cOH^* + cH^* + cHCO_3^* + 2\, cCO_3^* \tag{44}$$

However, this is inherent in the mass balances given above and the requirement can therefore be used as a test of the precision of the calculated concentrations.

Obviously the equilibrium concentrations in the pore water might also be obtained using a suitable standard program for calculation of thermodynamic equilibria in solutions. However, the cases considered here are simple and the speed required for the calculations is high. It was therefore thought desirable to avoid interfacing with a standard program.

4.4. Feed solution

The solution entering the crack may be equilibrated in advance by contact with excess $CaCO_3$. In this case equations (3), (8) and (9) in combination with $cH = K_w/(g_1^2 \cdot cOH)$ and the requirement about electroneutrality:

$$2\ cCa + cNa = cOH + cHCO_3 + 2\ cCO_3 \qquad (45)$$

are sufficient to calculate the composition of the solution. The hydrogen concentration is low and disregarded in (45) as elsewhere in the program, but cH and therefore pH can be obtained from (6). The concentration of sodium cNa must be known (e.g. = 0) and no other ions should be present.

The concentrations in the feed solution are introduced into the main part of the program as:

$$cCa_0 \quad cNa_0 \quad cOH_0 \quad cCO3_0 \quad cHCO3_0 \quad cH2CO3_0$$

where the indices i = 0 indicate a position outside the columns numbered from 1 to n.

The feed solution used in most of the example calculations has the composition: 2.00 mM Ca^{2+}, 0.0035 mM CO_3^{2-}, 3.99 mM HCO_3^{-1} and 0.55 mM dissolved CO_2 per litre at pH=7.21 and a CO_2 partial pressure of 0.014 atm. (see Table 3 and 4 in Section 7). The solution is in equilibrium with calcite and the chemical activity coefficients are g_1=0.92 and g_2=0.71 which means that the product of cCa_0 and $cCO3_0$ according to (3) must be a factor ~2 higher than the solubility product.
The solution may also contain a radioisotope considered not absorbed on the solids.

A synthetic calcite equilibrated calcium bicarbonate solution without sodium was used in many of the experiments, and the chemical analysis of this feed solution is in reasonable agreement with the above composition [6,7].

Solutions containing an excess of dissolved CO_2 in form of aggressive carbon dioxide may also be relevant for certain conditions, and will result in different development of the calcite cover in the crack, see Section 7, Table 3 and case $\mathbf{a_U}$.

The feed solution may contain other components influencing the formation of precipitates. The most important is probably Mg^{2+} which at high pH gives rise to difficult soluble $Mg(OH)_2$. This would be the case for the Risø tap water used as feed in some of the experiments.

For cracks in cementitious materials with high alumina contents, sulphate and chloride may also be of interest. These components are not included in the present version of the model, neither is the dissolved silicic acid associated with the C-S-H phase.

4.5. Inside the crack

As mentioned in Section 3 the flow inside the crack is supposed to be laminar with no mixing perpendicular to the flow direction except by diffusion. Equations (1) and (2) are generalised in the following for n columns with variable remaining crack width.

The amount passing through the crack is m ml/s and the corresponding mean velocity in column i is:

$$v_i = m/(crack_i \cdot b) \tag{46}$$

where $crack_i < a$ is the part of the crack not occupied by calcite deposit on column i.

With laminar flow the velocity is highest at the middle of the crack diminishing towards zero at the crack surfaces and following a parabolic expression like (1).

The pressure loss over the part of the crack with length L/n in column i is supposed to be given by:

$$\Delta h_i = \frac{12 \cdot m \cdot (L/n) \cdot \eta}{b \cdot crack_i^{\,3} \cdot g \cdot \rho_w} \tag{47}$$

where g is the acceleration due to gravity, η the viscosity and ρ_w the density of water at 20 ^oC. The total pressure loss over the crack lengths in the n columns is then obtained by summation.

In the individual columns the flow is initially distributed over the crack thickness a cm subdivided into $2N = 2 \cdot 10$ grid cells constituting the crack part of the columns. The layers are numbered from j=0 to j=-9 symmetrically about the mid-plane in the crack, see Fig.11 and 13. They are all of the same thickness dcx = a/2N (in the examples 0.02/20 cm = 10 μm).

Eventually some of the crack volume is filled by precipitate forming a layer with thickness x_{dist} on both surfaces of the crack, leaving only the distance:

$$crack_i = a - 2 \cdot x_{dist} \tag{48}$$

available for the flow. During a time step Δt the thickness of the precipitated layer increases according to:

$$x^*_{dist} = x_{dist} + \frac{ds_{CaCO3}}{M_{CaCO3} \cdot \rho_{CaCo3} \cdot (1 - \varepsilon_j)} \tag{49}$$

where ds_{CaCO3} is the amount of precipitated $CaCO_3$, M_{CaCO3} = 0.100 g calcite/mmol, ρ_{CaCO3} = 2.71 g/cm^3 is the density of calcite crystals and ε_j the porosity of the deposit.

The growth of the precipitate takes place within a certain cell j = LayNo (-9 to 0) defined by

$$|\,\mathrm{LayNo}\,| \cdot dcx < x_{dist} < (\,|\,\mathrm{LayNo}\,|+1) \cdot dcx$$
$$\text{or} \quad \mathrm{LayNo} = \mathrm{Trunc}(x_{dist}/(a/2N)) \tag{50}$$

In the general case the flow is distributed over N + LayNo-1 'empty' cells with thickness dcx= a/2N and the empty part dx = (1 - LayNo) · dcx - x_{dist} of the cell where build up of the layer takes place.

Combination with the velocity distribution typical for laminar flow is obtained from the summation of the products of local velocity and empty grid cross sections compared with the volumetric flow rate per unit breadth b of the crack:

$$\sum_{-9 \text{ to } \mathrm{LayNo}-1} dcx_j \cdot v_j \; + \; dx \cdot v_{\mathrm{LayNo}} \;\; = \;\; m/b \tag{51}$$

where the velocities are given by:

$$v_j \;\; = \;\; k\left((crack_i/2)^2 - y_j^{\,2}\right) \tag{52}$$

using $y_j \;\; = \;\; (j+9.5)\; dcx \qquad \text{for } j < \mathrm{LayNo}$

or $y_{\mathrm{LayNo}} = \;\; (j+9)\; dcx \; + dx/2 \qquad \text{for } j = \mathrm{LayNo}$

as distance from the crack mid-plane.

From this the value of the proportionality constant k can be calculated and used in (52) to obtain the parabolic distributed velocities in the various grid layers in the crack.

The amounts of solution flowing through one of the 'empty' cells is then :

$$w_j \;\; = v_j \cdot dcx \cdot b \qquad \text{ml/s} \tag{53}$$

and for the cell with the growing layer:

$$w_{\mathrm{LayNo}} \;\; = v_{\mathrm{LayNo}} \cdot dx \cdot b \qquad \text{ml/s} \tag{54}$$

with dissolved materials corresponding to the concentrations in the various layers.

When the thickness of the deposited layer is changing from column i-1 to i a correction is necessary to take account of the redistribution of liquid and dissolved materials over the different cross-sectional area available for the flow.

The situation is illustrated in Fig. 13 for decreasing thickness of the calcite layer up through the columns. The flow entering each cell in the i'th column is divided into a part $w_{i,j}$ moving up through the cell above and a part $ww_{i,j}$ which is diverted into the cell to the left.

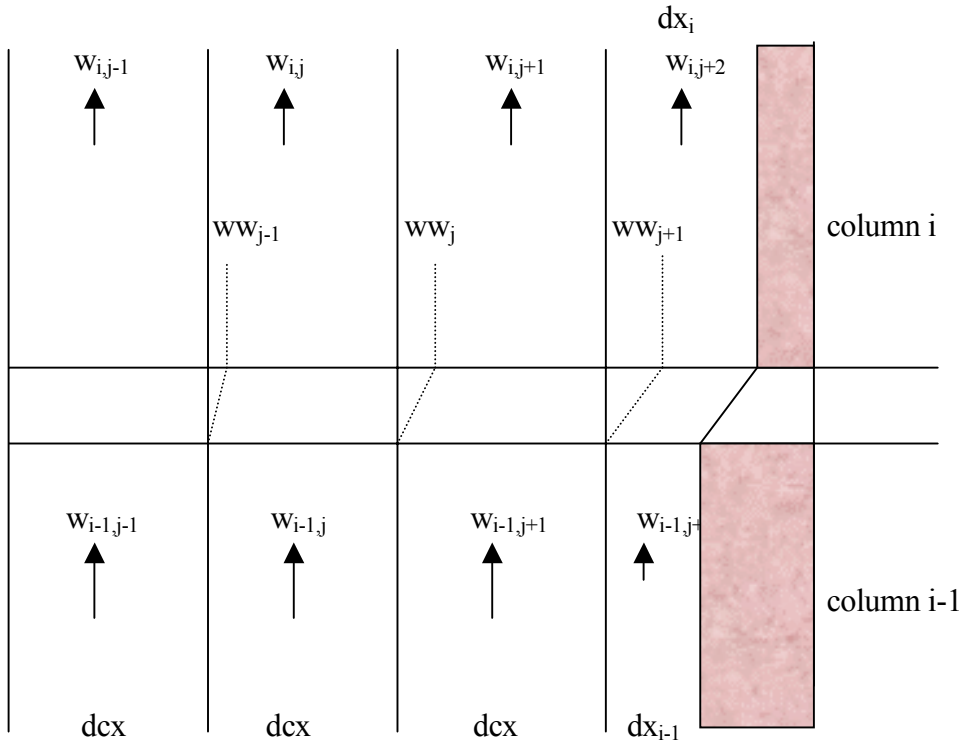

Fig. 13. Redistribution of solution flow over the grid cells in the right hand side of the crack when the thickness of the precipitated layer is decreasing in the flow direction. In the example j = -8, LayNo = -6.

The mass balance for the flow through cell i,j is then:

$$w_{i,j} = ww_{i,j-1} + w_{i-1,j} - ww_{i,j} \tag{55}$$

or

$$dcx \cdot v_{i,j} = ww_{i,j-1} + dcx \cdot v_{i-1,j} - ww_{i,j} \tag{56}$$

where $v_{i,j}$ and $v_{i-1,j}$ are obtained from (52) and dcx, where relevant, must be substituted with the open parts dx_i and dx_{i-1} for the layers with growing calcite

The redistribution is then obtained successively starting with $ww_{i,-10} = 0$ because there is no side flow through the mid-plane due to crack symmetry.

Similar procedures can be used when the thickness of the deposit is increasing in the flow direction, a situation typical for cracks exposed to aggressive carbonate feed solution. In case of different cell numbers j = LayNo of the growing layers in column i and i-1 some further complications must be taken into account.

The redistribution of flow and dissolved material is included in the program but is for simplification omitted in the following mass balances.

The concentrations in the solution entering $cell_{i,j}$ from the $cell_{i-1,j}$ below (or as the feed solution when i-1 = 0) are:

$$cCa_{i-1,j}\ \ cNa_{i-1,j}\ \ cOH_{i-1,j}\ \ cCO3_{i-1,j}\ \ cHCO3_{i-1,j}\ \ cH2CO3_{i-1,j}$$

The concentrations in the solution leaving $cell_{i,j}$ are:

$$cCa^*_{i,j}\ \ cNa^*_{i,j}\ \ cOH^*_{i,j}\ \ cCO3^*_{i,j}\ \ cHCO3^*_{i,j}\ \ cH2CO3^*_{i,j}$$

or simplified $cCa^*\ \ cNa^*\ \ cOH^*\ \ cCO3^*\ \ cHCO3^*\ \ cH2CO3^*$.

The mass balances, equations (13) to (18) in Section 3.2. must therefore for cell numbers -9 to LayNo be supplemented by additional terms taking the flow into account:

$$\Delta m_{CaCO3} + A\,\Delta qCa - A\,\Delta x\,\varepsilon\,(cCa^* - cCa) + w_j\cdot(cCa_{i-1,j} - cCa^*) = 0 \quad (57)$$

$$\Delta m_{CaCO3} + \Delta HCO_3 + A\,\Delta qCO3 - A\,\Delta x\,\varepsilon\,(cCO_3^* - cCO_3) + w_j\,(cCO3_{i-1,j} - cCO3^*) = 0 \quad (58)$$

$$-\Delta HCO_3 + \Delta H_2CO_3 + A\,\Delta qHCO3 - A\Delta x\,\varepsilon\,(cHCO_3^* - cHCO_3) + w_j(cHCO3_{i-1,j} - cHCO3^*) = 0 \quad (59)$$

$$-\ \Delta H_2CO_3 + A\,\Delta qH2CO3 - A\,\Delta x\,\varepsilon\,(cH_2CO_3^* - cH_2CO_3) + w_j\,(cH2CO3_{i-1,j} - cH2CO3^*) = 0 \quad (60)$$

$$-\Delta HCO_3 - \Delta H_2CO_3 + A\,qOH - A\,\Delta x\,\varepsilon\,(cOH^* - cOH) + w_j\,(cOH_{i-1,j} - cOH^*) = 0 \quad (61)$$

$$A\,\Delta qNa - A\,\Delta x\,\varepsilon\,(cNa^* - cNa) + w_j\,(cNa_{i-1,j} - cNa^*) = 0 \quad (62)$$

Only CaseW 4 (no solids present) and CaseW 2 (only $CaCO_3$ present) are expected to be relevant for the flowing solution and in the layer of precipitate deposited on the original crack surface. $\Delta m_{Ca(OH)2}$ has therefore been removed from the mass balances.

Equation (62) alone is sufficient to determine cNa^* because only diffusion and no chemical reactions are involved:

$$cNa^* = (A\,\Delta qNa + A\,\Delta x\,\varepsilon\,cNa - w_j\,cNa_{i-1,j})/(A\,\Delta x\,\varepsilon + w_j) \quad (63)$$

For the other species computation of the change in concentrations due to diffusion and dilution is carried out separately and before the chemical equilibration. The procedure is described in Section 5 and gives a new set of concentrations: cCa', cOH', cCO_3', $cHCO_3'$ and cH_2CO_3' where

$$cCa' = (A\,\Delta qCa + A\,\Delta x\,\varepsilon\,cCa + w_j\,cCa_{i-1,j})/(A\,\Delta x\,\varepsilon) \quad (64)$$

with similar expressions for the other species.

Inserting in the equations above results in the removal of the Δq's and part of the dilution terms:

$$\Delta m_{CaCO3} - A\,\Delta x\,\varepsilon\,(cCa^{*} - cCa') - w_j\,cCa^{*} = 0 \quad (65)$$

$$\Delta m_{CaCO3} + \Delta HCO_3 - A\,\Delta x\,\varepsilon\,(cCO_3^{*} - cCO_3') - w_j\,cCO3^{*} = 0 \quad (66)$$

$$-\Delta HCO_3 + \Delta H_2CO_3 - A\,\Delta x\,\varepsilon\,(cHCO_3^{*} - cHCO_3') - w_j\,cHCO3^{*} = 0 \quad (67)$$

$$-\Delta H_2CO_3 - A\,\Delta x\,\varepsilon\,(cH_2CO_3^{*} - cH_2CO_3') - w_j\,cH2CO3^{*} = 0 \quad (68)$$

$$-\Delta HCO_3 - \Delta H_2CO_3 - A\,\Delta x\,\varepsilon\,(cOH^{*} - cOH') - w_j\,cOH^{*} = 0 \quad (69)$$

Eliminating ΔHCO_3 and ΔH_2CO_3 and introducing (23) and (24) give:

$$z = cCO_3^{*} = -R_1\,z/x - R_2\,z/x^2 + A\,\Delta x\,\varepsilon\,(cCO_3' + cHCO_3' + cH_2CO_3' + \Delta m_{CaCO3})/(A\,\Delta x\,\varepsilon + w_j) \quad (70)$$

$$x = cOH^{*} = R_1\,z/x + 2\,R_2\,z/x^2 + A\,\Delta x\,\varepsilon\,(cOH' - cHCO_3' - 2\,cH_2CO_3')/(A\,\Delta x\,\varepsilon + w_j) \quad (71)$$

Two cases must be distinguished:

CaseW 4: No solid is present, i.e. $m_{CaCO3}=0$ and $\Delta m_{CaCO3}=0$.
This is supposed to be the case for all the grid cells in the crack where there is no direct contact with already precipitated material (j<LayNo). A certain degree of oversaturation may occur in the inner cells, but this is not expected to cause any nucleation of suspended crystallites of calcite.

Solving (70) and (71) together gives:

$$cCO_3^{*} = z = S0w/(1 + R_1/x + R_2/x^2) \quad (72)$$

$$x^3 + (R_1 - S1w)x^2 + (R_2 - R1_2(S1w + S0w))x - R_2(2\,S0w + S1w) = 0 \quad (73)$$

where

$$S0w = A\,\Delta x\,\varepsilon\,(cCO_3' + cHCO_3' + cH_2CO_3')/(A\,\Delta x\,\varepsilon + w_j) \quad (74)$$

$$S1w = A\,\Delta x\,\varepsilon\,(cOH' - cHCO_3' - 2\cdot cH_2CO_3')/(A\,\Delta x\,\varepsilon + w_j) \quad (75)$$

The calcium concentration is given directly by (65) because solid phases are absent:

$$cCa^{*} = A\,\Delta x\,\varepsilon\,cCa'/(A\,\Delta x\,\varepsilon + w_j) \quad (76)$$

and the degree of oversaturation is: $cCa^{*} \cdot z/R3$. (77)

CaseW 2: $CaCO_3$ present

Introducing $cCa^* = R3/z$ and combining (65) and (70) gives:

$$cCO_3^* = z = (x-S1w)\, x^2/(R_1 x + 2\, R_2) \tag{78}$$

$$x^6 + (R_1 - 2\, S1w)\, x^5 + (R_2 + S1w(S1w-R_1) - R_1(S1w+S3w))\, x^4 + (S1w+S3w)(S1w\cdot R_1 - 2\, R_2)\, x^3 + (S1w\, R_2(S1w+2\, S3w) - R_1^2 \cdot R_3)\, x^2 - 4\, R_1\, R_2\, R_3\, x - 4\, R_2^2\, R_3 = 0 \tag{79}$$

where S1w is given by equation (75) above and

$$S3w = A\, \Delta x\, \varepsilon\, (cCO_3' + cHCO_3' + cH_2CO_3' - cCa')/(A\cdot dx\cdot \varepsilon + w_j) \tag{80}$$

When x and z are obtained $cCa^* = R3/z$

and the amount of dissolved $CaCO_3$ is calculated from (65) in the form:

$$\Delta m_{CaCO3} = A\, \Delta x\, \varepsilon\, (R_3/z - cCa') \tag{81}$$

Inside the precipitated layer, i.e. for $0 \geq j > LayNo$, no liquid flow is supposed to take place i.e. $w_j=0$. The formulas for CaseW2 are then similar to Case 2, see Section 4.3, except that the term $r_{Ca(OH)2}$ is irrelevant.

The total amount of calcium carbonate in the layer is

$$m^*_{CaCO3} = m_{CaCO3} - \Delta m_{CaCO3} \tag{82}$$

and the porosity is given by:

$$\varepsilon_j = 1 - m_{CaCO3}\, M_{CaCO3}/(\rho_{CaCO3}\, \Delta x_j\, A) \tag{83}$$

In case of the grid cell with the growing layer this formula gives the mean value for the porosity in the cell. This value is employed in the flux calculations described below.

The porosity of the calcite crystal agglomerate is assumed to have a specified value ε_{precip} when initially precipitated in an empty grid cell. This is used in calculating the thickness of the deposited layers x_{dist} as described above, see equation (49). When a grid layer cell is filled with calcite with porosity ε_{precip} further deposition of calcite results in decreasing porosity of the calcite in the cell. This is assumed to continue until a pre-selected porosity ε_{min} has been reached. Material from any continuing precipitation is then arbitrarily transferred to the next layer in the crack.

Obviously this is a somewhat artificial method to handle the growth of the calcite crystals constituting the covering layer. In Section 2 it is mentioned that 2 to 5 μm is a typical size of crystals found on uniform surface areas of the crack. This is not that much different from the 10 μm grid layer thickness used for calculations in the crack. The porosity decrease must be associated with growth in seems and hollows between existing calcite crystals which appears to be randomly oriented, see Fig. 4 and 5.

5. Pore systems

The cement mortar of the crack walls as well as the precipitated layer of calcium carbonate crystals are both porous materials characterized by a solution filled porosity ε. Using qualitative terms taken from percolation theory [10] and from [11] this porosity can be divided into different types:

ε_b: The backbone porosity represents the interconnected network of channels penetrating the sample. This may be subdivided into the flow porosity in form of coarse channels where convective transport preferentially takes place, and the diffusion porosity where the channels are so narrow that transport is predominantly by diffusion.

ε_d: The dead-end porosity represents channels or clusters of channels connected to the transmitting network at one point only. This is also called the storage porosity because dissolved materials are stored in the dead-end channels from where it might interact more or less slowly with the transmitting backbone network.

ε_c: The closed porosity represents pores or clusters of pores with no connection to the transmitting network.

The total porosity is the sum of the three types:

$$\varepsilon = \varepsilon_b + \varepsilon_d + \varepsilon_c \tag{84}$$

For cementitious materials with high w/c ratio the total porosity is also high, with a large fraction of coarse and well-interconnected capillary pores. The system is characterised by high connectivity and low constrictivity of the transmitting channels and the total porosity is dominated by ε_b.

When the materials are prepared with decrease w/c ratio, and particularly if fine grained additives such as micro silica are employed, the total porosity is somewhat decreased, but the important effect is that the pore system is more finely divided so that constrictivity is increased and connectivity decreased. The fraction of the total porosity associated with ε_b is therefore less and shifted towards diffusion porosity, while ε_d and maybe also ε_c are increased.

The release of ions from the cementitious material into the flowing solution in the crack is by diffusive leaching only. The concept of flow porosity is therefore irrelevant and the whole pore system could formally be regarded as clusters of dead-end pores connected to the exposed surface of the sample.

However, it is reasonable also in this case to maintain the concept of a backbone porosity representing the well interconnected part of the pore channels ensuring a reasonably homogeneously distributed connection with the deeper layers of the material.
Diffusion inside the pore system can be described in various manners. Three diffusion coefficients are relevant for each species: The effective diffusivity De (sometimes called the intrinsic diffusivity [6]), the pore diffusivity Dp, and the diffusivity in water Dw.

The diffusivities are related by the following expression:

$$De = Dp \cdot \varepsilon = Dw \cdot ff \cdot \varepsilon \quad (85)$$

where $\varepsilon = \varepsilon_b + \varepsilon_d$, i.e. the part of the porosity connected to the exposed crack surface.

The pore diffusivity is related to the diffusivity in water via the form factor ff taking the involved pathway through the pore system into account:

$$ff = \delta/\tau^2 \quad (86)$$

where τ is the tortuosity (the increase in path length relative to the sample thickness) and δ is the constrictivity of the pore system combining effects of connectivity and pore diameters on the movement of the dissolved species.

It should be noted that the form factor itself is correlated with porosity. The general tendency is that ff increases with increasing ε (with $ff \rightarrow 1$ for $\varepsilon \rightarrow 1$). However, the constrictivity in particular is also dependent on pore size distribution so that finely divided pores results in low ff values. This is the case for cementitious materials modified by addition of micro silica.

The solid surfaces of the pores are often negatively charged and this may also influence migration in the narrow channels due to anion exclusion. Such effects are also included in the constrictivity parameter δ.

In addition the movements of the major cat- and anions are linked via the electroneutrality requirement. The different mobilities of the various ions (as expressed by the different Dw values) gives rise to a diffusion potential, which will influence the movement of all electrically charged species. This is discussed in Section 5.2.

When a minor species is in local equilibrium with the solids as specified by the sorption capacity or distribution coefficient K_D so that

$$c_{solid} = K_D \cdot c_{solution} \quad (87)$$

an apparent diffusivity Da can be defined by:

$$Da = De/(\varepsilon + K_D \cdot \rho) \quad (88)$$

The proportionality 'constant' $\alpha = (\varepsilon + K_D \cdot \rho)$ is sometimes called the capacity factor [6] because it is a measure for the combined amount of a species which can be stored in the liquid and solid part of that particular porous material.

The K_D concept cannot be used to describe the complicated relationships between the major dissolved components and the solids in cementitious materials. For minor species such as radioisotopes K_D based chemical retardation can easily be introduced into the programme, but so far only migration of non-interacting minor components have been handled by the code.

5.1. Diffusion of single species

The flux q_i and the concentration change with time during one-dimensional diffusive transport of the dissolved species i across solution layers in the crack and inside the pore structure of the solid materials are described by Fick's first and second law. In differential terms:

$$q_i = Dp_i \cdot \varepsilon \frac{\delta c_i}{\delta x} = De_i \frac{\delta c_i}{\delta x} \tag{89}$$

$$\varepsilon \frac{\delta c_i}{\delta x} = \frac{\delta q_i}{\delta x} = \frac{\delta De_i (\delta c_i / \delta x)}{\delta x} = De \frac{\delta^2 c_i}{\delta x^2} \tag{90}$$

where the simplified expression to the right requires that the effective diffusivity $De_i = Dp_i \cdot \varepsilon$ is independent of the concentration in the pore solution c_i, the time t and the position x.

For simple cases these equations can be solved analytically together with the relevant boundary conditions. For more complicated systems numerical methods must be used.

It is instructive to derive the numerical expressions from Fick's first law applied on a section of a grid structure like the one described above and shown schematically in Fig. 14.

The layers numbered from j-1 to j+1 are characterised geometrically by the layer thickness dx and the porosity ε, and for the particular diffusing species i by the diffusivity De_i and the concentration c_i in the pore solution. Note that the concentration is per volume of pore solution not per volume of the porous material. The concentrations must therefore be multiplied by the porosity ε to account for the volume taken up by solids.

The flux passing through any individual interface of the column is then according to Fick's first law:

$$q_i = Dp_i \cdot \varepsilon \frac{\Delta c_i}{\Delta x} \tag{91}$$

and because the flux entering and leaving any particular interface must be identical it follows that the flux through the interface e.g. between layers j and j+1 can be written:

$$q_{j,j+1} = Dp_j \varepsilon_j \frac{c_j - C_{j,j+1}}{½\Delta x_j} = Dp_{j+1} \varepsilon_{j_{+1}} \frac{C_{j,j+1} - c_{j+1}}{½\Delta x_{j+1}} \tag{92}$$

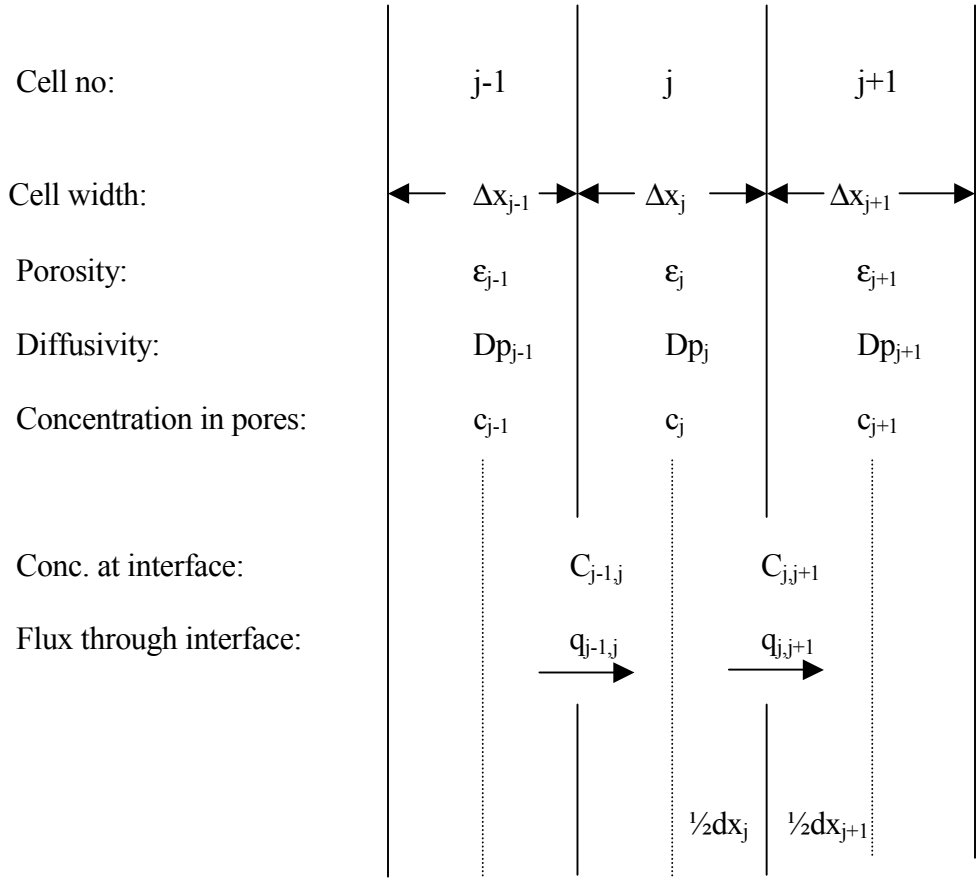

Fig. 14 Grid or layer structure for derivation of the numerical expression for diffusive transport of a single dissolved species i. (For simplicity the indices i are omitted).

Eliminating the unknown concentration $C_{j,j+1}$ at the interface gives:

$$q_{j,j+1} = \frac{2\ Dp_j\ \varepsilon_j \cdot Dp_{j+1}\ \varepsilon_{j+1}}{Dp_j\ \varepsilon_j\ \Delta x_{j+1} + Dp_{j+1}\ \varepsilon_{j+1}\ \Delta x_j}\left(c_j - c_{j+1}\right) = k_{j,j+1}\left(c_j - c_{j+1}\right) \qquad (93)$$

which for constant Dp, ε and Δx values reduces to:

$$q_{j,j+1} = \frac{2\ Dp\ \varepsilon}{\Delta x}\left(c_j - c_{j+1}\right) \qquad (94)$$

In the same manner the flux through the interface between layer j-1 and j is given by:

$$q_{j-1,j} = \frac{2\ Dp_{j-1}\ \varepsilon_{j-1} \cdot Dp_j\ \varepsilon_j}{Dp_{j+1}\ \varepsilon_{j+1}\ \Delta x_j + Dp_j\ \varepsilon_j\ \Delta x_{j-1}}\left(c_{j-1} - c_j\right) = k_{j-1,j}\left(c_{j-1} - c_j\right) \qquad (95)$$

Introducing these fluxes into the mass balance expression for layer j:

$$vol_j \; \Delta c_j \;\; = \;\; (q_{j-1,j} \; - q_{j,j+1}) \; \Delta t \tag{96}$$

where $vol_j = \varepsilon_j \, \Delta x_j$ is the pore volume and $\Delta c_j = c^*_j - c_j$ is the change in concentration of the pore solution over the time step $\Delta t = t^* - t$ gives:

$$c^*_j \;\; = \;\; c_j \; + \; \Delta t \; (q_{j-1,j} \; - q_{j,j+1}) \; / \; (\varepsilon_j \, \Delta x_j) \tag{97}$$

or inserting expressions (82) and (84):

$$c^*_j \;\; = \;\; c_j \; + \; \Delta t \; \frac{k_{j-1,j} \; c_{j-1} - \left(k_{j-1,j} \; c_j + k_{j,j+1} \; c_j\right) + k_{j,j+1} \; c_{j+1}}{\varepsilon_j \; \Delta x_j} \tag{98}$$

If the pore diffusivity and porosity are the same in all the layers this reduces to:

$$c^*_j \;\; = \;\; c_j \; + \; \Delta t \; \frac{2 \; Dp}{\Delta x_j} \left(\frac{c_{j-1} - c_j}{\Delta x_{j-1} + \Delta x_j} + \frac{c_{j+1} - c_j}{\Delta x_{j+1} + \Delta x_j} \right) \tag{99}$$

and when all the Δx values are the same:

$$c^*_j \;\; = \;\; c_j \; + \; \Delta t \; \frac{Dp \;\; \left(c_{j-1} - 2c_j + c_{j+1}\right)}{\Delta x^2} \tag{100}$$

which is the usual expression for the numerical approximation to Fick's second law using equidistant grid steps.

Because the concentration must be positive, i.e. $c^*_j \geq 0$ it is required that

$$c_{j-1} \; + \; c_{j+1} \; + \; c_j \; (\Delta x^2 \, / \, (Dp \; \Delta t) - 2) \;\; > \;\; 0 \tag{101}$$

This is always the case when

$$\Delta t \; < \; \Delta x^2 \, / \, (2 \; Dp) \tag{102}$$

or for grids which are not equidistant:

$$\Delta t \;\; < \;\; \frac{\Delta x_j \left(\Delta x_j + \Delta x_{j-1}\right)\left(\Delta x_j + \Delta x_{j+1}\right)}{2 \; Dp \left(2 \; \Delta x_j + \Delta x_{j-1} + \Delta x_{j+1}\right)} \tag{103}$$

Such limitations of the length of the time step are needed to obtain a stable numerical calculation procedure under all circumstances.

At the mid-plane of the crack it follows from the symmetry of the system that the flux is zero. Inserting $q_{j-1,j} = 0$ and the expression for $q_{j,j+1}$ (92) in the mass-balance equation for the first element (No. j = -9 in the model) gives:

$$c^*_{-9} = c_{-9} + \Delta t\, q_{-9,-8} / (\Delta x_{-9}\, \varepsilon_{-9}) \tag{104}$$

In same manner for the outer grid cell (No. j = 20 in the model) where $q_{j,j+1} = 0$:

$$c^*_{20} = c_{20} + \Delta t\, q_{19,20}/(\Delta x_{20}\, \varepsilon_{20}) \tag{105}$$

These boundary expressions together with the general expression (98) for grid cells Nos. j = -8 to 19 permit calculation of a new set of the 30 concentrations c^*_j after a time step Δt.

5.2. Multicomponent diffusion of ionic species

The majority of the species diffusing inside the pores of a cementitious material are either cat- or anions. Movement of the electrically charged ions results in the creation of an electric field so that the movement of the ions cannot be described independently from each other. The effects will first be considered for the major ions responsible for nearly the total electrical conductivity of the solution, and thereafter for minor ions, such as the radioisotopes.

5.2.1. Interaction of major ions

According to theory for dilute solutions taken from [12] the transport equation for diffusion of the ion i in water must be extended to:

$$q_i = -z_i\, u_i\, F\, c_i \frac{\delta \Phi}{\delta x} - Dw_i \frac{\delta c_i}{\delta x} \tag{106}$$

where z_i is the number of charges on the ion and F is Faradays constant (96487 C/equivalent). It follows that $z_i \cdot F$ is the charge per mol.

Multiplication with the strength of the electric field $\delta\Phi/\delta x$ and with the mobility of the ion u_i (cm^2 mol/J sec) gives the migration velocity which multiplied with the concentration gives the contribution to the flux caused by the electric field.

The current in an electrolyte solution is caused by the sum of the movement of all the ions:

$$i = F \Sigma z_i\, q_i \tag{107}$$

In addition the requirement about electroneutrality of the solution must be fulfilled:

$$\Sigma z_i\, c_i = 0 \tag{108}$$

Inserting (106) in the expression for the current gives:

$$i = -F^2 \frac{\delta\Phi}{\delta x} \Sigma z_i^2 u_i c_i - F \Sigma z_i D_i \frac{\delta c_i}{\delta x} \quad (109)$$

In absence of concentration gradients the last term disappears and the expression can be rewritten:

$$i = -\kappa \frac{\delta\Phi}{\delta x} \quad (110)$$

where

$$\kappa = F^2 \Sigma z_i^2 u_i c_i \quad (111)$$

is the conductivity of the solution.

Equation (106) can then be rearranged into:

$$\frac{\delta\Phi}{\delta x} = -\frac{i}{\kappa} - \frac{F}{\kappa} \sum_i z_i Dw_i \frac{\delta c_i}{\delta x} \quad (112)$$

where the last term is the diffusion potential created by the different diffusivities of the various ions.

For the systems considered here the actual current is zero and therefore the term i/κ disappears.

Incidentally when i=0 it follows that $\Sigma z_i q_i = 0$. This means that the electro neutrality condition will continue to be fulfilled in the diffusing system provided that this was the case initially. Equation (108) may therefore be used as a control on the calculations.

Eliminating $\delta\Phi/\delta x$ by inserting (112) with $i = 0$ into (106) gives:

$$q_i = \frac{z_i u_i F^2 c_i}{\kappa} \sum_i z_i Dw_i \frac{\delta c_i}{\delta x} - Dw_i \frac{\delta c_i}{\delta x} \quad (113)$$

or if the expression (111) for κ is introduced and n represents the other diffusing ions:

$$q_i = K_i \sum_n z_i Dw_n \frac{\delta c_n}{\delta x} - Dw_i \frac{\delta c_i}{\delta x} \quad (114)$$

where

$$K_i = \frac{z_i u_i c_i}{\sum_n z_n u_n c_n} \quad (115)$$

The first term in this expression for the flux of species i is a correction for the interaction between i and the other diffusing ionic species. It is seen that the correction is proportional to the weighed mean of the mobility and the concentration of species i and to the sum of the diffusivities mutiplied by the charge and the concentration gradient.

The mobility u_n of an ion is connected with the ionic equivalent conductance λ_n through the formula:

$$\lambda_n = |z_n| F^2 u_n \tag{116}$$

and the diffusivities for ions in water can also be calculated from the ionic equivalent conductance by use of the Nernst-Einstein relation:

$$D_n = \frac{R T \lambda_n}{|z_n| F^2} = R T u_n \tag{117}$$

For porous materials it will be assumed that diffusivities and mobilities are influenced in the same way by the pore system, so that the effective diffusivity, the pore diffusivity and the mobilities are related by :

$$De_n = D_p \varepsilon = Dw_n ff_n \varepsilon = R T u_n ff_n \varepsilon = R T up_n \varepsilon = R T ue_n \tag{118}$$

The proportionality between D_n and u_n and the corresponding effective values for movement inside the pore system means that the mobilities may be substituted with diffusivities in expression (115) for K_i:

$$K_i = \frac{z_i Dw_i ff_i c_i}{\sum_n z_n^2 Dw_n ff_n c_n} = \frac{z_i Dp_i c_i}{\sum_n z_n^2 Dp_n c_n} \tag{119}$$

where $ff_i = ff_n = 1$ in case of diffusion in water.

In a porous material the f-factors describing influence of constrictivity, connectivity and tortuosity are not necessarily the same for the different species. Data are not readily available but must be obtained from electrical conductivity or diffusivity measurements on the material.

The expression for the flux in a porous material is then

$$q_i = K_i \sum_n z_n Dw_n \varepsilon ff_n \frac{\delta c_n}{\delta x} - Dw_i \varepsilon ff_i \frac{\delta c_i}{\delta x} \tag{120}$$

which reduces to (103) when $\varepsilon = 1$ and $ff_n = ff_i = 1$ in case of unrestricted diffusion in solution.

Inserting $Dp_n = Dw_n ff_n$ and isolating species i from the other ions gives:

$$q_i = \varepsilon \left(\sum_{n \neq i} K_i \, z_n \, Dp_n \frac{\delta c_n}{\delta x} - Dp_i (1 - z_i \, K_i) \frac{\delta c_i}{\delta x} \right) \tag{121}$$

or as an example for a grid cell with three diffusing species, i = 1 and the others numbered 2 and 3:

$$q_1 = \varepsilon \left[K_1 \left(z_2 \, Dp_2 \frac{\Delta c_2}{\Delta x} + z_3 \, Dp_3 \frac{\Delta c_3}{\Delta x} \right) - Dp_1 (1 - z_1 \, K_1) \frac{\Delta c_1}{\Delta x} \right] \tag{122}$$

where

$$K_1 = z_1 \, Dp_1 \, c_1 / (z_1^2 \, Dp_1 \, c_1 + z_2^2 \, Dp_2 \, c_2 + z_3^2 \, Dp_3 \, c_3) \tag{123}$$

which is readily extended to the five diffusing ions considered in the present model.

Values for z, the ionic equivalent conductance and the diffusivity in water are given in Table 1 for the relevant ions. The values are taken from Table 75-1 in [13].

The two last columns gives the Dw and Dp values actually used in most of the example calculation in Section 7. The Dw values are reduced a factor 5 relative to the values at 25°C and infinite dilution. Only a factor 1.04 may be ascribed to the temperature reduction to 20°C while ionic interaction effects could explain part of the rest because the solutions are not infinitely diluted. However, the reduction was mainly introduced to avoid numerical instabilities for the very thin layers in the crack.

The Dp values are further reduced by an arbitrary form factor f = 0.05 supposed to be valid for all the diffusing species and for the pore system in the cementitious material as well as the precipitated calcite. This is obviously a simplification, but more specific data are not readily available.

Table 1. Ionic equivalent conductances and diffusivities at infinite dilution in water at 25°C, together with the Dw and Dp values used in the example calculations in Section 7.

Ion n	Charge z_n	Equivalent conductance λ_n mho cm^2/equiv	Diffusivity in water at infinite dilution Dw_n cm^2/sec	Values used for Dw_n cm^2/sec	Values used for porous material $Dp_n = Dw_n\ ff_n$ cm^2/sec
H^+	+1	349.7	$93.11\ 10^{-6}$		
Na^+	+1	50.1	$13.34\ 10^{-6}$	$2.668\ 10^{-6}$	$0.133\ 10^{-6}$
Ca^{2+}	+2	59.5	$7.92\ 10^{-6}$	$1.584\ 10^{-6}$	$0.079\ 10^{-6}$
OH^-	–1	198	$52.7\ 10^{-6}$	$10.54\ 10^{-6}$	$0.526\ 10^{-6}$
CO_3^{2-}	–2	69.3	$9.23\ 10^{-6}$	$1.864\ 10^{-6}$	$0.092\ 10^{-6}$
HCO_3^-	–1	44.5	$11.85\ 10^{-6}$	$2.370\ 10^{-6}$	$0.119\ 10^{-6}$
H_2CO_3	0	0	$4.8\ 10^{-6}$	$4.8\ 10^{-6}$	$0.24\ 10^{-6}$
Cs^+	+1	77.2	$20.56\ 10^{-6}$	$4.112\ 10^{-6}$	$0.206\ 10^{-6}$
Sr^{2+}	+2	59.4	$7.90\ 10^{-6}$	$1.580\ 10^{-6}$	$0.079\ 10^{-6}$

Data for H^+ is included for comparison although they are not used in the model.

The diffusivity in water for the uncharged H_2CO_3 specie is an estimate. The factor 5 reduction in the actually used value is omitted because ionic interactions are irrelevant.

The table also contains Dw and Dp values for the Cs^+ radioisotopes considered in the next section. Data for Sr^{2+} are included for comparison although no calculation examples are presented in this report.

The expression for the corrected flux may be introduced into mass balance equations for a finite element as it was done in the more simple case in Section 5.1.

Referring to the notation in Fig. 14 the flux passing through the interface between element j and j+1 can be written:

$$q_{i,jj+1} = \varepsilon_j \left[K_{i,j} \sum_{n\neq i} z_n Dp_n \frac{c_{n,j} - C_{n,jj+1}}{\tfrac{1}{2}\Delta x_j} - Dp_i \left(1 - z_i\ K_{i,j}\right) \frac{c_{i,j} - C_{i,jj+1}}{\tfrac{1}{2}\Delta x_j} \right] \tag{124}$$

$$= \varepsilon_{j+1} \left[K_{i,j+1} \sum_{n\neq i} z_n Dp_n \frac{C_{n,jj+1} - c_{n.j+1}}{\tfrac{1}{2}x_{j+1}} - Dp_i \left(1 - z_i\ K_{i,j+1}\right) \frac{C_{i,jj+1} - c_{i,j+1}}{\tfrac{1}{2}x_{j+1}} \right]$$

which together with the corresponding equations for the flux of the other $n\neq i$ ions may be used to eliminate the unknown concentrations $C_{i,jj+1}$ and $C_{n,jj+1}$ at the interfaces between the cells.

(The index jj+1 is dropped in the following and the interfaces concentrations are represented by C_1, C_2, C_3 . . .)

In the example with 3 diffusing ions 3 linear equations are obtained as exemplified by:

$$\frac{\varepsilon_j}{½\Delta x_j}[K_{1,j}\,(z_2\,Dp_2\,(c_{2,j}-C_2)+z_3\,Dp_3(c_{3,j}-C_3))\;\;-Dp_1\,(1-z_1\,K_{1,j})\,(c_{1,j}-C_1)] \qquad (125)$$

$$= \frac{\varepsilon_{j+1}}{½\Delta x_{j+1}}[K_{1,j+1}\,(z_2\,Dp_2\,(C_2-c_{2,j+1})+z_3\,Dp_3(C_3-c_{3,j+1}))\;\;-Dp_1\,(1-z_1\,K_{1,j+1})\,(C_1-c_{1,j+1})]$$

or

$$Dp_1\left(\frac{\varepsilon_j\left(1-z_1K_{1,j}\right)}{½\Delta x_j}c_{1,j}+\frac{\varepsilon_{j+1}\left(1-z_1K_{1,j+1}\right)}{½\Delta x_{j+1}}c_{1,j+1}\;-\left(\frac{\varepsilon_j\left(1-z_1K_{1,j}\right)}{½\Delta x_j}+\frac{\varepsilon_{j+1}\left(1-z_1K_{1,j+1}\right)}{½\Delta x_{j+1}}\right)C_1\right) \qquad (126)$$

$$-z_2\;Dp_2\left(\frac{\varepsilon_jK_{1,j}}{½x_j}c_{2,j}+\frac{\varepsilon_{j+1}K_{1,j+1}}{½x_{j+1}}c_{2,j+1}\;-\left(\frac{\varepsilon_jK_{1,j}}{½x_j}+\frac{\varepsilon_{j+1}K_{1,j+1}}{½x_{j+1}}\right)C_2\right)$$

$$-z_3\;Dp_3\left(\frac{\varepsilon_jK_{1,j}}{½x_j}c_{3,j}+\frac{\varepsilon_{j+1}K_{1,j+1}}{½x_{j+1}}c_{3,j+1}\;-\left(\frac{\varepsilon_jK_{1,j}}{½x_j}+\frac{\varepsilon_{j+1}K_{1,j+1}}{½x_{j+1}}\right)C_3\right)$$

or if $M_{1,j} = 2\,\varepsilon_j\,K_{1,j}/\Delta x_j$ and $M_{1,j+1} = 2\,\varepsilon_{j+1}\,K_{1,j+1}/\Delta x_{j+1}$

and $L_{1,j} = 2\,\varepsilon_j\,(1-z_1K_{1,j})/\Delta x_j$ and $L_{1,j+1} = 2\,\varepsilon_{j+1}\,(1-z_1K_{1,j+1})/\Delta x_{j+1}$

$$\begin{aligned} &Dp_1\,(L_{1,j}\,c_{1,j}+L_{1,j+1}\,c_{1,j+1}\;-(L_{1,j}+L_{1,j+1})\,C_1)\\ &-\;z_2\,Dp_2\,(M_{1,j}\,c_{2,j}+M_{1,j+1}\,c_{2,j+1}\;-(M_{1,j}+M_{1,j+1})\,C_2)\\ &-\;z_3\,Dp_3\,(M_{1,j}\,c_{3,j}+M_{1,j+1}\,c_{3,j+1}\;-(M_{1,j}+M_{1,j+1})\,C_3)\;=\;0 \end{aligned} \qquad (127)$$

or $$a_1\,C_1\;+\;b_1\,C_2\;+\;c_1\,C_3\;=\;k_1 \qquad (128)$$

where the definition of the constants a_1, b_1, c_1 and k_1 are given by comparison with the equation above.

The corresponding expressions for 5 ions are:

$$
\begin{aligned}
a_1 C_1 + b_1 C_2 + c_1 C_3 + d_1 C_4 + e_1 C_5 &= k_1 \\
a_2 C_1 + b_2 C_2 + c_2 C_3 + d_2 C_4 + e_2 C_5 &= k_2 \\
a_3 C_1 + b_3 C_2 + c_3 C_3 + d_3 C_4 + e_3 C_5 &= k_3 \\
a_4 C_1 + b_4 C_2 + c_4 C_3 + d_4 C_4 + e_4 C_5 &= k_4 \\
a_5 C_1 + b_5 C_2 + c_5 C_3 + d_5 C_4 + e_5 C_5 &= k_5
\end{aligned}
\qquad (129)
$$

where the constants are obtained by comparison with extended versions of (127):

$$
\begin{aligned}
a_1 &= - Dp_1 (L_{1,j} + L_{1,j+1}) \\
b_1 &= z_2 Dp_2 (M_{1,j} + M_{1,j+1}) \\
c_1 &= z_3 Dp_3 (M_{1,j} + M_{1,j+1}) \\
d_1 &= z_4 Dp_4 (M_{1,j} + M_{1,j+1}) \\
e_1 &= z_5 Dp_5 (M_{1,j} + M_{1,j+1})
\end{aligned}
\qquad (130)
$$

$$
\begin{aligned}
k_1 = &- Dp_1 (L_{1,j}\, c_{1,j} + L_{1,j+1}\, c_{1,j+1}) \\
&+ z_2 Dp_2 (M_{1,j}\, c_{2,j} + M_{1,j+1}\, c_{2,j+1}) \\
&+ z_3 Dp_3 (M_{1,j}\, c_{3,j} + M_{1,j+1}\, c_{3,j+1}) \\
&+ z_4 Dp_4 (M_{1,j}\, c_{4,j} + M_{1,j+1}\, c_{4,j+1}) \\
&+ z_5 Dp_5 (M_{1,j}\, c_{5,j} + M_{1,j+1}\, c_{5,j+1})
\end{aligned}
$$

and

$$
\begin{aligned}
a_2 &= z_1 Dp_1 (M_{2,j} + M_{2,j+1}) \\
b_2 &= - Dp_2 (L_{2,j} + L_{2,j+1}) \\
c_2 &= z_3 Dp_3 (M_{2,j} + M_{2,j+1}) \\
d_2 &= z_4 Dp_4 (M_{2,j} + M_{2,j+1}) \\
e_2 &= z_5 Dp_5 (M_{2,j} + M_{2,j+1})
\end{aligned}
\qquad (131)
$$

$$
\begin{aligned}
k_2 = &\; z_1 Dp_1 (M_{2,j}\, c_{1,j} + M_{2,j+1}\, c_{1,j+1}) \\
&- Dp_2 (L_{2,j}\, c_{2,j} + L_{2,j+1}\, c_{2,j+1}) \\
&+ z_3 Dp_3 (M_{2,j}\, c_{3,j} + M_{2,j+1}\, c_{3,j+1}) \\
&+ z_4 Dp_4 (M_{2,j}\, c_{4,j} + M_{2,j+1}\, c_{4,j+1}) \\
&+ z_5 Dp_5 (M_{2,j}\, c_{5,j} + M_{2,j+1}\, c_{5,j+1})
\end{aligned}
$$

and similarly for the other 3 sets of constants.

The unknown concentrations C_i must lay in the intervals $c_{i,j}$ to $c_{i,j+1}$ and when the set of linear equations are solved they are ordered accordingly so that C_1 corresponds to the highest value of $c_{i,j} + c_{i,j+1}$, C_2 to the next highest, etc. The equations can then be solved using the standard Gausian elimination principle.

When the concentrations at the interfaces are known the corresponding flux's from cell j to j+1 is obtained from (124):

$$q_{i,jj+1} = \varepsilon_j \left[K_{i,j} \sum_{n \neq i} z_n \, Dp_n \frac{c_{n,j} - C_{n,jj+1}}{½x_j} - Dp_i \left(1 - z_i \, K_{i,j}\right) \frac{c_{i,j} - C_{i,jj+1}}{½x_j} \right] \tag{132}$$

which for 5 diffusing species is written

$$\begin{aligned} q_{1,jj+1} &= - L_{1,j} \, Dp_1 \, (c_{1,j}-C_1) \\ &\quad + M_{1,j}(z_2 \, Dp_2 \, (c_{2,j}-C_2)+z_3 \, Dp_3(c_{3,j}-C_3)+z_4 \, Dp_4 \, (c_{4,j}-C_4)+z_5 \, Dp_5(c_{5,j}-C_5) \\ q_{2,jj+1} &= - L_{2,j} \, Dp_2 \, (c_{2,j}-C_2) \\ &\quad + M_{2,j}(z_1 \, Dp_1 \, (c_{1,j}-C_1)+z_3 \, Dp_3(c_{3,j}-C_3)+z_4 \, Dp_4 \, (c_{4,j}-C_4)+z_5 \, Dp_5(c_{5,j}-C_5) \end{aligned} \tag{133}$$

and similarly for the three others.

The diffusion caused change in the concentrations over the time step Δt are then given by five mass-balance equations (19) of the form:

$$\begin{aligned} c^*_{1,j} &= c_{1,j} + \Delta t \, (q_{1,j-1j} - q_{1,jj+1})/(\varepsilon_j \, \Delta x_j) \\ c^*_{2,j} &= c_{2,j} + \Delta t \, (q_{2,j-1j} - q_{2,jj+1})/(\varepsilon_j \, \Delta x_j) \qquad \text{etc.} \end{aligned} \tag{134}$$

Here it is utilized that the flux's $q_{i,j-1j}$ entering cell j from cell j-1 is known from the previous calculation of the flux leaving cell j-1. The boundary conditions at the mid-plane of the crack and on the outside of the concrete are given by equations (104) and (105) in Section 5.1.

5.2.2. Effects on minor ionic components.

Radioisotopes in the pore solution will often be present in form of ionic species at such low concentrations what they do not contribute significantly to the electrical conductivity of the solution. However, as ions they are still influenced by the diffusion potential created by the migration of the major ionic species. For an ionic radioisotope equation (106) can be written:

$$q_r = - z_r \, u_r \, F \, c_r \frac{\delta \Phi}{\delta x} \frac{\delta c_r}{\delta x} - Dw_r \tag{135}$$

while equations (107) to (112) are unchanged with index n representing the major species.

Eliminating $\delta\Phi/\delta x$ by inserting (112) with current i = 0 into (135) gives:

$$q_r = \frac{z_r \, u_r \, F^2 \, c_r}{\kappa} \sum_n z_n Dw_n \frac{\delta c_n}{\delta x} - Dw_r \frac{\delta c_r}{\delta x} \tag{136}$$

or if the expression (111) for κ is introduced:

$$q_r = K_r \sum_n z_n Dw_n \frac{\delta c_n}{\delta x} - Dw_r \frac{\delta c_r}{\delta x} \quad (137)$$

where

$$K_r = \frac{z_r u_r c_r}{\sum_n z_n^2 u_n c_n} \quad (138)$$

The first term in this expression for the flux of species r is a correction for the interaction between the isotope r and the other diffusing ionic species. As for major species the correction is proportional to the weighed mean of the mobility and the concentration of the minor species r and to the sum of the diffusivities for all the major species multiplied by the charge and the concentration gradient.

Assuming as previously that diffusivities and mobilities for the ions are influenced in the same way by the pore system, equation (138) can be written in analogy with (119):

$$K_r = \frac{z_r Dw_r ff_r c_r}{\sum_n z_n^2 Dw_n ff_n c_n} = \frac{z_r Dp_r c_r}{\sum_n z_n^2 Dp_n c_n} \quad (139)$$

where $ff_i = ff_n = 1$ in case of diffusion in water.

As remarked above for the major ions the ff-values describing influence of constrictivity, connectivity and tortuosity are not necessarily the same for different species. Data are not readily available but must be obtained from diffusivity measurements on the material.

The expression for the flux of a small amount of ionic radioisotope in a porous material is then:

$$q_r = K_r \sum_n z_n Dw_n \varepsilon ff_n \frac{\delta c_n}{\delta x} - Dw_r \varepsilon ff_r \frac{\delta c_r}{\delta x} \quad (140)$$

which reduces to (137) when $\varepsilon = 1$ and $ff_n = ff_r = 1$ in case of unrestricted diffusion in solution.

Inserting $Dp_n = Dw_n ff_n$ and $Dp_r = Dw_r ff_r$ gives the following analogue to equation (121):

$$q_r = \varepsilon \left(K_r \sum_n z_n Dp_n \frac{\delta c_n}{\delta x} - Dp_r \frac{\delta c_r}{dx} \right) \quad (141)$$

or as an example for a grid cell with three diffusing major species in addition to the isotope:

$$q_r = \varepsilon \left[K_r \left(z_1 Dp_1 \frac{\Delta c_1}{\Delta x} + z_2 Dp_2 \frac{\Delta c_2}{\Delta x} + z_3 Dp_3 \frac{\Delta c_3}{\Delta x} \right) - Dp_r \frac{\Delta c_r}{\Delta x} \right] \quad (142)$$

where

$$K_r = \frac{z_r\, Dp_r\, c_r}{z_1^2\, Dp_1\, c_1 + z_2^2\, Dp_2\, c_2 + z_3^2\, Dp_3\, c_3} \quad (143)$$

which is readily extended to other numbers of diffusing major ions.

The radioisotope (or other minor ionic components) have no significant influence on the behaviour of the major ions, and the correction on the flux of the radioisotope due to diffusion of the major ions can therefore be calculated independently when the transport behaviour of the major ions have been resolved according to the equations in Section 5.2.1.

Equation (141) for q_r may also be written:

$$q_r = Dp_r\, \varepsilon\, \frac{z_r c_r Cor - \Delta c_r}{\Delta x} \quad (144)$$

where

$$Cor = \frac{\Sigma\, z_n\, Dp_n\, \Delta c_n}{\Sigma\, z_n^2\, Dp_n\, \Delta c_n} \quad (145)$$

or for the example with three major ions

$$Cor = \frac{z_1\, Dp_1 \Delta c_1 + z_2\, Dp_2 \Delta c_2 + z_3\, Dp_3 \Delta c_3}{z_1^2\, Dp_1 \Delta c_1 + z_2^2\, Dp_2 \Delta c_2 + z_3^2\, Dp_3 \Delta c_3} \quad (146)$$

It follows that $z_r \cdot c_r \cdot Cor$ is a correction to the concentration gradient for species r caused by the migrating major ions. Cor can be positive or negative depending on the dominating ion, in cement often OH^-. A high out-flux of this anion will tend to increase the out-flux also of minor cations i.e. most of the radioisotope species.

Values for z, the ionic equivalent conductance λ and the diffusivity in water are included in Table 1 for Cs^+ and Sr^{2+} as examples of relevant radioisotopes.

Equating the expressions for the corrected flux of a minor species leaving and entering the interface between layers j and j+1 and eliminating the unknown concentration $C_{r,j,j+1}$ gives in analogy to the derivation of equation (125):

$$q_{r,jj+1} = \varepsilon_j\, Dp_{r,j}\, \frac{z_r c_{r,j} Cor_j - (C_{r,jj+1} - c_{r,j})}{½\Delta x_j} = \varepsilon_{j+1}\, Dp_{r,j+1}\, \frac{z_r c_{r,j+1} Cor_{j+1} - (c_{r,j+1} - C_{r,jj+1})}{½\Delta x_{j+1}} \quad (147)$$

or

$$q_{r,j,j+1} = k_{j,j+1}\, (\, z_r\, (c_{r,j}\, Cor_j + c_{r,j+1}\, Cor_{j+1}) + (c_{r,j} - c_{r,j+1})\,) \quad (148)$$

where

$$k_{j,j+1} = \frac{2\, Dp_j \varepsilon_j \cdot Dp_{j+1} \varepsilon_{j+1}}{Dp_j \varepsilon_j \Delta x_{j+1} + Dp_{j+1} \varepsilon_{j+1} \Delta x_j}$$

and Cor_j is obtained from equation (146) with $\Delta c_n = C_{n,j,j+1} - c_{n,j}$

and Cor_{j+1} similarly for $\Delta c_n = c_{n,j+1} - C_{n,j,j+1}$

The necessary information is readily obtained in connection with the solution of the set of linear equations in Section 5.2.1.

In the same manner the flux through the interface between layer j-1 and j is given by:

$$q_{r,j-1,j} = k_{j-1,j} \left(z_r \left(c_{r,j-1}\, Cor_{j-1} + c_{r,j}\, Cor_j\right) + \left(c_{r,j-1} - c_{r,j}\right) \right)$$

where (149)

$$k_{j-1,j} = \frac{2\, Dp_{j-1}\varepsilon_{j-1} \cdot Dp_j\varepsilon_j}{Dp_{j-1}\varepsilon_{j-1}\Delta x_j + Dp_j\varepsilon_j\Delta x_{j-1}}$$

and Cor_{j-1} is obtained from eqation (146) with $\Delta c_n = c_{n,j-1} - C_{n,j-1,j}$

and Cor_j similarly for $\Delta c_n = C_{n,j-1,j} - c_{n,j}$

The Cor_j value is therefore not the same in the two sets of equations.

When the corrected in- and out-fluxes are available, a mass-balance consideration as for equation (97) gives the new concentration of r in grid layer j:

$$c^*_{r,j} = c_{r,j} + \Delta t \frac{q_{r,j-1,j} - q_{r,j,j+1}}{\varepsilon_j\, \Delta x_j} \qquad (150)$$

which inserting equations (148) and (149) and assuming pore diffusivities, porosities and thicknesses to be the same in each layer reduces to:

$$c^*_{r,j} = c_{r,j} + \Delta t \frac{Dp\left(z_r\left(c_{r,j-1}Cor_{j-1} - c_{r,j+1}Cor_{j+1}\right) + c_{r,j-1} - 2\, c_{r,j} + c_{r,j+1}\right)}{\Delta x^2} \qquad (151)$$

In the model equations (148) and (149) are used in combination with (150) to calculate the corrected new concentrations.

6. Program structure and input requirements

The structure of the CRACK2 calculation program is shown schematically in Fig. 15 used as basis for the following discussion.

(Values in parentheses refer to a page in the report where the topic is described or where to find parameter values used in the example calculations in Section 7).

6.1. Input

The program uses a series of fundamental chemical and physical constants such as:

- Equilibrium constants for the carbonate system (p. 20)
- Solubility constants for $CaCO_3$ and $Ca(OH)_2$ (p. 19)
- Densities for the two solid minerals (p. 26)
- Diffusivites in water for the 6 dissolved major species:
  Ca^{2+}, Na^{+}, OH^{-}, CO_3^{2-}, HCO_3^{-} and H_2CO_3 (p. 44)
  and for radioisotopes such as R1, R2 = $^{137}Cs^{+}$.

The values must be given as input. They are functions of temperature, but this is presently disregarded. Readily available values valid for 20-25^{o}C are used in the example calculations.

The system must then be defined, comprising:

- Dimensions of the cracked cement block (p. 15, 83)
- Width of the crack (p. 15, 83)
- Initial porosity of the cementitious material (p. 18, 57, 90)
- Type and composition of the cementitious material (p. 57,90)
- Concentration of radioisotopes R1, R2 if present in the cement mortar (p. 57)

- Subdivision of the systems into n columns and for each column
  into 30 grid layers with specified thickness' (p.18)
- Assumptions about oversaturation, nucleation and porosity development
  in the solution filled cement mortar and calcite layers (p. 29, 33, 34)
- Estimate of the form factors decreasing the pore diffusivity
  relative to the free diffusivity in water. (p. 36, 44, 90)
  (The form factor can be specified differently for individual chemical species but are in the present version of the model considered constant and independent of material (calcite or cement mortar) and of the porosity changes.)

The number of columns, the grid layer thickness, the diffusivities and the time steps used in the calculations must be selected so that numerically stable solutions of the diffusion equations are obtained.

A subprogram calculates the initial equilibrium composition of the pore water in the cementitious material and of the solution present initially inside the crack (where the concentrations are assumed to be a fraction of the initial pore solution composition).

For the inflowing feed solution the following must be specified:

- Flow rate (p. 16)
- Concentrations of Ca^{2+}, Na^{+}, OH^{-}, CO_3^{2-}, HCO_3^{-}, and H_2CO_3. (p. 27)
- Concentration of radioisotopes R1, R2 if present in the feed solution

The solution must be in cat- anion equilibrium, but need not be in equilibrium with calcite although this is the case for the solution used in most of the test calculation. Presently the amount and composition of the inflowing solution is kept constant during a calculation but it is fairly simple to introduce variable compositions or flow.

6.2. Calculations

The development of the system with time is then calculated using a three-step procedure made necessary by the thin grid sections and the steep concentration gradients over the precipitated calcite layer:

The FlowSolution subprogram operates on very short time steps (e.g. dtc=0.01 to 0.04 sec). The solution entering the crack part of the column is the feed solution in case of the first column (i=1) or the out-flowing solution from the crack part in the previous column ($1< i < n$).

Diffusion from adjacent solution layers are calculated, starting at the mid-plane (j = -9) and proceeding towards the crack surface (j = LayNo). Correction for diffusion potential is carried out for each layer followed by calculation of change in composition caused by mixing with the incoming solution and the contributions from diffusive transport from the neighbouring layers.

Out- or indiffusion of radioisotopes is calculated with correction for the diffusion potential created by the migrating major species.

Oversaturation relative to calcite is permitted for the central part of the crack, while precipitation is supposed to occur instantaneously in the layer in contact with the cementitious material (j=0) or with an already precipitated calcite layer. The excess Ca^{2+} or CO_3^{2-} ions are removed as $CaCO_3$ which is added to the amount already present in the layer resulting in an increase in thickness of the deposited layer as calculated from the calcite mineral density and an assumed initial porosity of the precipitate ($\varepsilon_{pecip} = 0.50$). When a layer (e.g. j = 0) is filled completely precipitation is initiate in the adjacent layer (j = -1 which then is designated LayNo). The filled layer does not any longer participate in the advective flow of solution through the crack and the program distributes the flow over the diminished cross-section of the partly filled crack.

(p. 29,30)

However, some additional precipitation of $CaCO_3$ inside such a filled layer may still occur due to reaction between Ca^{2+} and $CO_3^{2-} + HCO_3^{-}$ diffusing in from the crack solution and $Ca^{2+} + OH^{-}$ diffusing out from the cementitious material. This additional precipitation decreases the porosity of

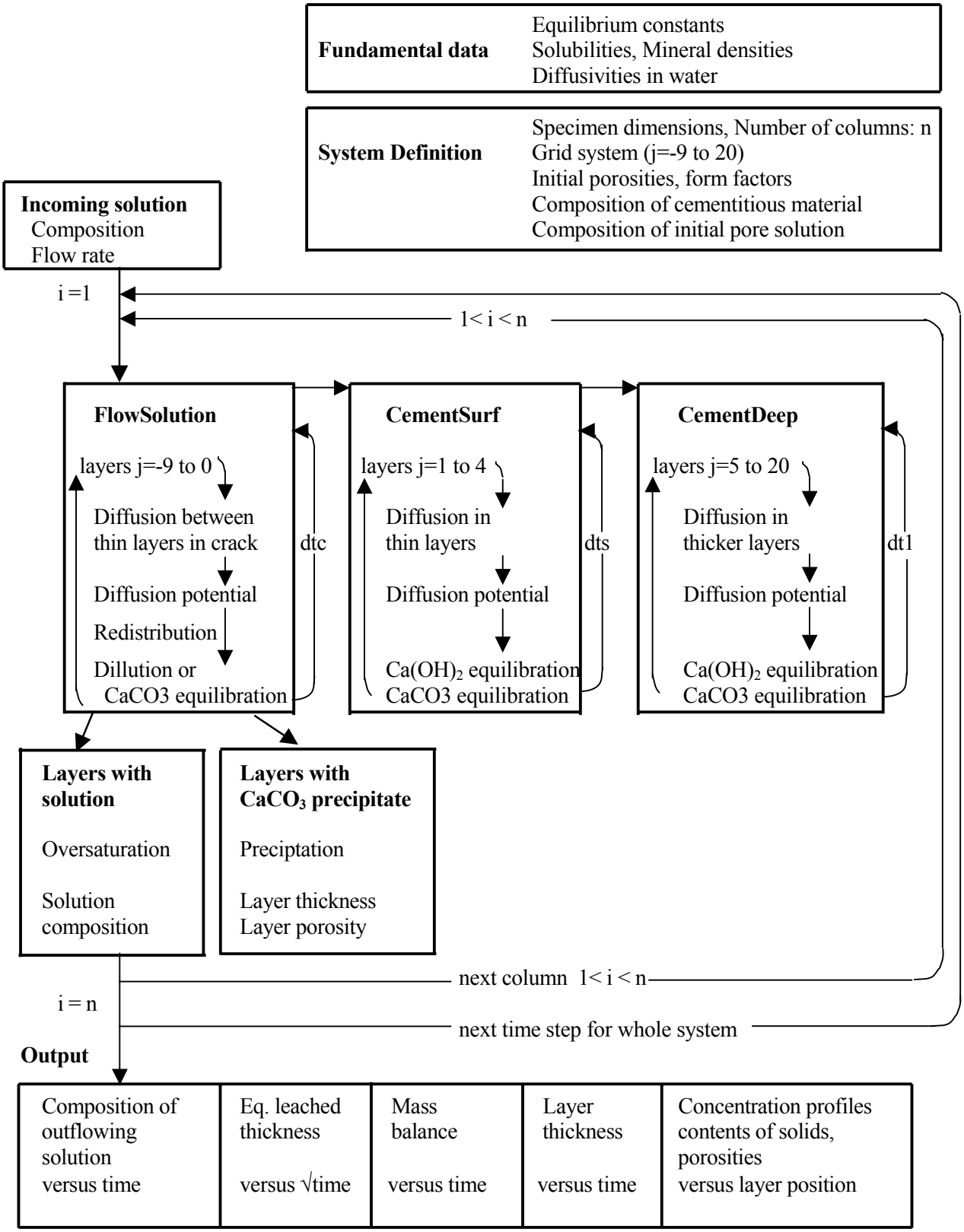

Fig. 15. Calculation structure for the Crack2 program.

the calcite layer and makes it eventually more or less impermeable corresponding to a certain minimum porosity (e.g. $\varepsilon_{min} = 0.001$) specified in the program. (p. 34)

The dtc time steps are repeated dts/dtc times under accumulation of the amount of material moved by the advective flow through the crack (used later as incoming material to the next column) and the diffusive flux through the j=0/j=1 interface (representing the flux into the cementitious material). The many repetitions of these calculations are mainly responsible for the long calculation times of the program, and some attempt to reduce this load should be made. The use of fewer and coarser grid layers in the middle of the crack is one possibility.

The diffusion in the four layers (j = 1 to 4) of the cementitious material nearest the original crack surface is calculated using a somewhat longer time step (e.g. dts = 12 sec). This is possible because the layers are thicker and the diffusivities lower than in the solution filled layers in the crack.

Calculations of diffusive fluxes from concentration gradients are again followed by correction for diffusion potential. The resulting solution is equilibrated with solid $Ca(OH)_2$ representing the cement paste. The calcium concentration is strongly influenced by OH^- from NaOH present in the pore solution. Eventually one or more of the outer layers may be depleted for solid $Ca(OH)_2$ leaving an inert material with increased porosity corresponding to the amount of dissolved $Ca(OH)_2$. $CaCO_3$ is precipitated if the solubility limits are exceeded.

The dts time steps are repeated dt1/dts times under accumulation of the diffusive flux through the j=4/j=5 interface which is then used as the flux into the deeper layers of the cementitious material. Calculation of the diffusion in these layers can be carried out using relatively long time steps (e.g. dt1 = 60 sec) due to the thicker layers. Otherwise the procedure is similar to the one used for the outer layers. The deeper layers are mainly serving as reservoir for the out-diffusion of sodium hydroxide.

At the end of each time step dt1 the accumulative amount of dissolved materials present in the outflowing solution from column i is used as feed solution for column i+1, and the procedure is repeated starting with the FlowSolution subprogram for this column.

When all the columns have been calculated the sequence of calculations are repeated for a new time step dt1 and this is repeated until the selected maximum calculation time has been reached.

6.3. Output and comparison with experiments

The calculations results are stored for up to 60 equidistantly spaced periods, and from these files results may be presented in different manners such as:

- The composition of the outflowing solution (as a mean over the flow in all the crack grid layers not blocked by precipitate).
- The equivalent leached thickness, i.e. the accumulative amount removed with outflowing solution per cm^2 internal crack area/divided by the original concentration of the component in the cementitious material. This is of special interest for sodium and for radioisotopes present in the cement mortar, because the leaching diffusivity D_{leach} obtained from the slope of the equivalent leached thickness L versus the square root of time according to:

$$L = 2\sqrt{\frac{D_{leach} \cdot t}{\pi}} \qquad (152)$$

can be compared directly with experimentally determined diffusivities. This is one manner to test whether reasonable values have been used for the form factor ff. Modifications of ff may then be used to calibrate the model. Some experimental values for D_{leach} are given in Table 2.

- Mass balances development based on the difference between the contents in incoming solution and the accumulative amounts of Na, Ca, carbonate species or radioisotopes removed with the out-flowing solution can also be compared with measurements on experimental systems.

Table 2. Recipes (g/100 g cement) and experimental D_{leach} values (10^{-7} cm^2/s) for Na, K and Cs for various types of cementitious materials.

		Cement mortar [5]				Cementitious backfills [7]		
		a	b	d	e	Gran	SFR	NRVB
cement		100	100	100	100	100	100	100
sand		200	140	140	120[1)]	-	540	148[2)]
water		45	38	28	28	70	134	136
porosity			~20%			50%	~25%	50%
D_{leach} 10^{-7} cm^2/s	Na	2.6	1.2	0.75	0.15			
	K	1.9	0.9	0.20	0.02	11	8.2	9.4
	Cs	0.5	0.2	0.03	0.001			

1) including 20 g micro silica. 2) finely ground chalk and calcium hydroxide

The following features illustrates the behaviour of the system and may explain experimental observation but are less accessible to comparison with experimental measurements:

- The thickness of the precipitated layers on the various columns as function of time supplemented with information about the porosity of the layers.
- Cross-sections at a selected time of the layers of precipitate and leached cement mortar for all columns with signatures for porosity and contents of $CaCO_3$ and $Ca(OH)_2$
- Concentration profiles over the layers in the individual columns at selected times during the calculation period. Another option is to specify a single time, e.g. the end of the calculation, and ask for a plot of the concentration profiles for all or a selected number of the individual columns.
- Similar plots can be made for the porosity, and for the contents of precipitated $CaCO_3$ or remaining $Ca(OH)_2$ in the various columns at selected times.
- Concentration profiles in the various layers inside the crack and in the cement mortar. The degree of solution saturation with $CaCO_3$ can also be plotted.

The information stored at the selected time intervals can be obtained as tables of concentrations, etc. The fluxes at the interface between the cementitious material and the layer of precipitate are also available as tables.

7. Example calculations

The example calculations presented in the following are based on data as given elsewhere in the report, see Section 6. Results for a main case and some variants are presented illustrating effects of parameter variations.

The main system simulates a 0.2 mm wide and 9 cm long crack in a cement mortar designated type b and used in experimental work at Risø, see Section 2. The mortar is prepared from 100 g SRPC (Danish sulphate resistant Portland cement) with 140 g sand and 38 g water. It is similar to a good construction concrete except that coarse aggregates are omitted. The water cement ratio is 0.38 and the density 2.32 g/cm^3. The material contains 0.21 g $Ca(OH)_2$/cm^3 (disregarding C-S-H, etc.) and 0.0017 g Na/cm^3 assumed to be dissolved in the pore solution as NaOH. The content of potassium is converted to the equivalent amount of sodium and included in the 0.0017 g/cm^3. The initial porosity of the mortar is assumed to be 20 vol%.

The minor components R1 and R2 both represent a Cs radioisotope assumed to be dissolved in the pore solution in the mortar, but R1 and R2 are handled somewhat differently as explained below. An arbitrary activity concentration of 10000 Bq/cm^3 is assumed for this mortar. Decay is not considered but would be simple to introduce.

The incoming solution is a synthetic calcium bicarbonate solution with composition as specified in Section 3.4. The flow rate is 4.3 ml/h corresponding to 0.17 mm/s as the initial water velocity in the crack and a residence time of 53 seconds.

The length of the crack is subdivided into 5 columns and each column is again divided into 30 grid sections of which 10 are in the crack and 20 in the cementitious material as described in Section 3.

The employed diffusivities in water Dw are given in Table 1 (Section 5.2.1.) together with the pore water diffusivities Dp obtained by multiplication of Dw with a form factor ff = 0.05 assumed to be valid for all the diffusing species and for the cementitious material as well as the layer of precipitated calcium carbonate. The form factor ff is also considered independent of changing porosity. For ionic species the Dw values have been reduced a factor 5 compared with the diffusivities at infinite dilution.

The modelled time is 14 days and the calculations typically took about 50 to 150 hours (2 to 6 minutes/hour model time and column) on a high speed PC. Most of this was spent on calculating diffusion in the thin layers in the crack.

Results from a series of calculations for this system and variants of the system are presented in the following. An overview of variations in the employed parameters is presented in Fig. 16.

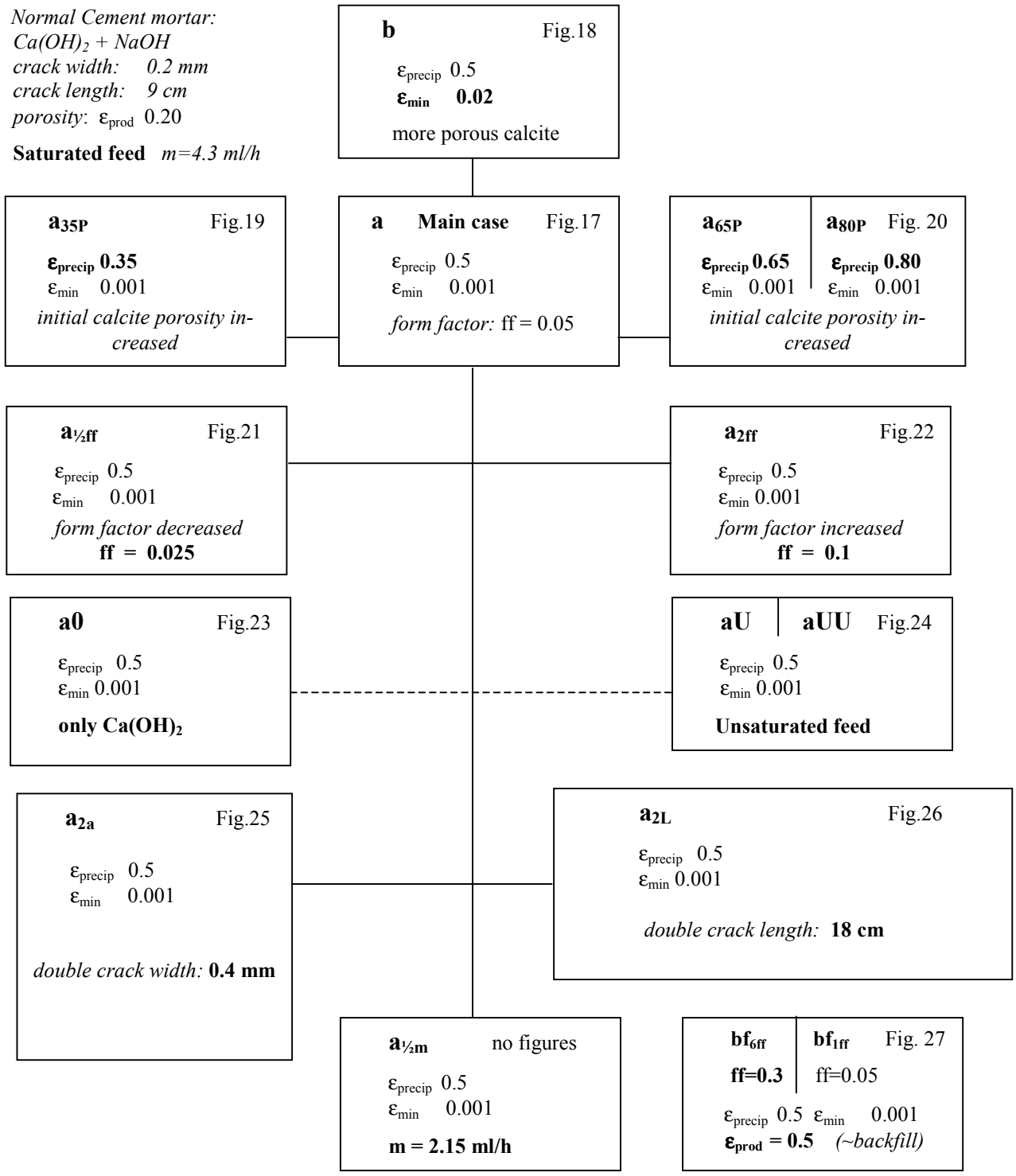

Fig. 16. Schematic presentation of parameters used in the example calculations. The variants comprise different assumptions about porosity of the mortar and the calcite layer, ff values and pore diffusivities in the mortar and calcite, mortar containing only calcium hydroxide or with unsaturated calcium bicarbonate used as feed solution. Two examples of other crack geometries are compared with effects of reduced solution flow rate. Calculations on porous backfill material are also included.

Input data for the main case **a** are given in Table 3. The minimum porosity ε_{min} of the calcite layer is assumed to be 0.1 %. Case **b** is similar, except that ε_{min} is increased to 2 %. Effects of variation of the assumed value for porosity of the initially precipitated calcite layer ε_{precip} are illustrated by cases $\mathbf{a_{35P}}$, $\mathbf{a_{65P}}$ and $\mathbf{a_{80P}}$.

The influence of changes in pore diffusivities Dp = ff · Dw are illustrated by the cases $\mathbf{a_{½ff}}$ and $\mathbf{a_{2ff}}$.

In individual calculations ff is considered constant.

Table 3. Input data for the main example calculation **a** (and **aU**) as listed by the model.

Model calculation of CaCO3 crackfilling in concrete – Crack2a.pas
Testcase 1, type b mortar = Ca(OH)2 with NaOH

a = 0.0200 b = 3.50 length = 9.00 cm
Number of columns 5
ConcCaOH2= 0.210 ConcNa= 0.0017 g/cm^3 (case a0: ConcNa= 0)
ConcR1= 10000 Bq/cm3
ConcR2= 10000 Bq/cm3
epsilon= 0.20 epsilonPrecip= 0.50 epsilonMin= 0.0010 (case b: epsilonMin = 0.002)

kCO2= –1.403 k1= –6.383 k2= –10.378 kw= –14.000 kCaCO3= –8.452 kCa(OH)2= –5.222

	Ca	Na	OH	CO3	HCO3	H2CO	R1	R2	
Dw =	1.5840	2.6680	10.5200	1.8460	2.3700	4.8000	4.1120	4.1120	e-6 cm2/sec
ff =	0.0500	0.0500	0.0500	0.0500	0.0500	0.0500	0.0500	0.0500	
Dp =	0.0792	0.1334	0.5260	0.0923	0.1185	0.2400	0.2056	0.2056	e-6 cm2/sec

dt1 = 60 should be < 380 sec dts = 3.0 < 95 sec dtc = 0.04 < 0.048 sec (values down to 0.01 were also used)
Number of tables = 56 dt-steps/table = 360 Tmax = 336 hours

m = 4.30 ml/h Mean flow rate = 0.017 cm/sec
Laminar flow: 14.94 14.64 14.04 13.15 11.95 10.45 8.65 6.55 4.16 1.46 % relative in layer –9 to 0
Total ideal pressure loss at start: 0.0048 cm H2O
Ingoing solution, Ca: 2.000 CO3: 0.0035 HCO3: 3.993 H2CO3: 0.550 mMol/L pCO2= 0.0139 at pH= 7.21
Is: 0.00600 g1: 0.919 g2: 0.713 CaCO3oversat: 1.000

Calculation from 25-6-2002

Case aU as above, but with
Ingoing solution, Ca: 2.000 CO3: 0.0014 HCO3: 3.997 H2CO3: 1.408 mMol/L pCO2= 0.0356 at pH= 6.80
Is: 0.00600 g1: 0.919 g2: 0.713 CaCO3oversat: 0.392 i.e. undersaturated feed solution

Calculation from 6-11-2002

The specimen consists of the type b mortar (simplified to $Ca(OH)_2$ + NaOH) except for Case **aO** where the NaOH content has been left out, and Case **bf** with an especially porous material.

The incoming solution is mostly assumed to be in equilibrium with calcite. A slightly aggressive feed solution is used in Case **aU** with composition as indicated in the bottom part of Table 3. Effects of a nearly pure CO_2 solution have also been considered, Case **aUU**.

Effects of increased crack width or crack length are illustrated by cases $\mathbf{a_{2a}}$ and $\mathbf{a_{2L}}$ (i.e. with double crack width or crack length).

For the Main Case **a** the output table at the end of the calculation period for column 5 (the column at the outlet) is shown in Table 4. For the various grid layers the table lists:

- position of the midplane of the layer (or surface of calcite layer where precipitate is present),
- layer porosities, with $\varepsilon_{min} = 0.001$ reached in layer 0 nearest the original surface,
- remaining $Ca(OH)_2$, with layer 1 nearly but not completely depleted,
- precipitated $CaCO_3$, in layers 0, –1 and –2 in the crack and very little in the leached mortar,
- concentration profiles for Ca, Na, OH, CO_3, HCO_3, H_2CO_3,
- a difference between the sums of an- and cations better than 10^{-7} equivalents/litter,
- degree of calcite saturation of the solution ($cCa \cdot cCO3 \cdot g_2^2 / L_{CaCO3} = 1$ in calcite-containing layers, >1 in the open crack and <1 in the pore solution in mortar without $CaCO_3$),

The two last columns show the concentration of the radioisotopes R1 and R2 (cesium without retention on the solids) when electrical interactions with migrating major ions are taken into account (R1) and where this is disregarded (R2).

The bottom part of the table contains some overall mass-balance results for the run:

2.890 – 1.916 + 2.679 = 3.653 mMol Ca precipitated as $CaCO_3$ in agreement with that

6.569 – 2.800 – 0.075 – 0.040 – 0.000 = 3.654 mMol carbonate species are removed from the solution during passage of the crack.

The an – cation difference as well as the mass-balances serve as control on correct calculation and shows that numerical dispersion or other mathematical difficulties has not give rise to problems (although beginning effects of that type can be seen). In general the performance is better for low values of the time step dtc, but with rapidly increasing calculation time as consequence.

For the Main Case **a** reduction in the crack cross-section due to precipitated calcite results in a very slight increase in pressure loss over the system: from 0.0048 to 0.0116 cm H_2O as calculated from flow rate and the crack dimensions according to equation (2).

Table 4. Porosity, contents of $Ca(OH)_2$ and $CaCO_3$, and concentration profiles for Case a, Column 5 after 28 days. The cat- anion balance for the concentrations and the degree of oversaturation of the solution relative to $CaCO_3$ are also given.
Summary data for the whole simulation are shown in the lower part of the table.

Table No: 56 for column 5 at time t = 336 hours

	mm		mMol in layer		mMol/L solution								Bq/ml	
j	x	eps	sCaOH2	sCaCO3	cCa	cNa	cOH	cCO3	cHCO3	cH2CO3	An-Cat	Oversat	cR1	cR2
-9	-0.0095	1	0	0	1.445	0.704	0.000	0.0046	3.584	0.328	0.0000	1.02	124	91
-8	-0.0085	1	0	0	1.444	0.705	0.000	0.0046	3.583	0.328	0.0000	1.02	124	91
-7	-0.0075	1	0	0	1.442	0.707	0.000	0.0046	3.581	0.327	-0.0000	1.01	124	91
-6	-0.0065	1	0	0	1.439	0.710	0.000	0.0046	3.579	0.327	-0.0000	1.01	124	91
-5	-0.0055	1	0	0	1.436	0.713	0.000	0.0046	3.575	0.326	-0.0000	1.01	125	91
-4	-0.0045	1	0	0	1.431	0.717	0.000	0.0046	3.571	0.326	0.0000	1.01	125	92
-3	-0.0035	1	0	0	1.427	0.722	0.000	0.0046	3.566	0.325	0.0000	1.00	126	92
-2	-0.0021	0.9647	0	0.0121	1.421	0.727	0.000	0.0046	3.560	0.324	0.0000	1.00	127	92
-1	-0.0020	0.3713	0	0.2147	1.312	0.868	0.000	0.0049	3.482	0.281	0.0000	1.00	143	103
0	-0.0005	0.0010	0	0.3411	0.010	31.4	28.4	1.514	0.0089	0.0000	-0.0000	1.00	3643	4008
1	0.0050	0.2891	0.036	0.0160	5.321	55.7	66.3	0.0048	0.00001	0	-0.0000	1.00	6422	8038
2	0.0150	0.2843	0.545	0.00003	5.730	57.6	69.9	0,0047	0.00001	0	-0.0000	1.00	6642	8310
3	0.0275	0.1985	0.720	0	5.366	61.4	72.1	0.0046	0.00001	0	-0.0000	0.91	7078	8743
4	0.0450	0.1993	0.897	0	4.862	67.4	77.1	0.0046	0.00001	0	-0.0000	0.78	7760	9432
5	0.0675	0.1997	1.074	0	4.324	74.8	83.5	0.0045	0.00001	0	-0.0000	0.65	8617	10317
6	0.0950	0.1999	1.252	0	3.796	83.8	91.4	0.0044	0.00001	0	-0.0000	0.52	9642	11403
7	0.1275	0.2	1.430	0	3.304	94.2	100.8	0.0042	0.00001	0	-0.0000	0.40	10830	12690
8	0.1650	0.2	1.609	0	2.863	106.1	111.8	0.0040	0	0	0.0000	0.30	12177	14182
9	0.2075	0.2	1.788	0	2.478	119.4	124.3	0.0037	0	0	-0.0000	0.22	13682	15880
10	0.255	0.2	1.788	0	2.149	134.0	138.3	0.0034	0	0	0.0000	0.16	15340	17783
11	0.305	0.2	1.788	0	1.882	149.2	153.0	0.0030	0	0	-0.0000	0.11	17064	19786
12	0.355	0.2	1.788	0	1.673	164.2	167.6	0.0027	0	0	-0.0000	0.08	18768	21782
13	0.405	0.2	1.788	0	1.506	178.9	181.9	0.0024	0	0	-0.0000	0.06	20451	23759
14	0.455	0.2	1.788	0	1.370	193.2	196.0	0.0021	0	0	-0.0000	0.05	22113	25707
15	0.505	0.2	1.788	0	1.259	207.2	209.7	0.0019	0	0	-0.0000	0.04	23752	27614
16	0.655	0.2	8.939	0	1.015	247.6	249.6	0.0012	0	0	-0.0000	0.01	28570	33182
17	0.905	0.2	8.939	0	0.811	297.0	300.5	0.0005	0	0	0.0000	0.00	35685	40342
18	1.155	0.2	8.939	0	0.715	332.8	334.2	0.0002	0	0	0.0000	0.00	41369	45035
19	1.405	0.2	8.939	0	0.667	252.7	354.1	0.00004	0	0	-0.0000	0.00	45551	47760
20	1.765	0.2	16.81	0	0.609	369.5	370.7	0	0	0	0.0000	0.00	50000	50000

ingoing solution:	2.000	0.000	0.0002	0.0035	3.993	0.550			0	0
outgoing solution:	1.439	0.709	0.000	0.005	3.579	0.327			124	91
Total mMol	Ca	Na	OH	sumCO2					Bq	
in 1445 ml incoming solution:	2.890	0.000		6.569					0	0
in 1445 ml outgoing solution:	1.916	2.311		2.800					390016	312427
outdiffused from concrete:	2.679	2.309	7.857	-0.075	-0.040	-0.000			390016	312497

pressure loss over system: 0.0118 cm H2O

7.1. Main case

Plots illustrating the developments in the Main Case **a** simulation are shown as Figs. 17a to r. The figures also demonstrate the various output facilities available in the program.

Fig. 17a shows the calculated concentrations of Ca, Na and OH in the solution leaving the crack. The horizontal lines indicate the concentrations in the feed solution. It is seen that the calcium concentration initially is increasing. This is due to $Ca(OH)_2$ dissolution from the freshly exposed crack surfaces. Then the concentration decreases to about 10^{-4} M for about four days where after it increases to a value slightly below the concentration in the feed solution. During the same period the OH concentration drops from 10^{-2} to about $3 \cdot 10^{-7}$ M, only slightly above the OH^- concentration in the feed solution. Simultaneously the Na concentration is decreasing but eventually reaches a nearly steady value.

Fig. 17b shows the corresponding concentration developments for the carbonate species. It is seen that HCO_3^- and H_2CO_3 concentrations increases from the original low values towards the concentrations found in the feed solution, while CO_3^{2-} initially increases towards 10^{-3} M and then decreases towards the concentration in the feed solution.

What happens during the first about 8 days is that out-diffusing alkali metal hydroxide and some calcium hydroxide from the cement mortar reacts with bicarbonate in the feed solution resulting in an increased CO_3^{2-} concentration so that the solubility product for calcite is exceeded. Precipitation of $CaCO_3$ removes calcium and carbonate ions from the solution The calcite precipitates as a covering layer on the crack surfaces thereby diminishing the possibility for contact between the alkaline components in the cement mortar and the incoming calcium bicarbonate solution. Eventually a nearly unchanged feed solution is passing through the crack.

The shape of the curves in Figs. 17a and b are in general agreement with what has been found by measurements on experimental systems, see Section 2 Figs. 6a,b and 8. The deviations from smooth curves are supposed to be arte facts of the grid structure and reflects e.g. the successive emptying for $Ca(OH)_2$ of surface layers on the five columns.

The mass balance development of the system calculated from the contents in the feed and the out-flowing solution is shown in Fig. 17c. Similar calculations can be carried out for experimental systems and also here there is principal agreement between model and experiments, see Fig. 7. However, the period with variation in Ca-concentration is about 20 days not 10 as in the calculation example.

Precipitated calcite is given by the CaCO3 curve (obtained from carbonate removed from the solution). The Ca curve represents the amount of calcium removed from the system i.e. the accumulative difference between calcium entering with the feed and leaving with the outflowing solution. The Ca-leach curve represents calcium leached out from the mortar, but not necessarily out in the solution: The difference between the two Ca-curves represents the amount of calcium in the $CaCO_3$ originating as leached Ca from the mortar. The rest is from the feed solution, which also contributes all the necessary carbonate species.

The OH curve represents hydroxyl ions lost with outflowing solution, not the total amount of OH^- leached from the mortar, which typically is about twice as high. The additional OH^- is used in calcite precipitation, see also Section 7.9.

Figs. 17d, e and f show the concentration profiles for dissolved Ca^{2+}, CO_3^{2-} and HCO_3^- in pore solution in the cement mortar (yellow), in the precipitated calcite layer (white with red surface), and in the crack. In this type of figure the height of the blue columns indicates the concentration of the species in the incoming feed solution. Only the inner 0.8 cm of the 2 cm right hand side of the crack is shown in these and following figures. The vertical lines show the employed grid structure. Both sides of the crack are drawn indicating the symmetry of the system. The scale of the distances in the crack is increased a factor 10. The Ca-concentrations at the end of the calculation (i.e. after 14 days) are shown in logarithmic scale for all 5 columns. It is seen that they are rather similar and that the calcium concentration is high in the crack and the mortar but low in the calcite. For carbonate the opposite is the case with high CO_3 concentration in the calcite layer. The bicarbonate concentration decreases in through the calcite to very low levels in the mortar. For the carbonate species only the curves for the first and last column are shown in the figure.

Figs. 17g, h and j show the time development of the concentration profiles for dissolved sodium, the radioisotope R1 (Cs) and hydroxyl ions in column 1 (at the crack inlet). The concentrations are shown on a linear scale and low values can therefore not be seen. The fully drawn curves are for 14 days exposure and the horizontal line (points) at the top of the figures illustrates the initial situation at t = 0. It is seen that the three sets of curves in general are of similar shape. This is because the OH^- concentration is dominated by the contribution from NaOH and because R1 (Cs^+) is supposed not to be retained and as an alkali metal hydroxide behaves much like Na^+. In general the concentrations in the pore solution in the mortar layers near the crack drop rapidly during the first week of exposure. Then when the calcite layer is building up the concentration behind the more and more impermeable layer start to increase, eventually reaching a steady state determined by the concentration gradient and the possibility for diffusion through the remaining porosity.

Figs. 17j and k show the effect of the calcite barrier on the calculated leach curves for Na and R1. The apparent diffusivities corresponding to the initial slope of the curves are somewhat higher than the pore diffusivities corresponding to the porosity and the assumed ff value for the mortar, but after about one week the slope decreases resulting in apparent diffusivities about a factor two lower, see also Table 5 in Section 7.9.

Fig. 17k also illustrates the effect of including the electrical interaction between migration minor and major ions. For R1 (Cs^+) such effects have been included using theory as described in Section 5.2.2 while they are omitted for R2 (also Cs^+). The increased rate of diffusion for R1 is due to the high mobility of the OH^- ion and the drag this anion exercise on the slower moving Cs^+ ion.

Fig. 17l shows the degree of calcite saturation in the pore solution as obtained from concentration the profiles for Ca and CO_3 shown in Figs. 17d and e. Nucleation of calcite crystals in the central part of the laminar flow in the crack will be slow and is supposed not to take place. Calcite is only precipitated in contact with existing solids, either the cement mortar or already precipitated calcite. This means that OH^- diffusing into the central part of the crack and converting some HCO_3^- to CO_3^{2-} gives rise to a certain oversaturation of the solution. In contact with calcite the saturation is by

Fig. 17a **a**

Main Case

ε_{precip}=0.5 ε_{min}=0.001

Concentrations versus time for Ca, Na and OH in solution leaving the crack together with and Ca-concentration in the feed solution (horizontal line)

Compare with the experimental example in Fig 6a.

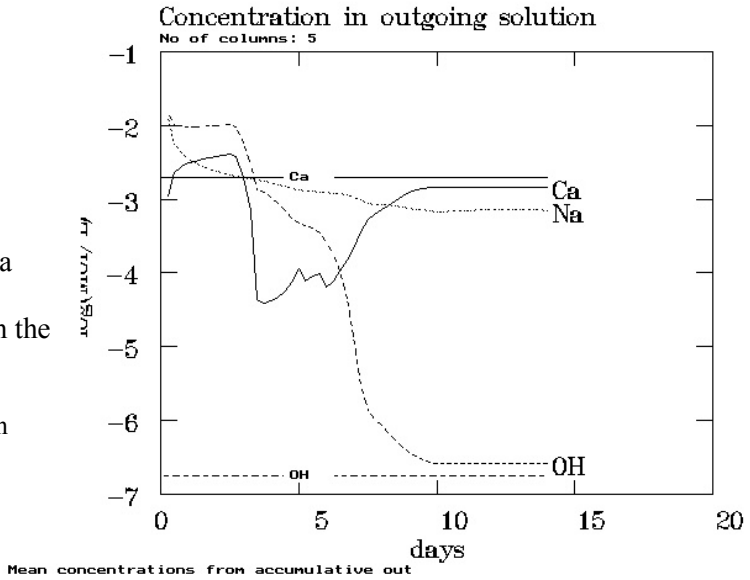

Fig. 17b **a**

Concentration versus time for H_2CO_3, HCO_3 CO_3 and OH in solution leaving the crack.

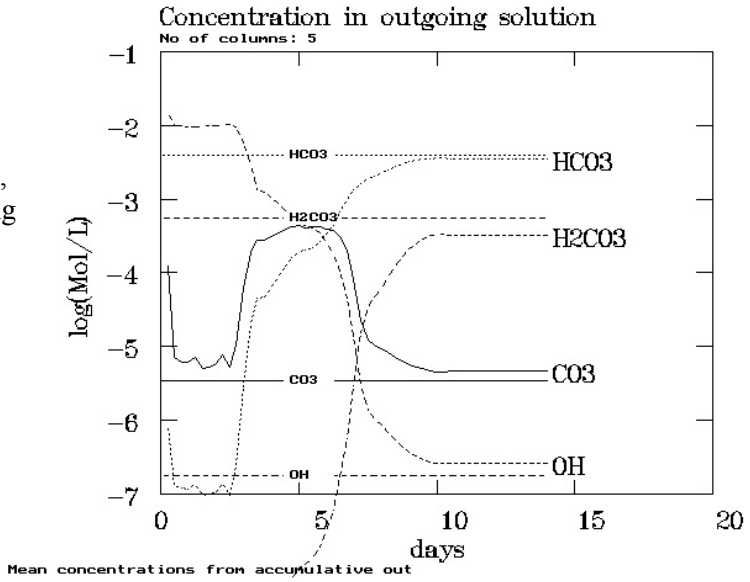

Fig. 17c **a**

Cumulative amounts of precipitated calcite, and (shown negative) Ca removed from the system with the outflowing solution, and calcium, potassium and hydroxide leached from the mortar.

Compare with the experimental example in Fig 6c.

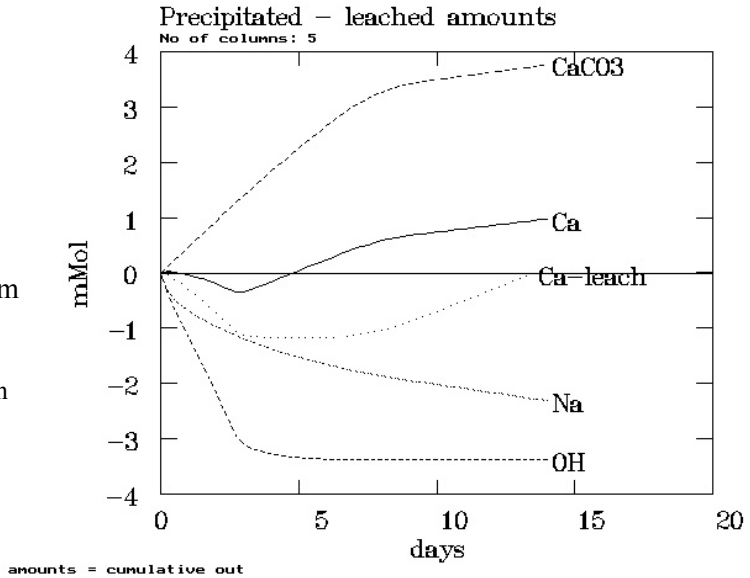

Fig. 17d **a**

Main Case

Concentration profiles after 14 days for dissolved calcium in pore water in the mortar (yellow), calcite layer (white with red outer surface) and in the solution in the crack (blue, the surface level indicates concentration in feed solution). Curves for all five columns are shown but are not very different. For time development se Fig. 17p

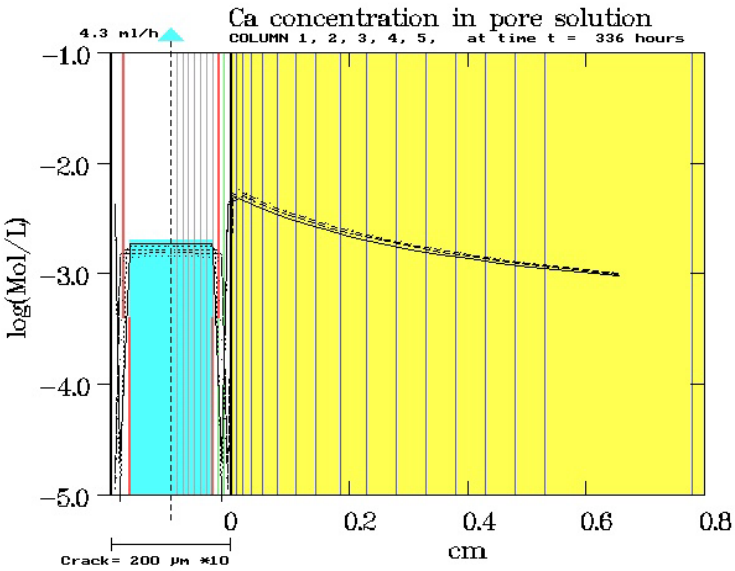

Fig. 17e **a**

Concentration profiles after 14 days for carbonate ions in pore water and in the crack. Only the curves for column 1 (at the feed entrance, fully drawn) and 5 are shown.

The large concentration variations can only be shown in logarithmic scale.

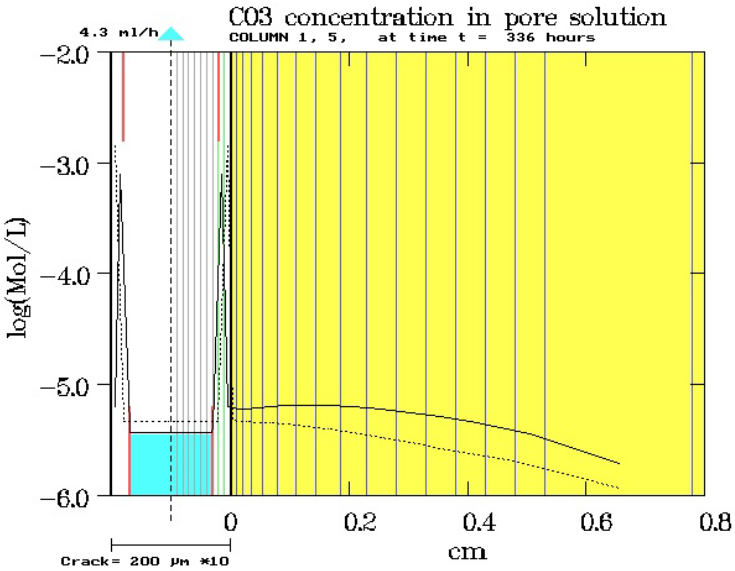

Fig. 17f **a**

Concentration profiles for bicarbonate ions in pore water and in the crack. Only the curves for column 1 (at the feed entrance, fully drawn) and 5 are shown.

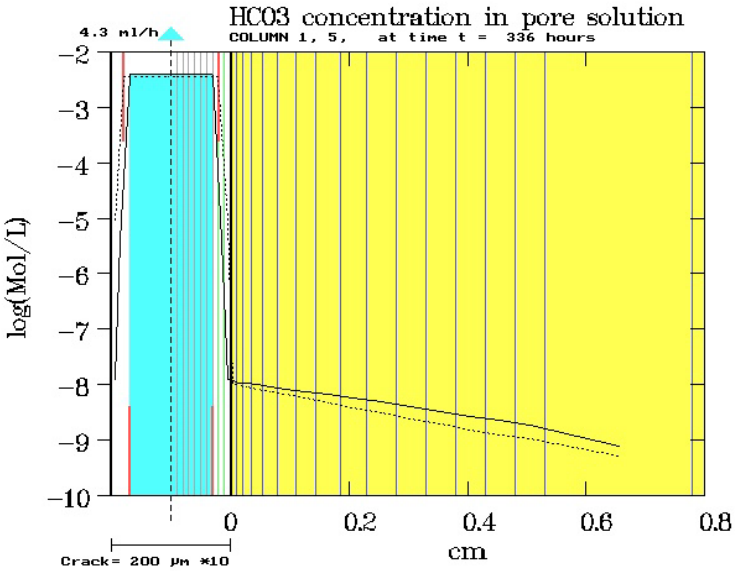

Fig. 17g **a**

Main Case

Concentration profiles for dissolved sodium in pore water in the mortar (yellow) and in the calcite layer (white with red outer surface). There is no Na in the feed and the concentration of the leached sodium in the crack is too low to be seen clearly in this linear presentation.
Curves for 0 (horizontal) and 3½, 7, 10½ and 14 days exposure. The fully drawn curve is at 14 days.

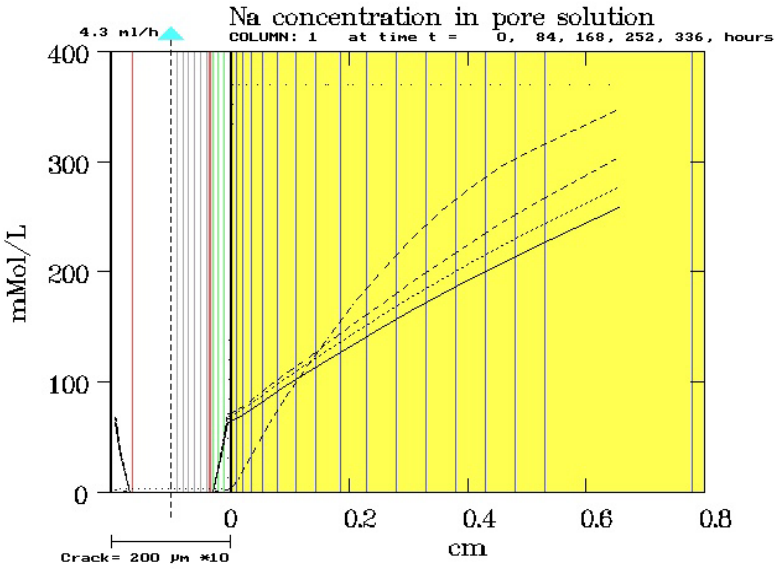

Fig. 17h **a**

Concentration profiles for the radioisotope R1 (Cs) in pore water in the mortar and in the calcite layer after t=0 (horizontal) and 3½, 7, 10½ and 14 days exposure.

The calculation includes correction for electrical interactions with the major migrating ions

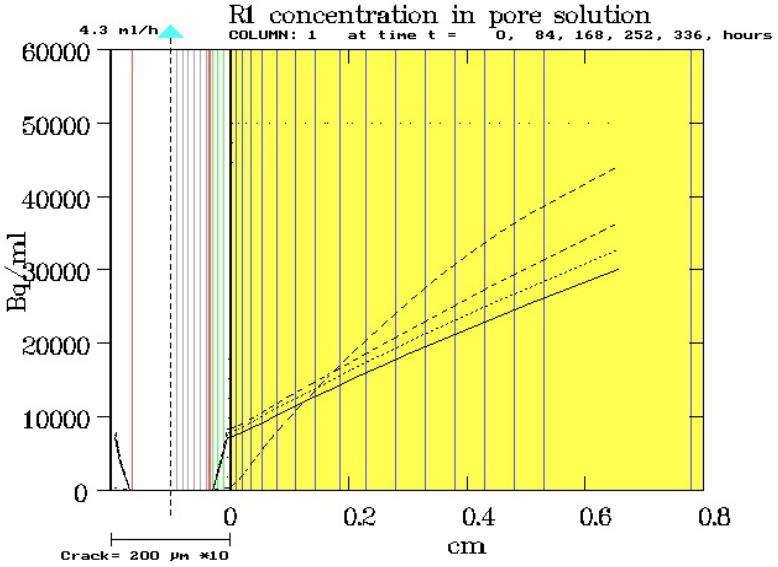

Fig. 17i **a**

Concentration profiles for hydroxyl ions in pore water the mortar and in the calcite layer after 0 (horizontal) and 3½, 7, 10½ and 14 days exposure.

The curves are nearly, but not quite similar to the sodium curves in Fig. 17g. (The different shape of the 3½ days curve is caused by OH from $Ca(OH)_2$).

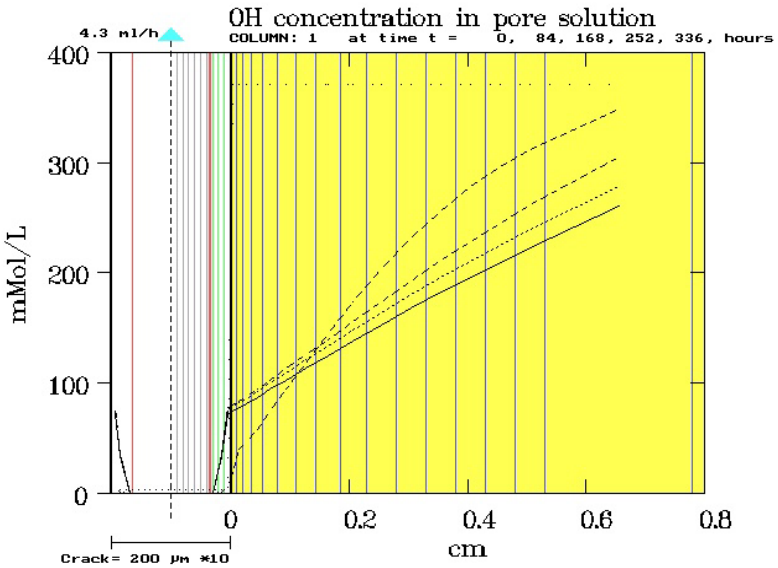

Fig. 17j **a**

Main Case

Leach curve for sodium. The equivalent leached thickness is plotted versus the square root of time. After about a week the slope of the curve decrease considerably.

Diffusivities corresponding to the two slopes are given in the figure.

Compare with the experimental examples in Fig. 6d. and 7.

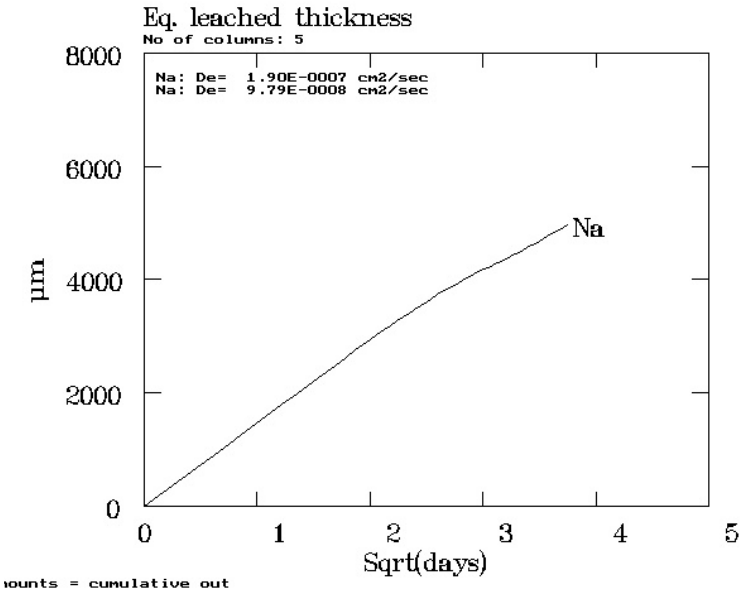

Fig. 17k **a**

Leach curve for the radioisotopes R1 and R2 (both Cs).
The equivalent leached thickness is plotted versus the square root of time. R1 is calculated with correction for electrical interaction with migrating major ions and R2 without such corrections.

Diffusivities corresponding to the two slopes of the curves are given in the figure.

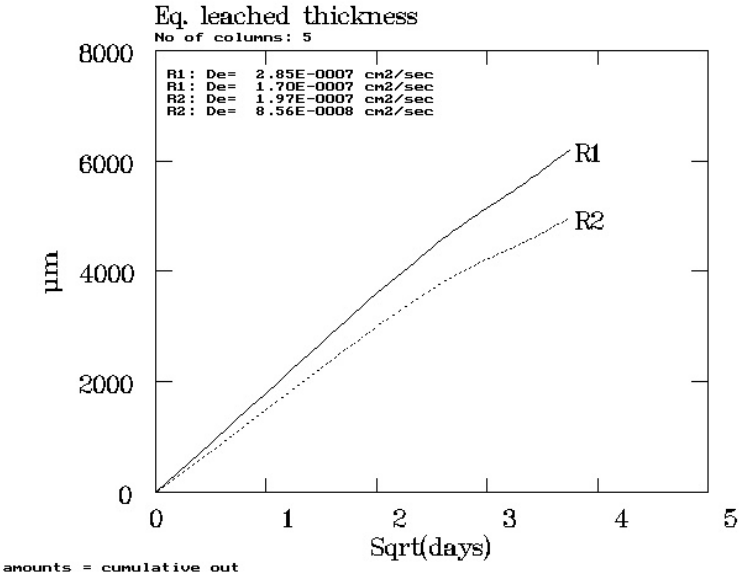

Fig. 17l **a**

Degree of calcite saturation in various layers along the length of the crack.

The solution is oversaturated in the crack (in layers -9 to –3), saturated in the layers with calcite (-2 to 2) and unsaturated in the deeper part of the mortar (3 to 20).

The outflowing solution is oversaturated after mixing.

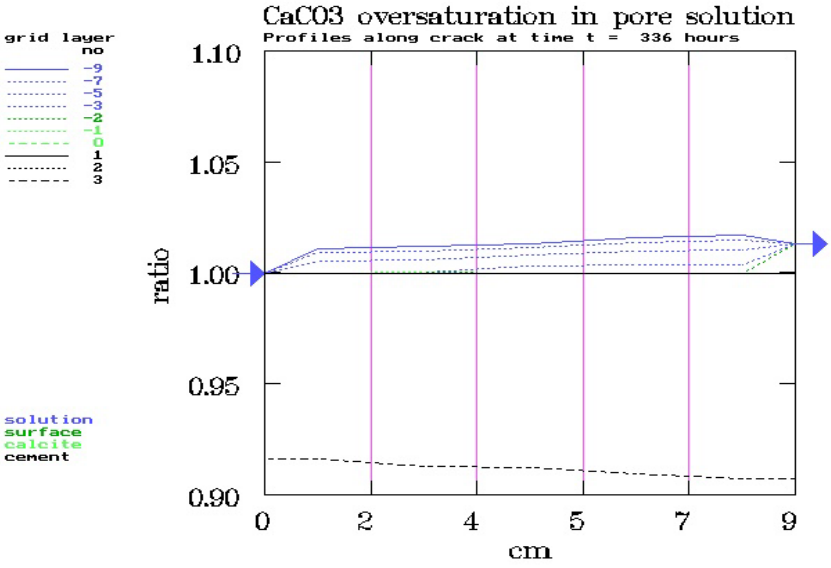

Fig. 17m **a**

Main Case

Growth of the calcite layers on top of the 5 column surfaces constituting the inner surface of the crack. The thickness x1 is for column 1 at the feed entrance while x5 is at the outlet.

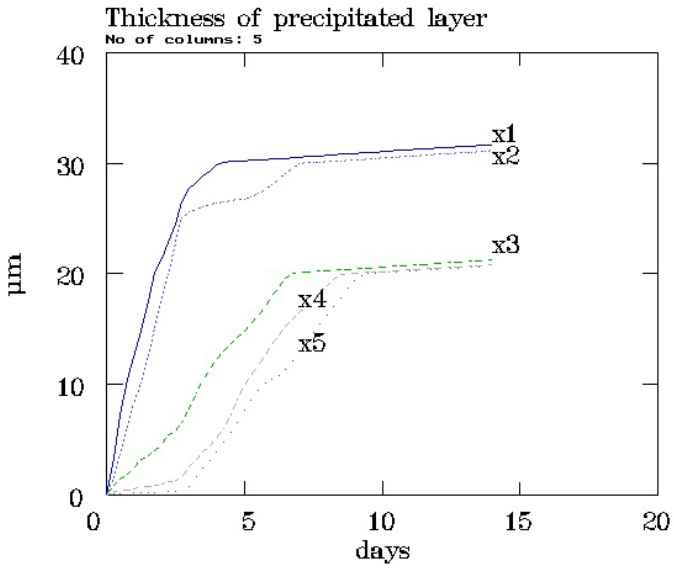

Fig. 17n **a**

Growth of the calcite layer on column 1 with porosity decreasing from 50% towards 0.1% as represented by the decreasing number of white points. Especially the layer between 10 and 20 µm is rapidly getting very dense.

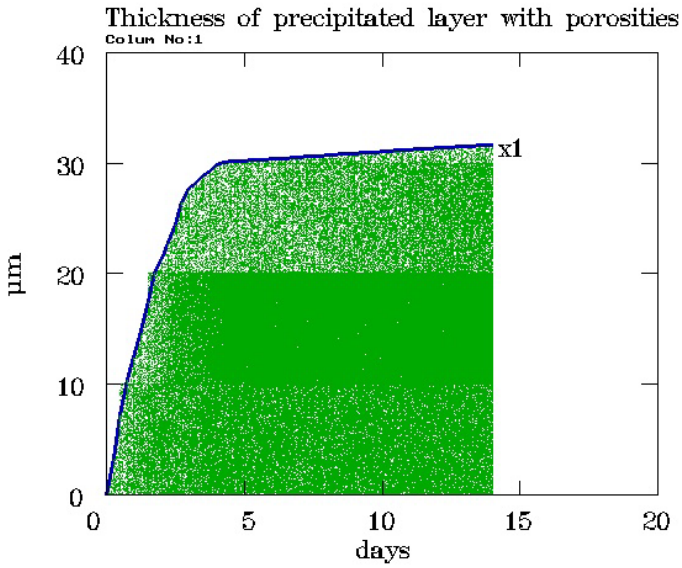

Fig. 17o **a**

Cut through the five-column system showing the 6 upper layers in the mortar and (on a larger scale) 4 layers in the crack. The grey dots represents sand, red points are $Ca(OH)_2$, yellow is C-S-H etc (considered inert) and green is calcite. White represents porosity. It is seen that at least one grid layer with dense, low porosity layer covers all 5 columns. Practically no calcite is deposited below the original

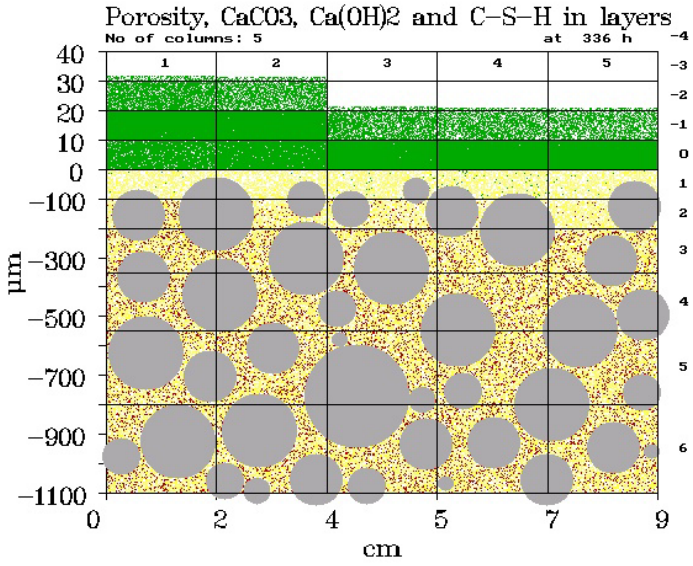

Fig. 17p **a**

Main Case

Concentration profiles for dissolved calcium in pore water in the mortar, the calcite layer and the solution in the crack. Curves for column 1 (at the feed entrance) at t = 0 (horizontal) and after 1, 3, 7 and 14 days exposure. The fully drawn curve is for 14 days and is also fairly representative for the other four columns at that time, see Fig. 17d.

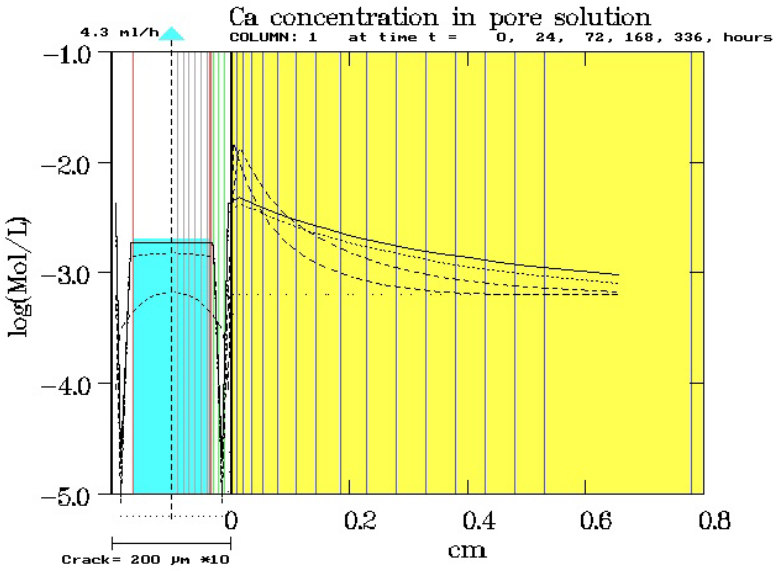

Fig. 17q **a**

Leach profile for $Ca(OH)_2$ in column 1 after 14 days. One outer layer of the mortar is completely depleted.

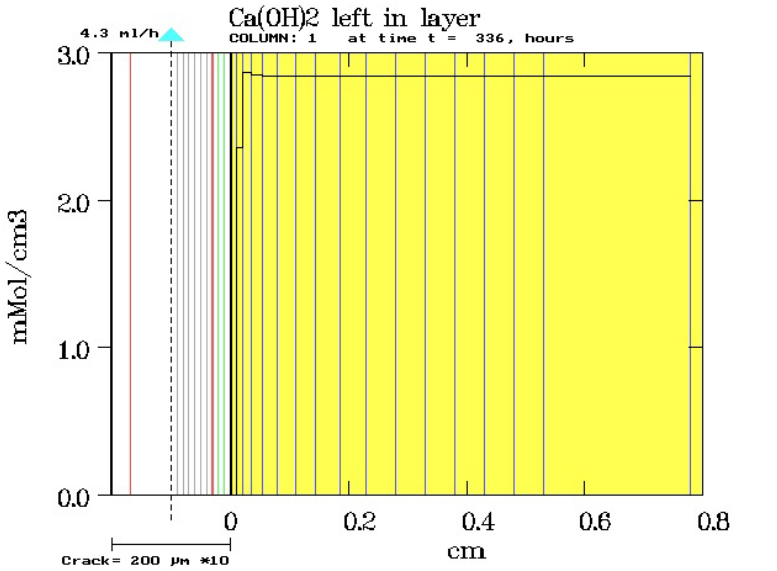

Fig. 17r **a**

Porosity of the layers in column 1 after 14 days. Leaching of $Ca(OH)_2$ increases the porosity of the outer mortar layers. Only one of the three grid layers with calcite has low porosity.

The blue curve shows the velocity profile for the solution in the crack.

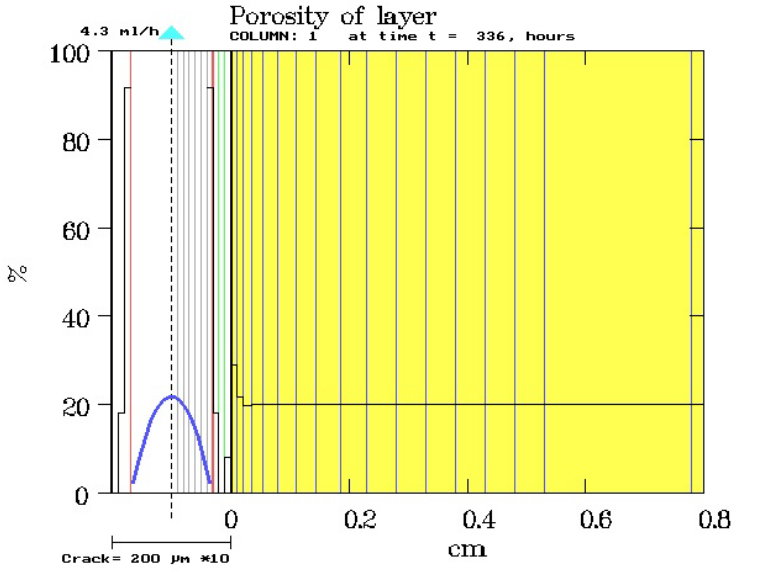

definition one, and inside the mortar the pore solution is undersaturated. The figure shows the of saturation degree along the length of the crack for selected grid layers. For layers without solids in the values are above 1, for the layers containing calcite the value is 1, and at the bottom of the figure is the first layer (No. 3 in the mortar) where the solution is unsaturated. This is for the situation after 14 days where calcite layers covers all 5 columns. While the layers are being established the appearance of the saturation curves is more complicated.

The solution leaving the crack is a mixture of the solutions flowing through the not calcite-filled of the 10 grid layers in the crack. The program calculates the composition of this mixture, which is also oversaturated as illustrated by the arrow to right in the Fig. 17l. This is in agreement with observations from the experiments where fanciful crystal aggregates (mounts, tubes etc.) were often formed around the outlet from the crack, see Figs. 3a and b.

Figs. 17m, n and o show the development of the calcite layer. In Fig. 17m the increasing thickness' of the calcite layer on top of the original crack surface in the five columns are depicted as function of time. A rapid increase is seen to be followed by a period with much slower growth of the layer.

As illustrated by Fig. 17n for column 1 a simultaneous decrease of porosity in the calcite layers is also taking place due to precipitation of calcite internally in remaining pores in already precipitated calcite. The initially precipitated calcite is assumed to have 50 % pores while a minimum porosity of 0.1% is supposed to remain even in the densest calcite. Such a layer is here developed as the second grid layer in the deposit. The formation of a diffusion barrier in form of dense calcite will be further discussed in Section 8.

Fig. 17o represents a general cut through all five columns after 14 days. The calcite layer (green with white pores) as deposited in the crack on top of the original column surfaces is drawn to an increased scale. One grid layer on each column has reached the minimum porosity and has therefore high diffusion resistance. The presence of this barrier prevents leaching and gives rise to the steep concentration gradients over the calcite as seen for Na, R1 and OH in Figs.17g, h and i.

The grid layers in the mortar are thicker than in the crack. The randomly distributed grey dots represent sand particles. They are drawn to scale and with a size distribution as typical for the experimental work. The number of red points is proportional to the amount of remaining $Ca(OH)_2$. Calcium hydroxide is seen to be absent in the mortar layer right below the calcite and also in the second layer in column 5 indicating more pronounced leaching due to the later formation of a covering layer on this column (see curve x5 in Fig. 17m). A very few green points represents the small amount of calcite deposited inside the leached mortar. Inert material (in the model including C-S-H) is represented by yellow points, while pores are white.

That the calcite practically exclusively is deposited as a covering layer on the crack surface and not in the partly leached cement paste in between the sand particles was also observed in the experiments. While wet the calcite layers were soft and could easily be scraped from the crack surface without removing sand particles, see also Section 2.

Fig. 17p is (like Fig. 17d) a presentation of concentration profiles for dissolved calcium in pore solution and crack but in this case for column 1 after 0, 1, 3, 7 and 14 days exposure to the incoming bicarbonate solution. The original Ca-concentration in the mortar is low (the horizontal dotted line) due to $Ca(OH)_2$ solubility suppression by high OH^- concentration from

dissolved NaOH. When the sodium hydroxide initially is rapidly leached the Ca-concentration increases to about 0.01 M. Later when the protective calcite layer is formed and the NaOH concentration again is increased in the leached grid layers of the mortar (Figs. 17g and i) the solubility of calcium hydroxide is again suppressed and the concentration curves become more flat.

Fig. 17q shows remaining $Ca(OH)_2$ in the grid layers of column 1 after 14 days. The layer nearest the crack is completely and the second layer partly depleted. As a curiosity it can be seen that the abnormal calcium concentration curves shown in Fig. 17p with the high concentrations at the surface have resulted in some back diffusion of Ca into the deeper mortar layers and precipitation of a small but visible amount of calcium hydroxide.

Fig. 17r shows the porosity also for column 1 at 14 days. The porosity of the mortar is somewhat increased at the crack surface due to leaching of $Ca(OH)_2$. The blue curve in the crack represents the relative velocity of the laminar solution flow in the crack. The formation of the calcite layer narrows the crack so that the residence time for the solution in the crack is decreased from 53 to 40 seconds. At the same time the pressure loss over the crack is slightly increased (from 0.0048 to 0.0116 cm H_2O), but the crack was nowhere near complete closure.

The above Main Case **a** has been selected as the basic illustrating example because it in many ways represents a reasonable approximation to experimental observations. In the following effects of some parameter variations will be described, see Fig. 16 for specifications.

7.2. High final porosity of calcite layer.

In Case **b** the assumption is that the minimum porosity of the calcite layers is 2 %, i.e. ε_{min}= 0.02, or a factor 20 higher than assumed in Case **a**. This results in a somewhat longer period with low Ca^{2+} and high CO_3^{2-} concentrations in the outflowing solution as seen by comparing Figs. 18a and b with Figs. 17a and b. The concentrations of calcium and bicarbonate ions after formation of the calcite layers remain considerably below the concentration in the feed solution. This is because the remaining 2 % porosity of the calcite permits considerable diffusive leaching from the mortar out into the flowing solution.

The result is a near disappearance of the sodium concentration gradient over the calcite layer and as a consequence somewhat higher calcium concentrations in the pores near the crack (compare Figs. 18e and d with Figs. 17g and d).

A plot of the sodium leach curve is shown in Fig. 18c. It is seen to be a practically straight line without the decline in apparent diffusivity after formation of the calcite layer as seen for Case **a** in Fig. 17j. Such a decline was typically found in the experimental work and indicates that formation of a relatively porous calcite layer is not what occurs in reality, see also the discussion in Section 8.

The thickness of the precipitated layer is higher in Case **b** than in the Main Case **a**, (compare Figs. 18f and 17o). Two grid layers have reached the 2 % porosity, but as diffusion barrier this is not as efficient as the one layer with 0.1% porosity in the Main Case **a**.

Fig. 18a **b**

High final calcite porosity
ε_{precip}=0.5 ε_{min}=0.02

Concentrations versus time for Ca, Na and OH in solution leaving the crack and Ca concentration in the feed solution (horizontal line).

Compare with Fig 17a

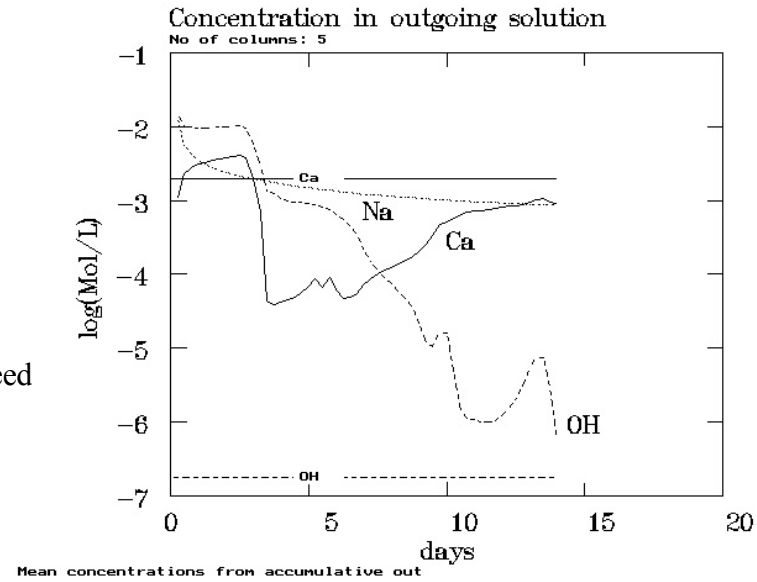

Fig. 18b **b**

Concentrations versus time for H_2CO_3, HCO_3 CO_3 and OH in solution leaving the crack, and concentrations in feed solution (horizontal lines).

Compare with Fig. 17b.

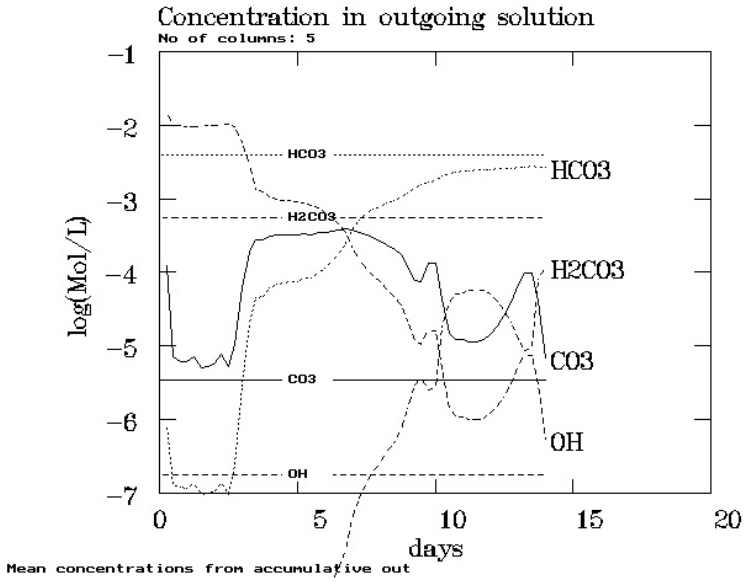

Fig. 18c **b**

Leach curve for sodium. The equivalent leached thickness plotted versus the square root of time. The line is nearly straight as indicated also by the diffusivities values corresponding to the slope of the initial and the last part of the curve.

Compare with Fig. 17j.

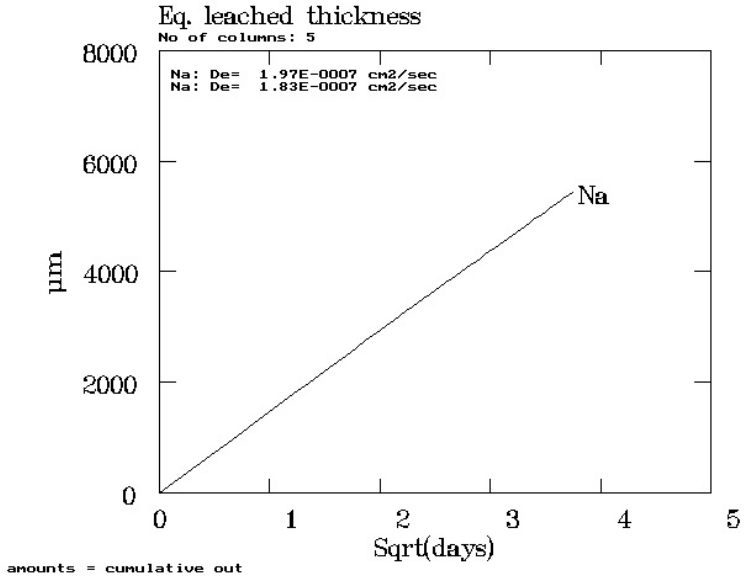

Fig. 18d **b**

High final calcite porosity

ε_{precip}=0.5 ε_{min}=0.02

Concentration profiles after 14 days for dissolved calcium in pore water in the mortar (yellow), calcite layer (white with red outer surface) and the solution in the crack (blue, the level indicates concentration in feed solution). Curves for columns 1 (at feed entrance, points) and 5 (whole line) are shown but are not very different.

Compare with Fig. 17d.

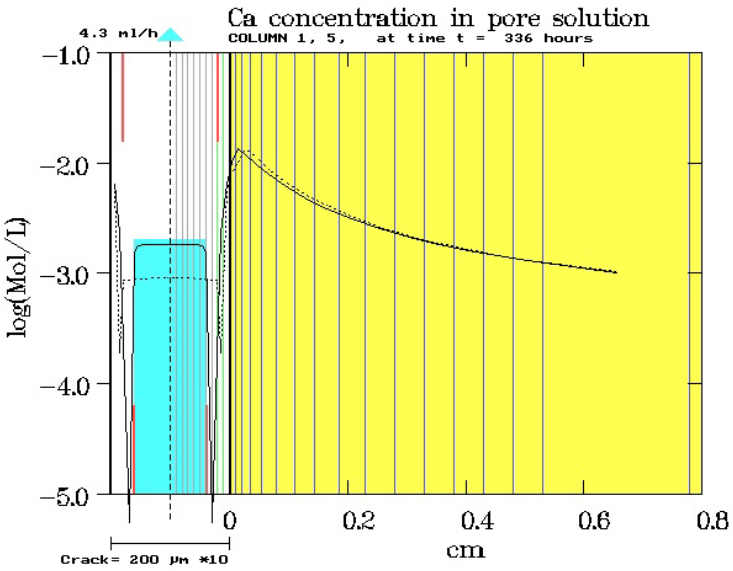

Fig. 18e **b**

Concentration profiles after 14 days for dissolved sodium in pore water in the mortar and in the calcite layer. There is no Na in the feed and the concentration of the leached sodium in the crack is too low to be seen clearly in linear presentation. Curves for column 1 after 0 (horizontal) and 7, 14, 21 and 28 days exposure are shown. The fully drawn curve is at 28 days.

Compare with Fig. 17g

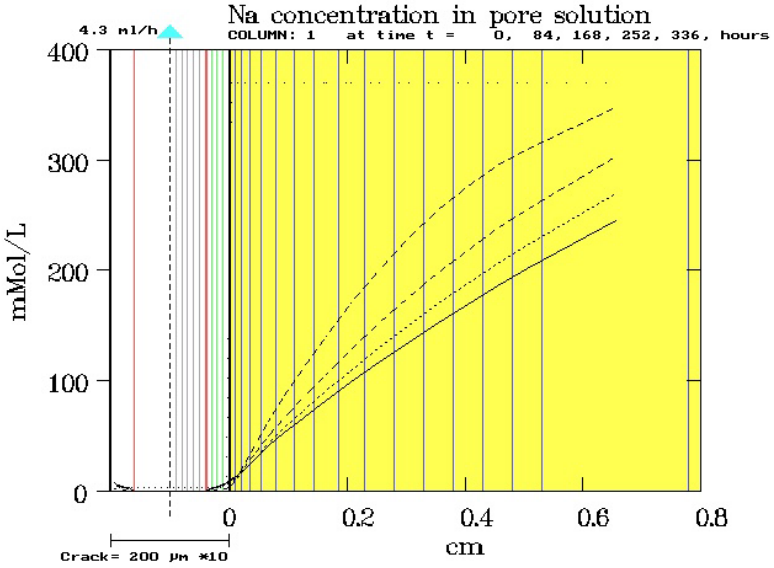

Fig. 18f **b**

Cut through the five-column system showing the 6 upper layers in the mortar and (on a larger scale) 5 layers in the crack. The grey dots represents sand, red points are $Ca(OH)_2$, yellow is C-S-H etc. (considered inert) and green is calcite. White represents porosity.
It is seen that two grid layers with 2 % porosity covers all 5 columns.
Practically no calcite is deposited below the original surface.

Compare with Fig. 17o

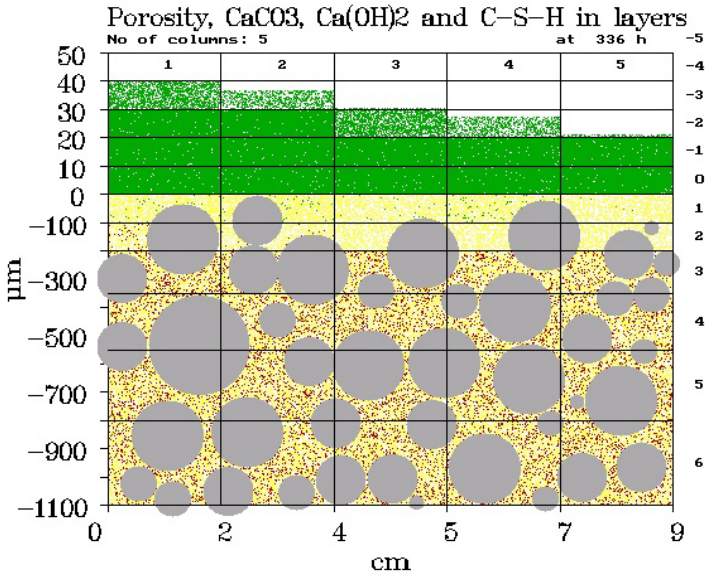

7.3. Variation of initial porosity of calcite layer

It is supposed that precipitation of calcite from solution in the open part of the crack can only take place in grid layers with already existing solid material. An assumption about the porosity ε_{precip} of such initially precipitated calcite (or rather the porosity between the calcite crystals) is needed to simulate the growth of a calcite layer inside the grid layer (ε_j in equation (49), see Section 4.5).

Effects of assuming ε_{precip}= 0.35, 0.5, 0.65 and 0.80 while the final porosity is maintained at ε_{min} = 0.001 are illustrated by Cases **a_{35P}**, **a**, **a_{65P}** and **a_{80P}**.

Assuming initial precipitation of a relatively dense calcite shorten the period with low calcium concentration in the outflowing solution while a more loose initial precipitate increases the period, compare Figs. 19a with 17a and 20a. The distribution of calcite over the columns is different with formation of a somewhat thicker layer in case of high initial porosity (Figs. 19c, 17o, 20b and in particular 20c). Closure of the crack is approaching in the later case with 80 % initial porosity in the calcite. However, after 14 days 26 % of the crack still remains open on column 2 and the calculated pressure loss has only reached 0.075 cm water. Grid layers with 0.1% porosity have developed on column 1 and 2, but not yet on columns 3, 4 and 5 although this probably would have occurred relatively soon. Out-diffusion of sodium will then decrease as in the normally observed manner as seen for the systems in Figs. 19b and 17j.

The assumption about a relatively loose initial precipitate may be in better agreement with experiments than the 50 % assumed in the Main Case **a.** In the experimental work the period with low calcium concentration in the outflowing solution was in general somewhat longer than obtained in the model calculations. Clogging of cracks with weak solid materials resulting in temporary pressure build-up followed by resumed flow after slight mechanical vibration was sometimes observed for 0.2 mm wide cracks.

Flow of solution is only assumed to take place in the open part of the crack outside the calcite layers. This is questionable when the initial precipitate is very porous, especially if a pressure gradient is building up.

7.4. Pore diffusivities and the form factor ff

The assumptions about pore diffusivities are open for discussion: Can the Dp values defined by equation (85) be obtained from the diffusivities in water by multiplication with a single form factor ff describing geometrical properties of the pore system, and should this ff value be the same for the pore system in cement mortar and in the calcite precipitate ? Should migrating cat- and anions have similar ff values or should ion-exclusion of anions be taken into account ? This will not be investigated here, only the effects of simple halving or doubling of the ff value used in the Main Case **a** calculation are presented as Cases **$a_{½ff}$** and **a_{2ff}**:

The use of half the Dp values produces the calcium concentration curve shown in Fig. 21a. The concentration starts low and the suppression around 5 days is not very pronounced. This behaviour is not in agreement with experimental observations. The leach curves for Na, R1 and R2 in Fig. 21b show the decline in slope associated with the formation of a tight calcite layer.

The amount of precipitate is about 10 % less than for the Main Case **a** (see also Table 5 in Section 7.9) and the distribution of calcite over the columns is different, compare Figs. 21c and 17o.

The use of double the Dp values gives a calcium curve starting higher than for Case **a** and with a well-developed period with suppression of the calcium concentration, see Fig. 22a. The initial slopes of the leach curves for Na, R1 and R2 are increased corresponding to the employed higher Dp values. The slopes show the usual decline after 4 – 5 days due to formation of the calcite layer. This is simultaneous with build-up of the sodium concentration behind the calcite layer as shown in Fig. 22b. The amount of precipitated $CaCO_3$ is increased about 12 % compared with Case **a**. The calcite layer is relatively thick, in this case (as for Case b) especially on column 1 at the feed entrance. However, the crack is not yet half filled and the calculated pressure loss only 0.014 cm H_2O.

The behaviour of an especially porous cement mortar (backfill) where an even higher ff value must be assumed is described in Section 7.8.

7.5. Mortar without NaOH

A different type of parameter variation is tried in Case **a0**. Here it is assumed that the cement mortar contains no alkali metals, i.e. the material is approximated by pure calcium hydroxide mixed with inert material. The absence of alkali metals is not a realistic possibility with commercial cements but effects of the unavoidable small contents of Na and KOH dissolved in pore water are often disregarded in theoretical discussions of cementitious materials.

Comparison of Figs. 23a and b with 17a and b shows that the main features of the time development of calcium, hydroxide and carbonate concentrations in the outflowing solution is similar with and without alkali metals present. However, the initial calcium leaching is somewhat enhanced and the later suppression of the calcium concentration and increase of CO_3^{2-} concentration is of short duration. It should be noticed that the calcium concentration returns completely to the value in the feed solution after formation of the calcite layer. This is because there is not the same possibility for build-up of a high hydroxide gradient over the calcite and the associated slow release through remaining pores when alkali metals are not present.

The concentration profiles for dissolved calcium and CO_3^{2-} in the crack and the pores of the calcite layer and cement mortar are shown in Figs. 23d and e for column 1 and 5 after 14 days. The calcium curve is flat without the characteristic suppression of calcium hydroxide dissolution caused by alkali metal hydroxides. The CO_3^{2-} concentration is low inside the mortar. The concentration profile for carbonate as well as calcium appears flat inside the crack but when the concentrations are combined a characteristic oversaturation profile is obtained as shown in Fig. 23f.

Fig. 19a **a_{35P}**

Low initial porosity of calcite
ε_{precip}=0.35 ε_{min}=0.001

Concentrations versus time for Ca, Na and OH in solution leaving the crack and Ca concentration in the feed solution (horizontal line)

Compare with Fig. 17a

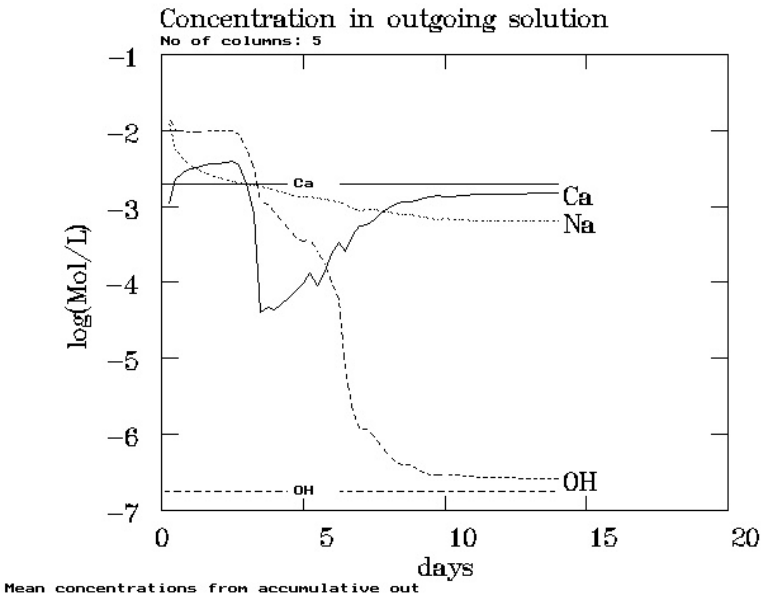

Fig. 19b **a_{35P}**

Leach curve for sodium. Equivalent leached thickness plotted versus square root of time. After about two weeks the slope of the curve decrease considerably.
Diffusivities corresponding to the two slopes are indicated in the figure.

Compare with Fig. 9j.

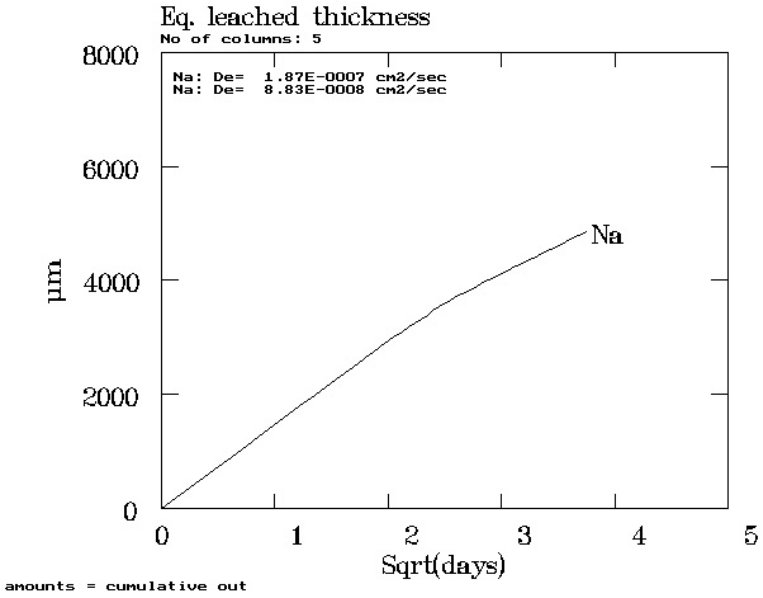

Fig. 19c **a_{35P}**

Cut through the five column system showing the 6 upper layers in the mortar and (on a larger scale) 4 layers in the crack. The grey dots represents sand, red points are $Ca(OH)_2$, yellow is C-S-H etc and green is calcite. White represents porosity. It is seen that at least one grid layer with dense, low porosity calcite covers all five columns.

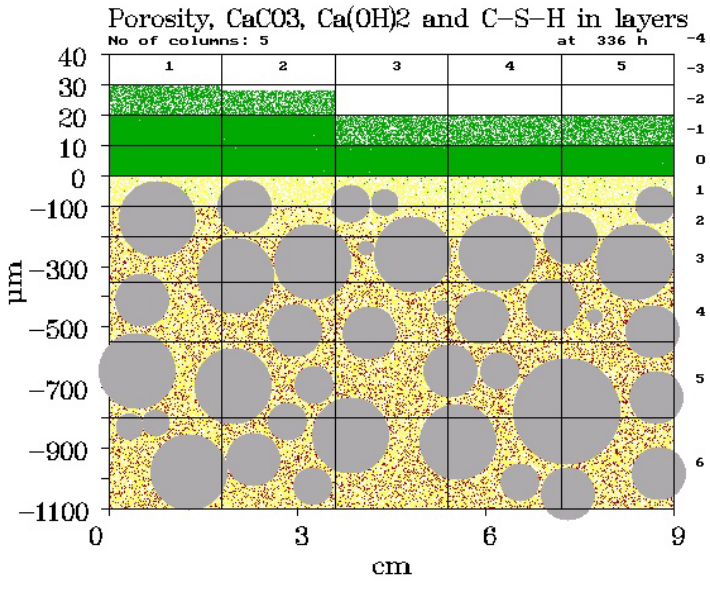

Fig 20a **a_{65P}**

High initial porosity of calcite

ε_{precip}=0.65 ε_{min}=0.001

Concentrations versus time for Ca, Na and OH in solution leaving the crack, and Ca concentration in the feed solution (horizontal line)

Compare with Figs. 17a and 19a

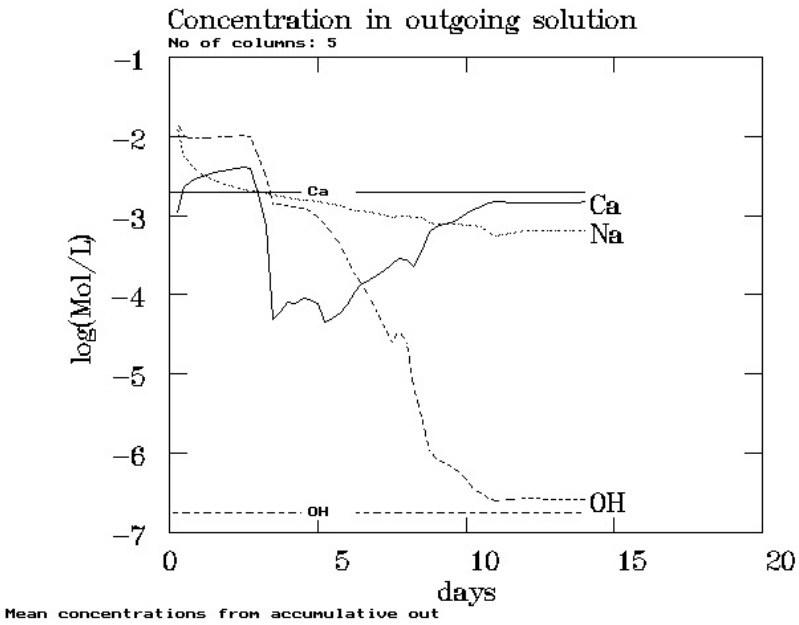

Fig. 20b **a_{65P}**

Cut through the five-column system after 14 days showing the 6 upper layers in the mortar and (on a larger scale) 4 layers with calcite in the crack. At least one grid layer with dense, low porosity layer covers all five columns.

Compare with Figs. 17o and 19c.

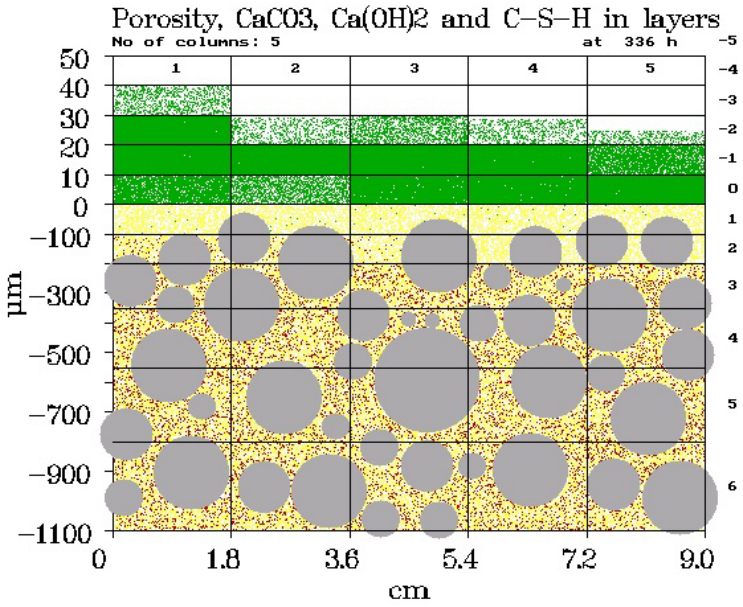

Fig. 20c **a_{80P}**

Very high initial porosity of calcite layer

ε_{precip}=0.80 ε_{min}=0.001

Cut through the five-column system showing the 6 upper layers in the mortar and (on a larger scale) 8 layers in the crack. One or two grid layers with relatively low porosity calcite covers all five columns but ε_{min} has (so far) only been reached in column 1 and 2

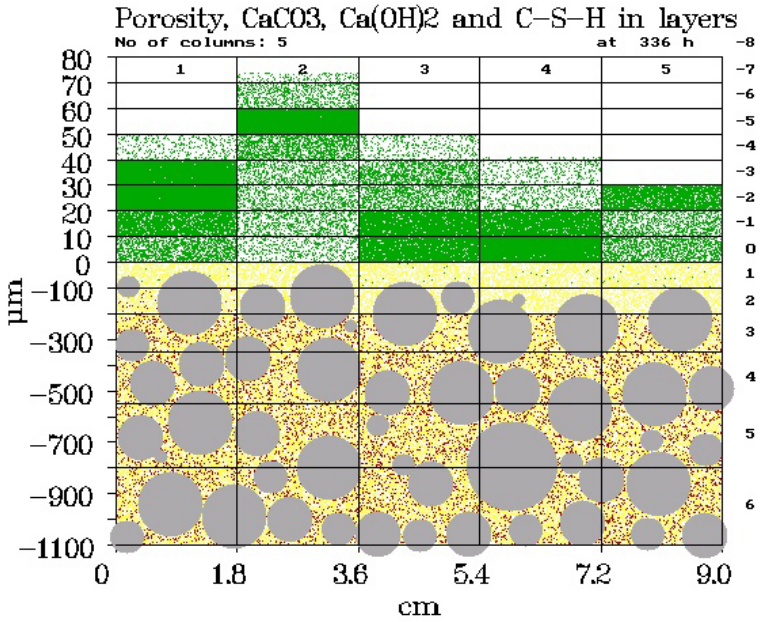

Fig. 21a **a½ff**

Decreased pore diffusivity in cement mortar: ff = 0.025

Concentrations versus time for Ca, Na and OH in solution leaving the crack and Ca concentration in the feed solution (horizontal line). The initial calcium concentration is low and the suppression in concentration around 5 days is relatively slight.

Compare with Fig. 17a.

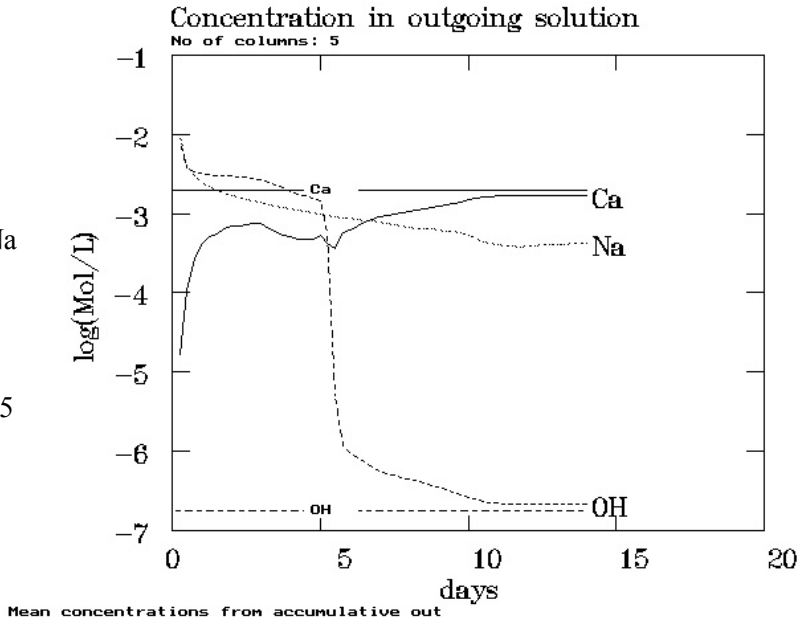

Fig. 21b **a½ff**

Leach curves for sodium, R1 and R2 (incidentally nearly the same as for sodium). Equivalent leached thickness versus square root of time. After about nine days the slope of the curves decreases considerably. Diffusivities are indicated in the figure.

Compare with Fig. 17j.

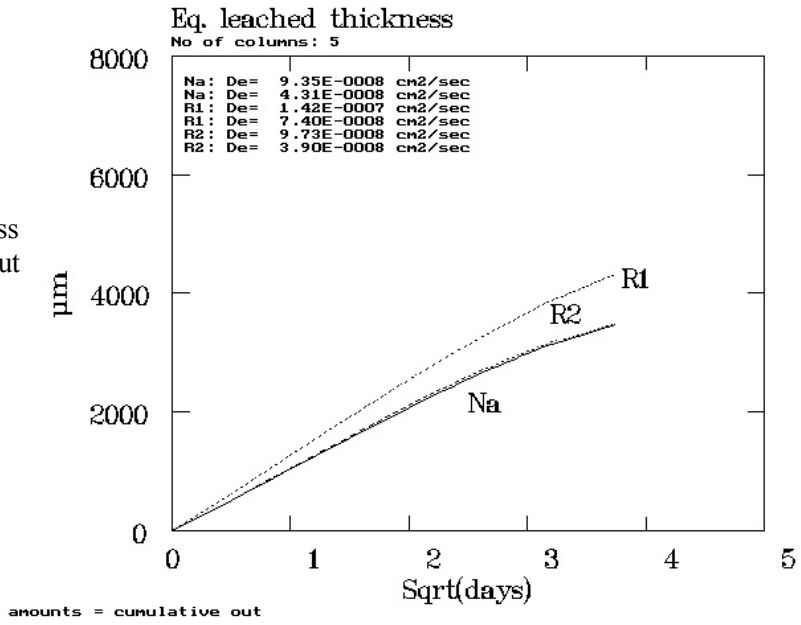

Fig. 21c **a½ff**

Cut through the five-column system showing the 6 upper layers in the mortar and (on a larger scale) 4 layers in the crack. Leaching of $Ca(OH)_2$ is incomplete in the upper mortar layer in column 1 due to the decreased diffusivity and rapid sealing of the surface by dense calcite. The calcite layer is thickest in the middle.

Compare with Fig. 17o.

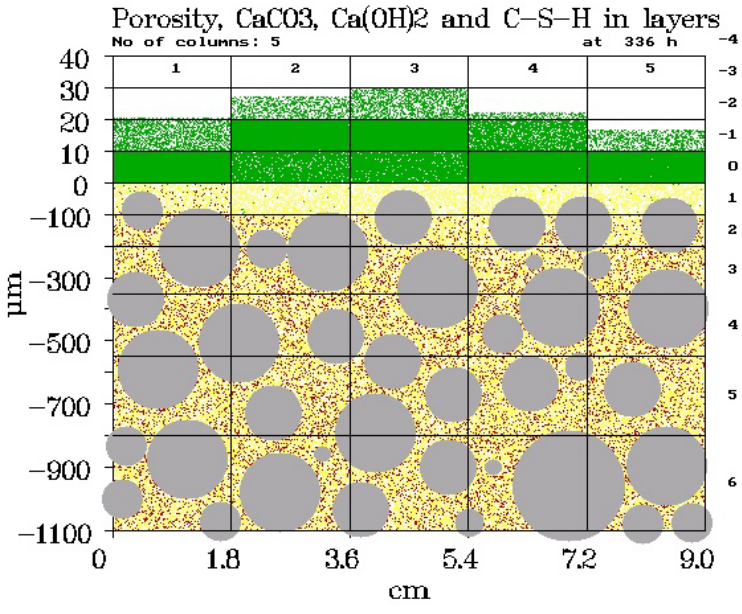

Fig. 22a a_{2ff}

Increased pore diffusivity in cement mortar ff = 0.100

Concentrations versus time for Ca, Na and OH in solution leaving the crack and Ca-concentration in the feed solution (horizontal line). The general appearance is similar to Fig. 17a but the initial calcium concentration is higher and more calcium is leaking out at the end after formation of the covering layer

Compare with Fig. 17a and 21a.

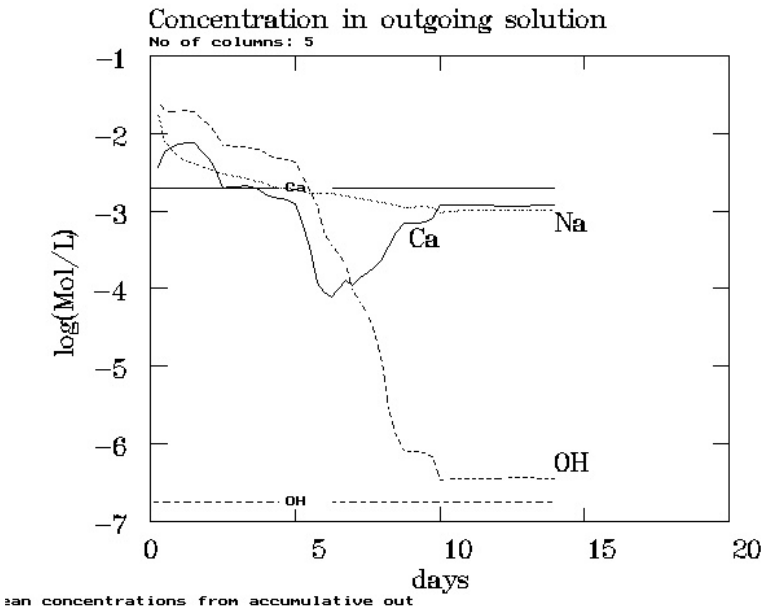

Fig. 22b a_{2ff}

Leach curves for sodium, R1 and R2 (incidentally nearly the same as for sodium). Equivalent leached thickness versus square root of time. After about four days the slope of the curves are somewhat decreased. Diffusivities are indicated in the figure.

Compare with Fig. 17j and 21b.

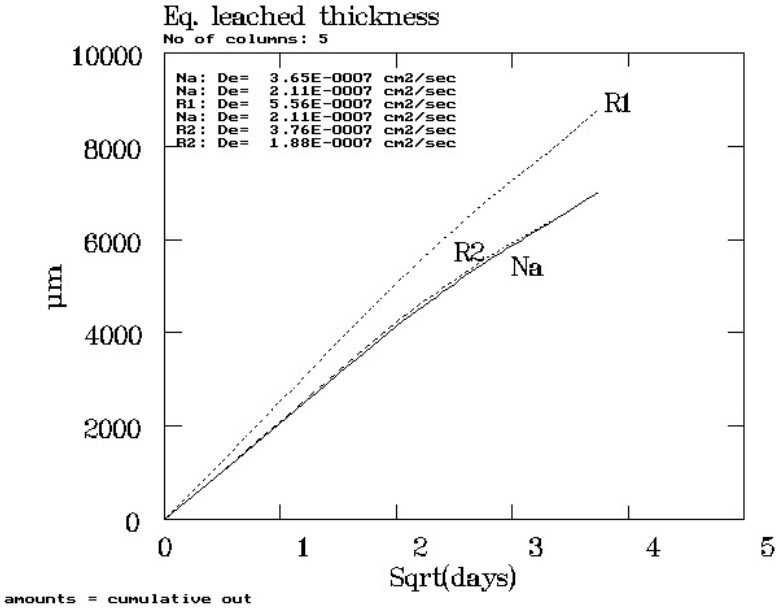

Fig. 22c $a_{½ff}$

Cut through the five-column system showing the 6 upper layers in the mortar and (on a larger scale) 5 layers in the crack. The calcite layer is thickest on the first column but the middle ones have two layers of dense calcite.

Compare with Fig. 17o.

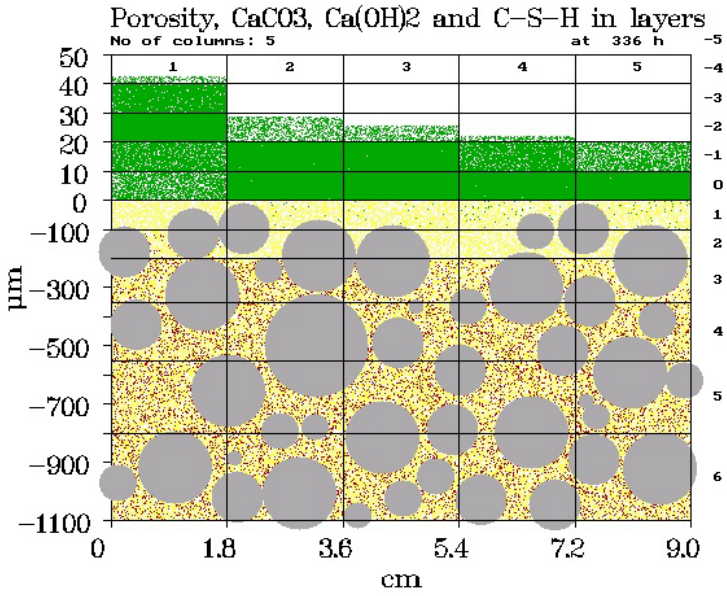

Fig. 23a **a0**

$Ca(OH)_2$ without NaOH, KOH

Concentrations versus time for Ca and OH in solution leaving the crack and Ca concentration in the feed solution (horizontal line)

Compare with Fig. 17a.

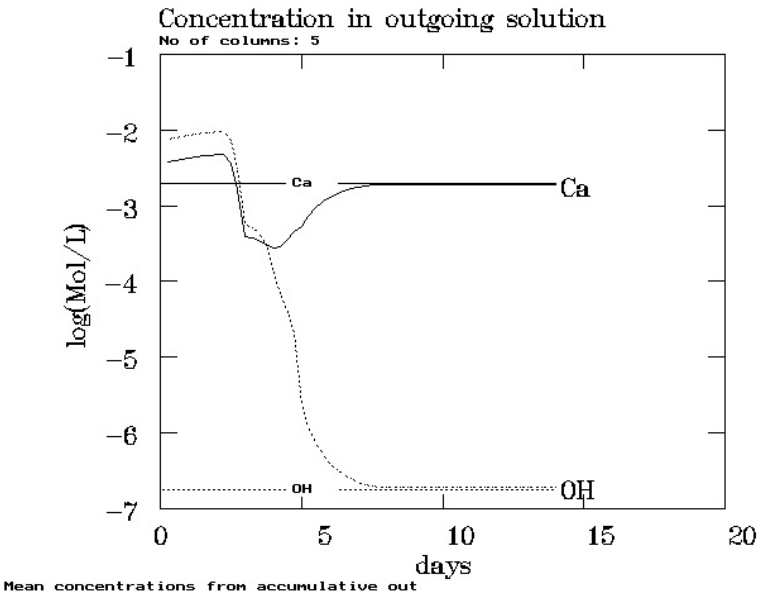

Fig. 23b **a0**

Concentrations versus time for H_2CO_3, HCO_3, CO_3 and OH in solution leaving the crack and concentrations in feed solution (horizontal lines)

Compare with Fig. 17b.

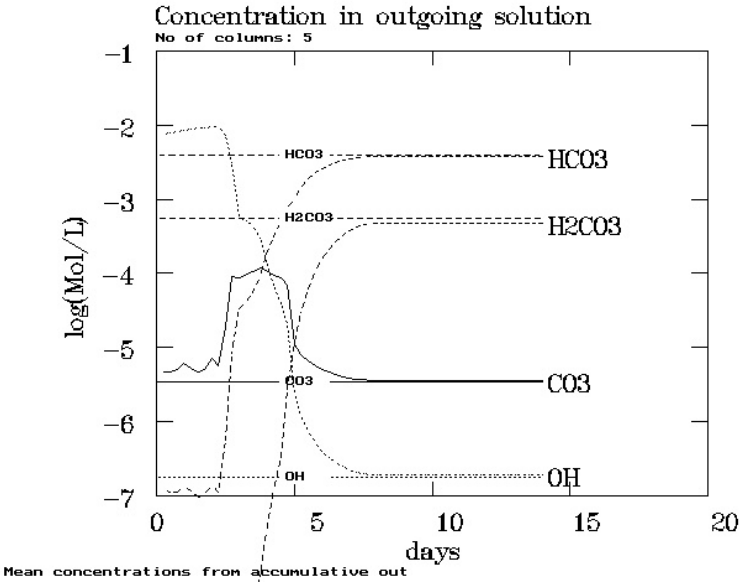

Fig. 23c **a0**

Cut through the five-column system showing the 6 upper layers in the mortar and (on a larger scale) 4 layers in the crack. The grey dots represents sand, red points are $Ca(OH)_2$, yellow is C-S-H etc, and green is calcite. White represents porosity. One grid layer with low porosity is present in all five columns.

Compare with Fig. 17o.

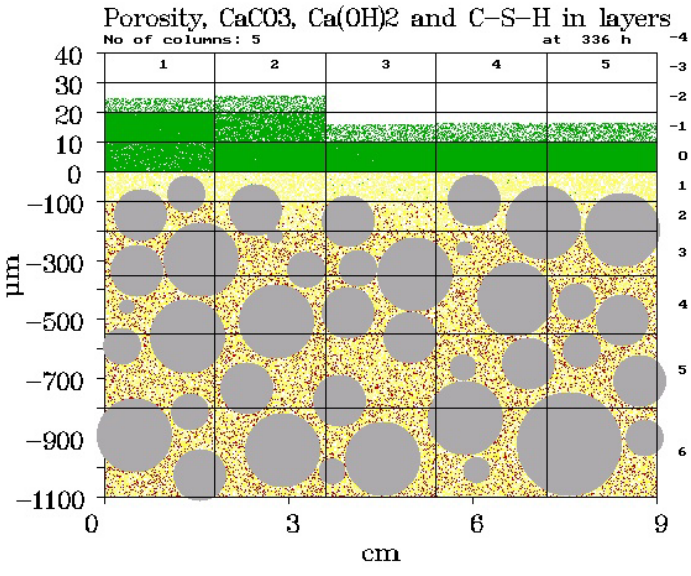

Fig. 23d **a0**

$Ca(OH)_2$ without NaOH, KOH

Concentration profiles for dissolved calcium in pore water in the mortar and calcite layer and in the crack solution. Curves for column 1 (at the feed entrance) and 5 (outlet) after 14 days (fully drawn).

Compare with Fig. 17d

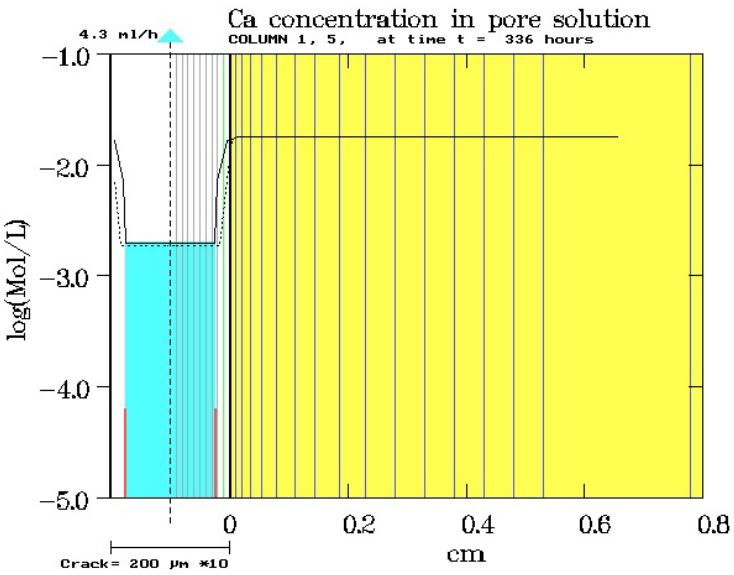

Fig. 23e **a0**

Concentration profiles for CO_3^{2-} in pore water in the mortar and calcite layer and in the crack solution. Curves for column 1 (at the feed entrance) and 5 (outlet) after 14 days (fully drawn).

Compare with Fig. 17e

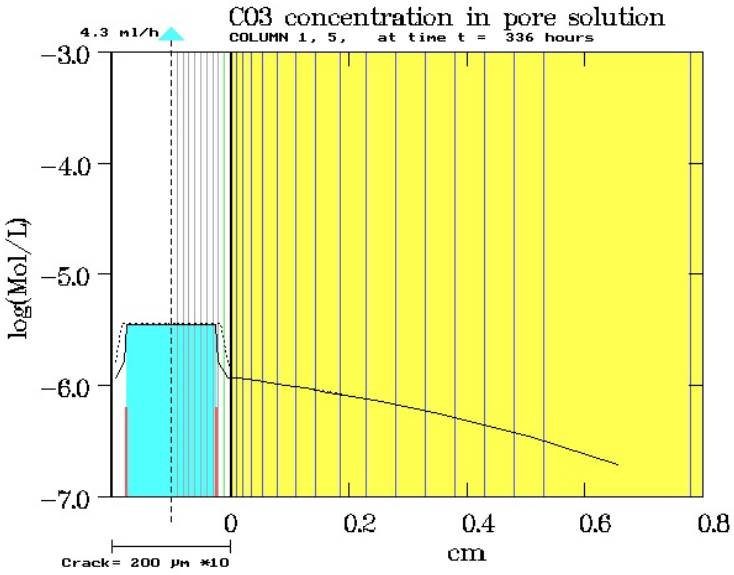

Fig. 23f **a0**

Degree of calcite saturation as obtained from the concentration curves in Figs. 23d and e.

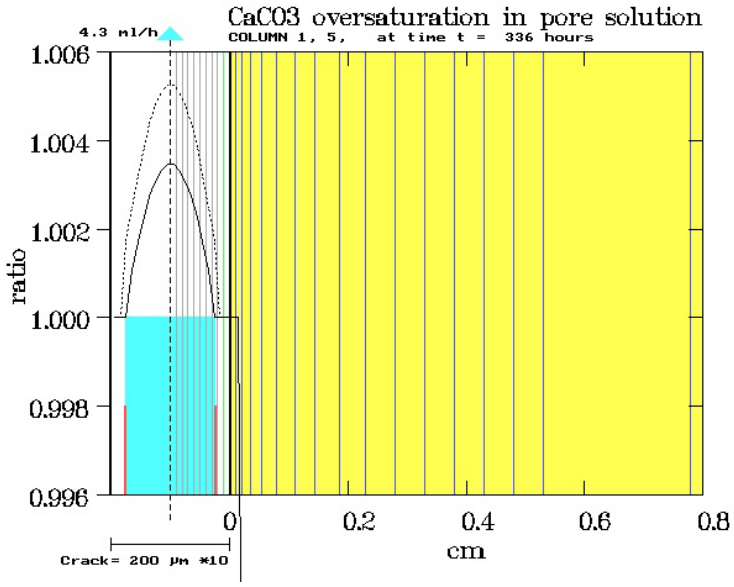

7.6. Aggressive feed solution

In reality the incoming feed solution may not always be in equilibrium with calcite. When sources of excess carbon dioxide are present – most likely biological degradation of organic materials in the soil or in buried waste – the partial pressure p_{CO2} and the concentration c_{H2CO3} of dissolved CO_2 are increased while the pH is somewhat decreased. When passing through a crack in cementitious material such a solution requires additional hydroxyl ions or will dissolve already precipitated calcite before it is equilibrated and can co-exist with solid $CaCO_3$.

Case **aU** illustrates effects of the use of such an aggressive solution as feed into a cracked cement mortar specimen of the same type and other conditions as in the Main case **a**. The feed solution composition is specified in the lower part of Table 3. Compared with the normal saturated solution pH is decreased from 7.21 to 6.80 and the content of undissociated dissolved H_2CO_3 is increased a factor 2.6 to 1.40 mMol/litter corresponding to 3.56 vol % CO_2 as partial pressure (outside the system). The dominating species is still HCO_3^- and the total content of carbonate species is increased a factor 1.24 to 5.62 mMol/litter.

Comparing the variation of composition of the outflowing solution for Case **aU** (Figs. 24a and b) with the corresponding curves for the Main Case **a** (Figs. 17a and b) shows a less pronounced period with low Ca-concentration, and that the calcium curve returns to nearly the exact level of the feed solution (not somewhat below) while the bicarbonate curve is slightly above the level of the feed solution not slightly below as when the feed is saturated. The explanation is that alkali metal hydroxide diffusing out from the mortar is used for converting undissociated H_2CO_3 into HCO_3^- ions but is insufficient to precipitate calcium from the incoming solution.

Fig. 24d shows the degree of calcite saturation in the various grid-layers along the crack after 14 days exposure. It is seen that the degree of $CaCO_3$ saturation increases from 0.4 in the entering feed to slightly above 1 in the solution leaving the crack.

Fig. 24e shows that a thin layer of calcite is also developing on the crack surface with the aggressive solution. A temporary layer of initially precipitated $CaCO_3$ is re-dissolved after some few days from columns 1 and 2, but one grid-layer with dense calcite (ε_{min}=0.001) remains on all 5 columns. This layer is maintained due to balancing of OH^- diffusing out through the calcite pores and the diffusion of aggressive H_2CO_3 in opposite direction through the solution-filled layers in the crack. The presence of the dense calcite layers has the usual effect of decreased slope of the leach curves for Na, R1 and R2 (Fig. 24c) and the associated build-up of sodium concentrations etc. behind the barrier layer.

Other types of aggressive solutions with less or no calcium may also be envisaged. Case **aUU,** has been calculated using a feed solution with as above 5.62 mMol carbonate species per litter but no calcium. The CO_2 partial pressure is then 0.13. This more aggressive solution produces the layer profile shown in Fig. 24f with no calcite retained on top of the first column, but significant amounts precipitated in the first grid layer of the cement mortar reducing the porosity from 26 to 14 %. Otherwise the curves are more extreme versions of Case **aU** in Figs. 24a,b,c and d. The calcite saturation curves increases from 0 at the entrance ~1 in the outflowing solution. Some mass-balance problems were encountered and Case **aUU** is on the margin of what can be handled by the model.

7.7. Double solution residence time

An idea about the effects of change in geometrical dimensions of the crack can be obtained from Case $\mathbf{a_{2a}}$ where the crack width is doubled from 0.2 to 0.4 mm, and Case $\mathbf{a_{2L}}$ where the crack length is doubled from 9 to 18 cm. Otherwise the model is unchanged, i.e. the column and grid numbers are unchanged, but the grid dimensions are doubled in thickness (from 10 to 20 μm in the crack) or in column cross-section ($18 \cdot 3.5/5 = 13.6$ in stead of 6.8 cm^2). Feed rate and other parameters are unchanged. In both cases the initial residence time for the solution in the crack is increased a factor 2, from 53 to 106 seconds.

A Case $\mathbf{a_{½m}}$ with half the flow rate employed in the other examples have also been included. This is another manner to obtain a double initial solution residence time of 106 seconds.

For Case **a2a** with double crack width Figs. 25a shows – compared with the Main Case Fig. 17a – that the decrease in calcium concentration in the outflowing solution is less in degree but drawn out over a longer period. The 14 days calculation period is not sufficient for development of grid layers with $\varepsilon_{min} = 0.001$ on the columns. The minimum values for the porosity were only reduced to 0.3, 0.3, 4, 10 and 25 % on column 1 to 5. This may simply be because more calcite is needed to reach low porosity in a 20 μm than in a 10 μm thick grid cell, see also Fig. 25f.

The development of a diffusion barrier with 0.3 % porosity is reflected in the Ca-concentration profiles for column 1 shown in Fig. 25d. The Ca-concentration curve after 7 days exposure shows the effect of OH^- build up behind the calcite barrier. The distances in the wider crack is also in this case shown multiplied with a factor 10 relative to the distances in the mortar.

More calcite is precipitated in Case $\mathbf{a_{2a}}$: 5.36 mMol against 3.77 in the main case (see Fig. 25b and 17c and Table 5). The reason is probably a combination of longer residence time and longer time required for development of a dense calcite layers functioning as diffusion barrier. The later is also reflected in the absence of a decrease in slope of the leach curves in Fig. 25c.

Fig. 25d shows the porosity of the layers in column 1 after 14 days (the two outer layers of the mortar is depleted for $Ca(OH)_2$ while the Main Case **a** only had one, see Fig. 17r). The laminar flow profile in the crack is also shown.

For Case $\mathbf{a_{2L}}$ with double crack length the period with $Ca(OH)_2$ leaching from freshly exposed mortar is extended and the period with decreased calcium concentration is delayed and does not end within the 14 days calculation period. Additional time will be required before sufficient calcite is available for generation of a dense layer on the last two columns resulting in the return of the calcium concentration towards the value in the feed.

In Case $\mathbf{a_{2L}}$ the amount of deposited calcite is 6.27 mMol, even higher than in Case $\mathbf{a_{2a}}$, while the amount of unprecipitated carbonate species passing through the crack is 0.44 mMol, the lowest in any of the calculation examples. As it is seen from Fig. 26f the calcite is deposited near the feed entrance, primarily on column 1. The solution is thereby depleted for carbonate species, which explains the slow formation of a covering layer on the later columns. However, the minimum 0.1% porosity was reached for calcite layers on column 1, 2 and 3, and some decrease in slope of the leach curves in Fig. 26c can already be seen.

Fig. 24a aU

Unsaturated feed solution

Concentrations versus time for Ca, Na and OH in solution leaving the crack and Ca concentration in the feed solution (horizontal line)

Compare with Fig. 17a.

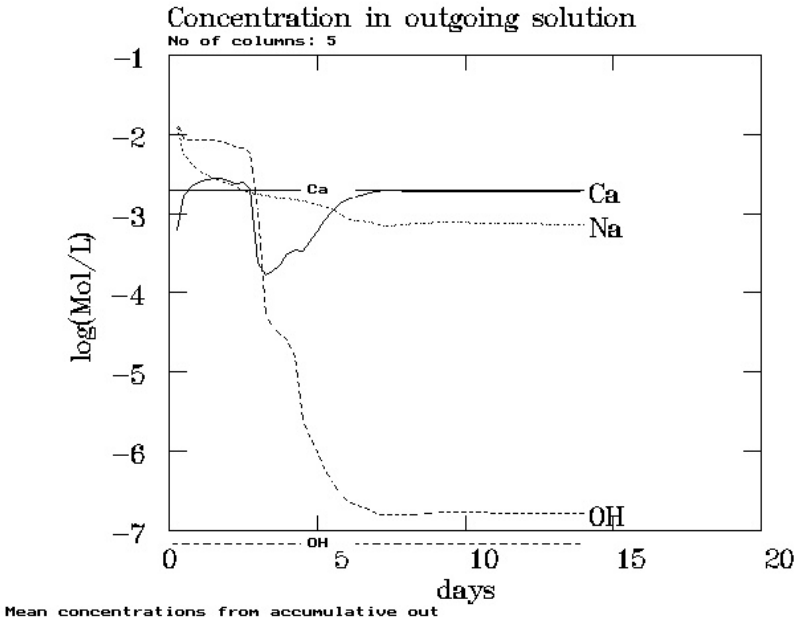

Fig. 24b aU

Concentrations versus time for H_2CO_3, HCO_3, CO_3 and OH in solution leaving the crack.
and concentrations in feed solution (horizontal lines)

Compare with Fig. 17b.

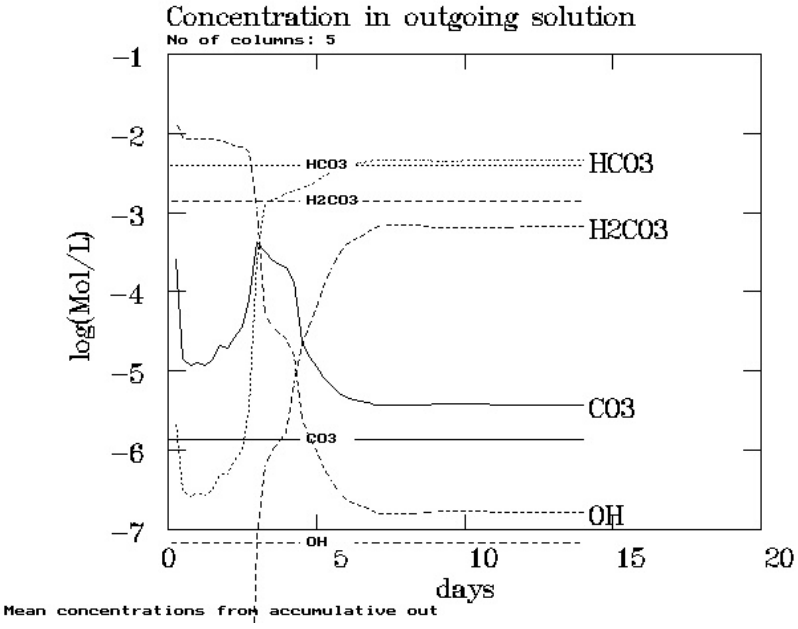

Fig. 24c aU

Leach curves for sodium, R1 and R2 (incidentally nearly the same as for sodium). Equivalent leached thickness versus square root of time. After about one week the slope of the curves are somewhat decreased. Diffusivities are indicated in the figure.

Compare with Figs. 17j,k and 21b

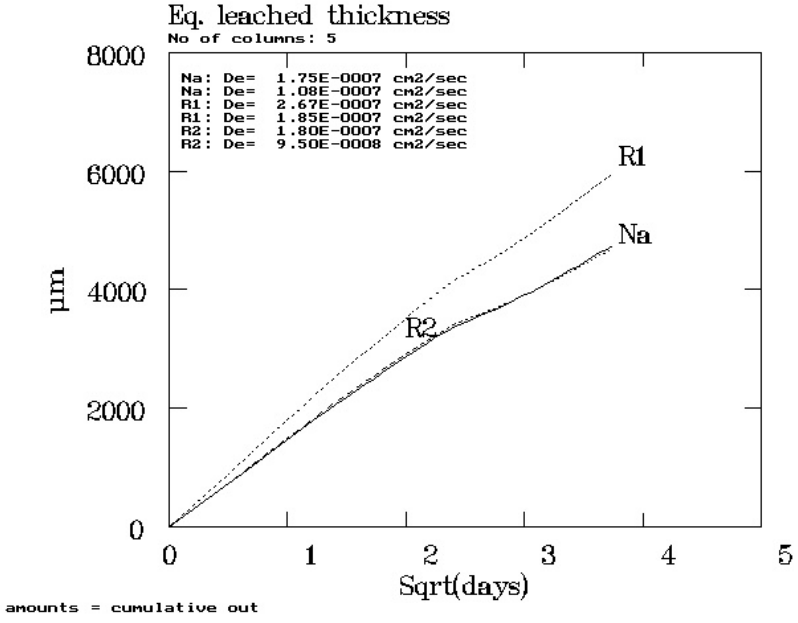

Fig. 24d **aU**

Unsaturated feed solution

Degree of calcite saturation in various grid layers along the length of the crack. The solution in the crack remains unsaturated until column five. The pore solution is saturated in layers with calcite (-1 and 0) and unsaturated in the deeper part of the mortar. The out-flowing solution is slightly oversaturated after mixing.

Compare with Fig. 17l.

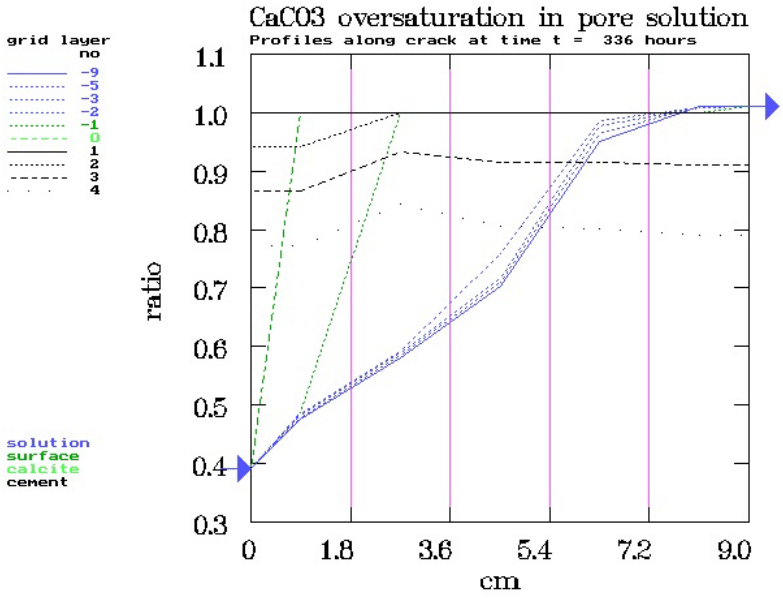

Fig. 24g **aU**

Cut through the five column system showing the 6 upper layers in the mortar and (on a larger scale) 4 layers in the crack after 14 days exposure.
A thin but low-porosity calcite layer is present on all columns.

Compare with Fig. 17o

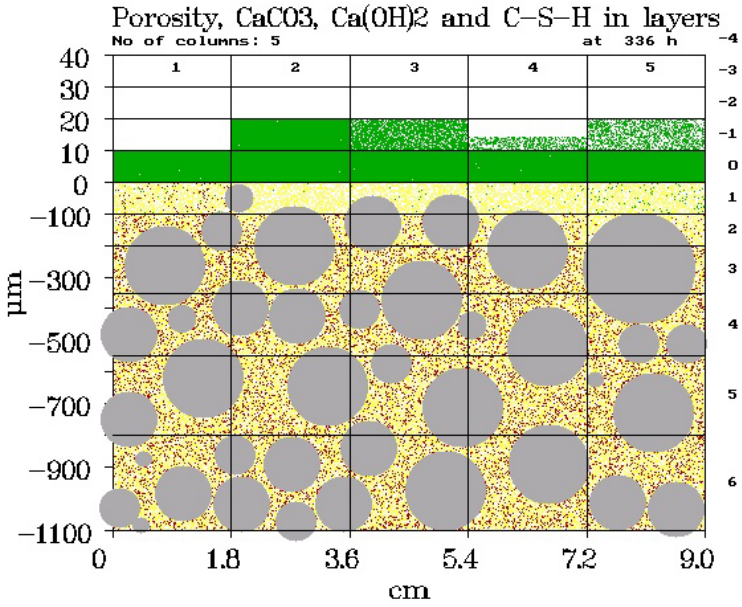

Fig. 24f **aUU**

Aggressive, pure CO_2 solution

Cut through the five-column system after 14 days exposure.
Aggressive corrosion and deposition of calcite in the outer mortar layer of the first column.
A thin low-porosity layer covers the other four columns.

Compare with Fig. 24g

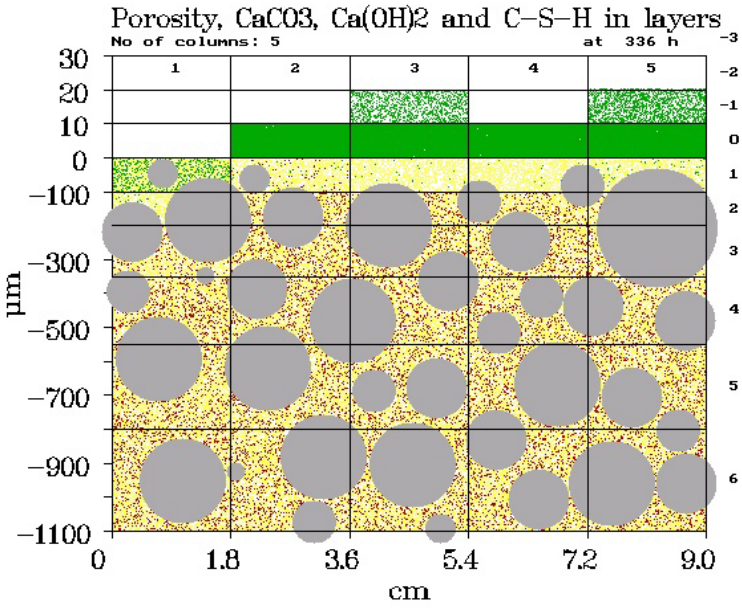

Fig. 25a **a_{2a}**

Double crack width:

a = 0.4 mm

Concentrations versus time for Ca, Na and OH in solution leaving the crack, and Ca concentration in the feed solution (horizontal line)

Compare with Fig. 17a

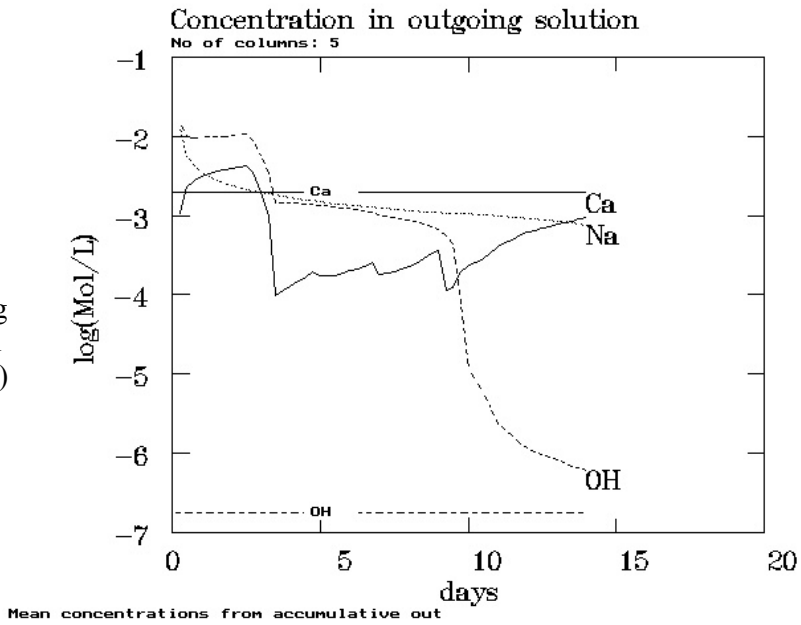

Fig. 25b **a_{2a}**

Cumulative amounts of precipitated calcite, and (negative) Ca removed from the system with the outflowing solution, and calcium, potassium and hydroxide leached from the mortar.

Compare with Fig. 17c.

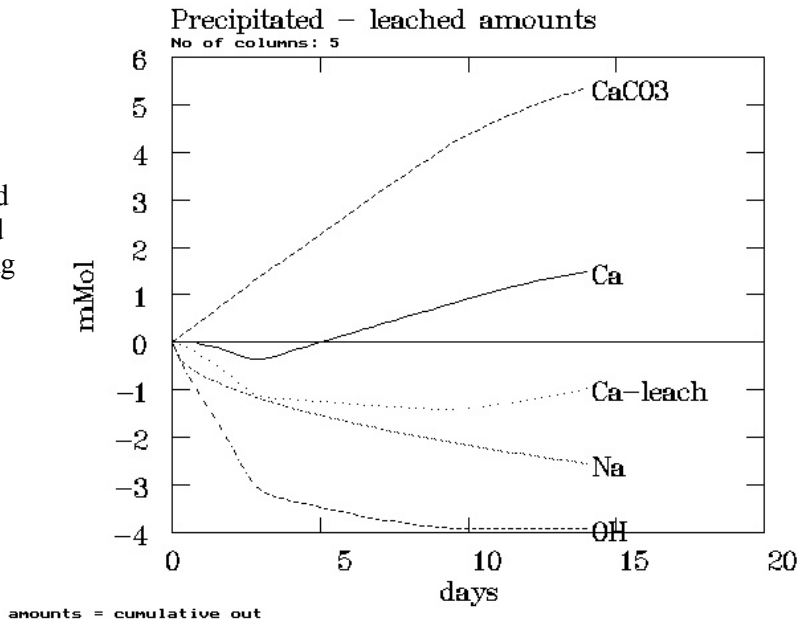

Fig. 25c **a_{2a}**

Leach curve for sodium and a radioisotope (Cs) calculated with (R1) and without (R2) correction for electrical interactions. The equivalent leached thickness is plotted versus the square root of time. Diffusivities corresponding to the slopes of the nearly straight lines are indicated in the figure.

Compare with Figs. 17j and k.

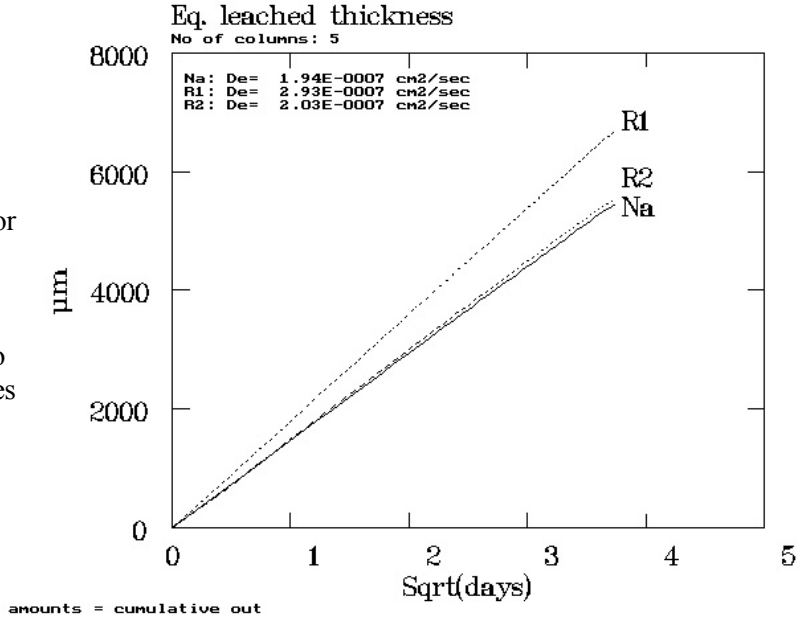

Fig. 25d a_{2a}

Double crack width:
a=0.4 mm

Concentration profiles for dissolved calcium in pore water in the mortar, calcite layer and the solution in the crack. Curves for column 1 (at the feed entrance) at t = 0 (horizontal) and after 3½, 7, 10½ and 14 days exposure. The fully drawn curve is for 14 days and shows the effect of formation of the covering layer.

Compare with Fig. 17p.

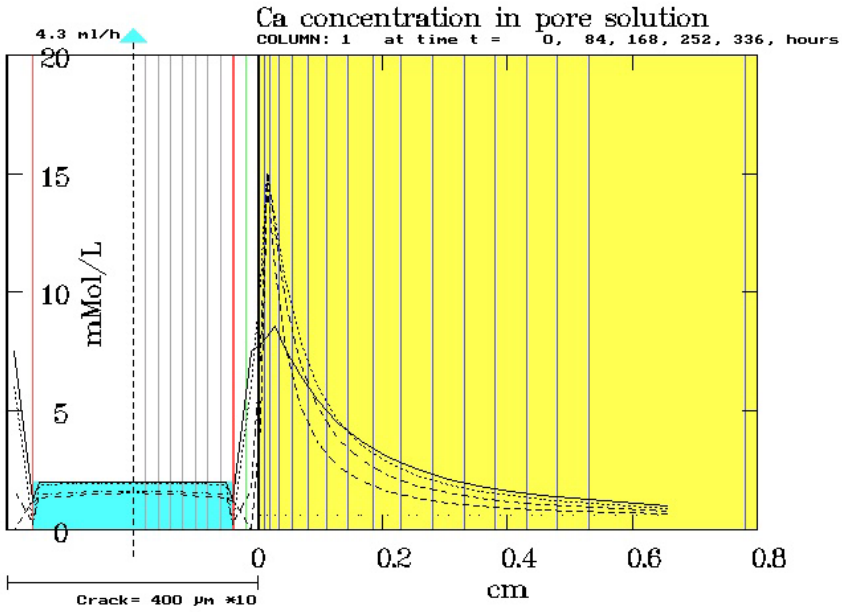

Fig. 25e a_{2a}

Porosity of the layers in column 1 after 14 days.
Leaching of $Ca(OH)_2$ increases the porosity of the outer mortar layers. The outer of the two grid layers with calcite has low porosity.
The blue curve shows the velocity profile for the solution in the crack.

Compare with Fig. 17r.

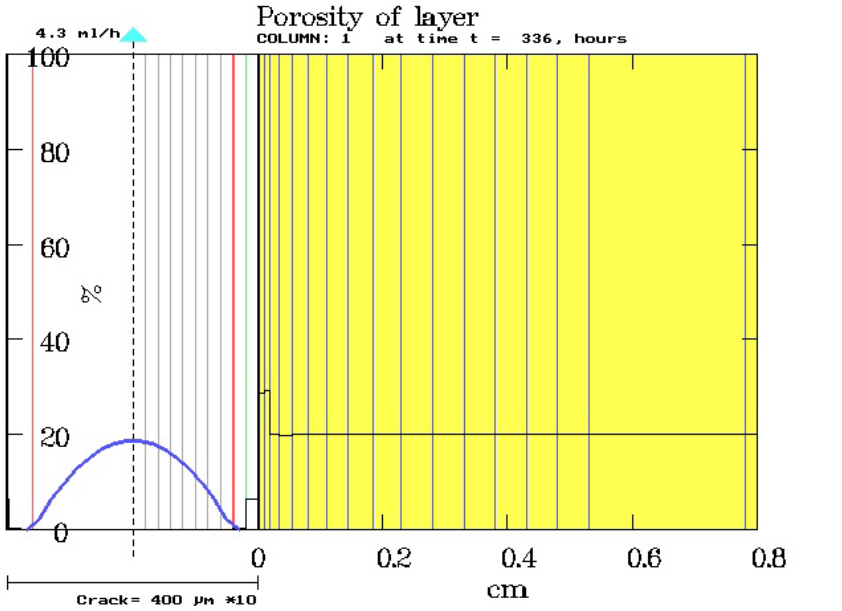

Fig. 25f a_{2a}

Cut through the five-column system showing the 6 upper layers in the mortar and (twice as thick as normally) 3 layers in the crack. The grey dots represents sand, red points are $Ca(OH)_2$, yellow is C-S-H etc, and green is calcite. White represents porosity. The grid layers on the last columns has not yet reached low porosity.

Compare with Fig. 17j and k

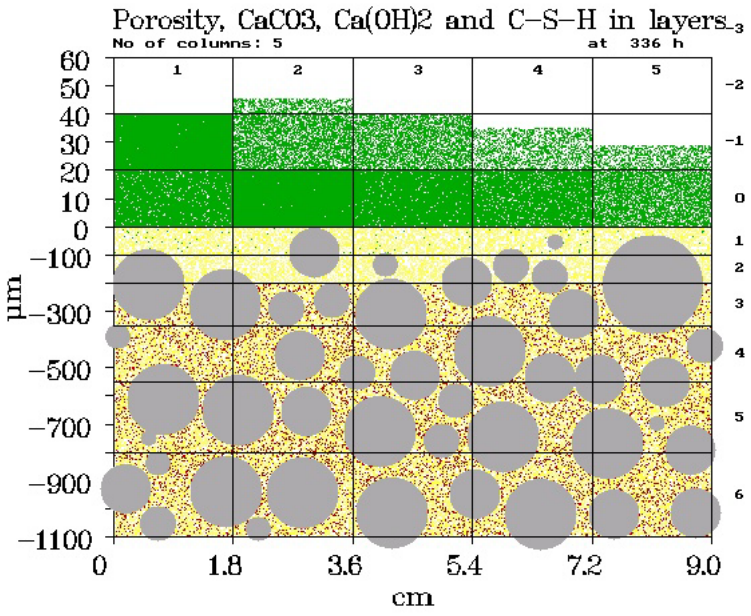

Fig. 26a a_{2L}

Double crack length:

L = 18 cm

Concentrations versus time for Ca, Na and OH in solution leaving the crack and Ca-concentration in the feed solution (horizontal line).

Compare with Fig. 17a.

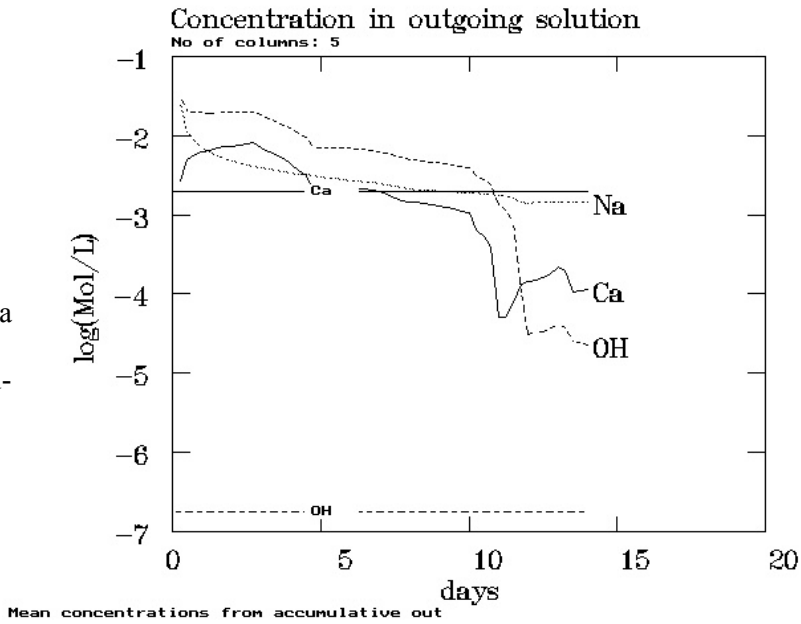

Fig. 26b a_{2L}

Calculated amounts of precipitated calcite, and (negative) removed calcium, and calcium, sodium and hydroxide leached from the mortar.

Compare with Fig. 17c.

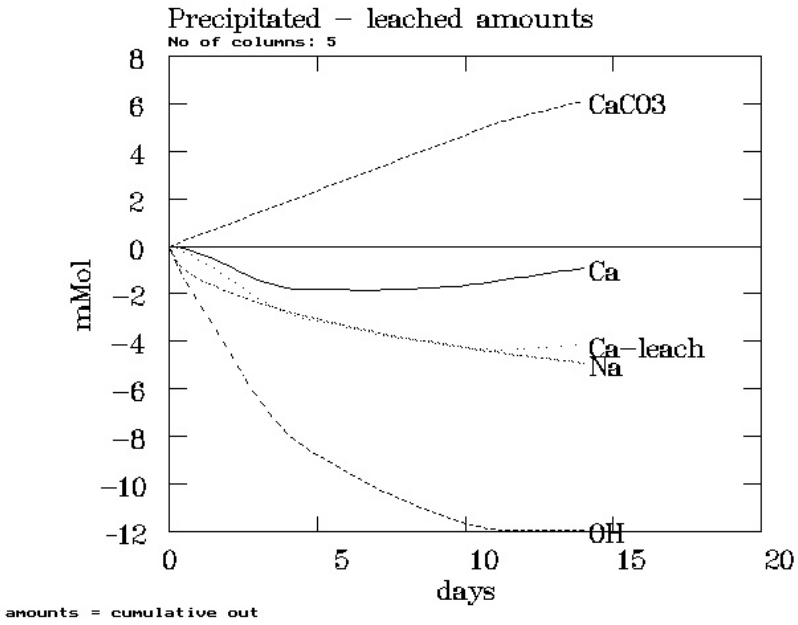

Fig. 26c a_{2L}

Leach curve for sodium and a radioisotope (Cs) calculated with and without correction for electrical interactions. The equivalent leached thickness is plotted versus the square root of time. Diffusivities corresponding to the slopes of the beginning and the end of the curves are indicated in the figure.

Compare with Figs. 17j and k.

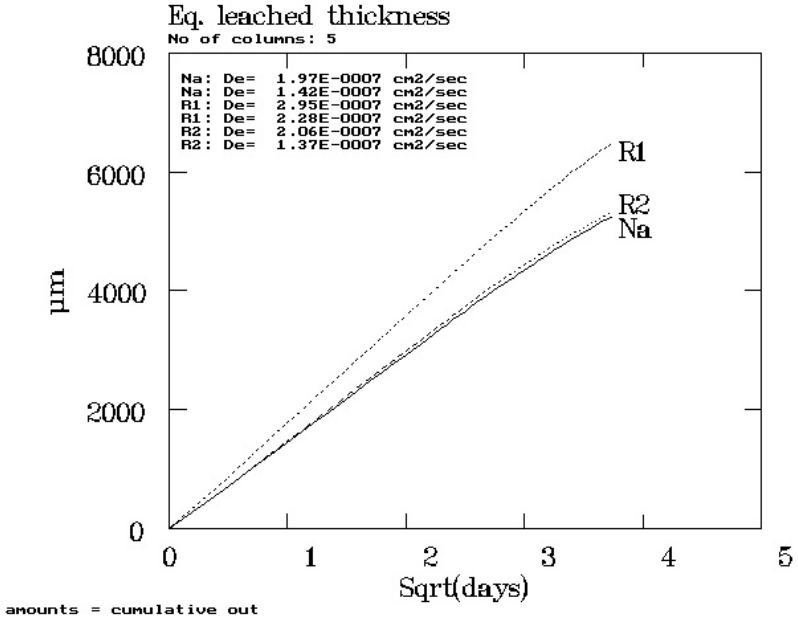

Fig. 26d **a_{2L}**

Double crack length:
L = 18 cm

Concentration profiles for sodium in pore water in the mortar, calcite layer and (not visible) the solution in the crack. Curves for column 1 (at the feed entrance) at t = 0 (horizontal) and after 3½, 7, 10½ and 14 days exposure. The fully drawn curve is for 14 days and shows the effect of formation of a tight covering layer.

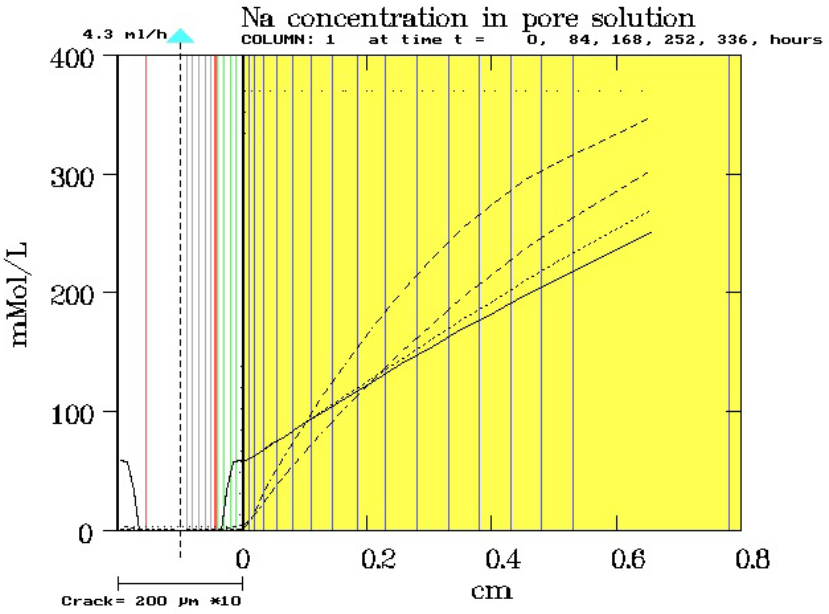

Fig. 26e **a_{2L}**

Porosity of the layers in column 1 after 14 days. Leaching of $Ca(OH)_2$ has increased the porosity of the outer mortar layers. The third of the four grid layers with calcite has low porosity. The blue curve shows the velocity profile for the solution in the crack.

Compare with Fig. 17r

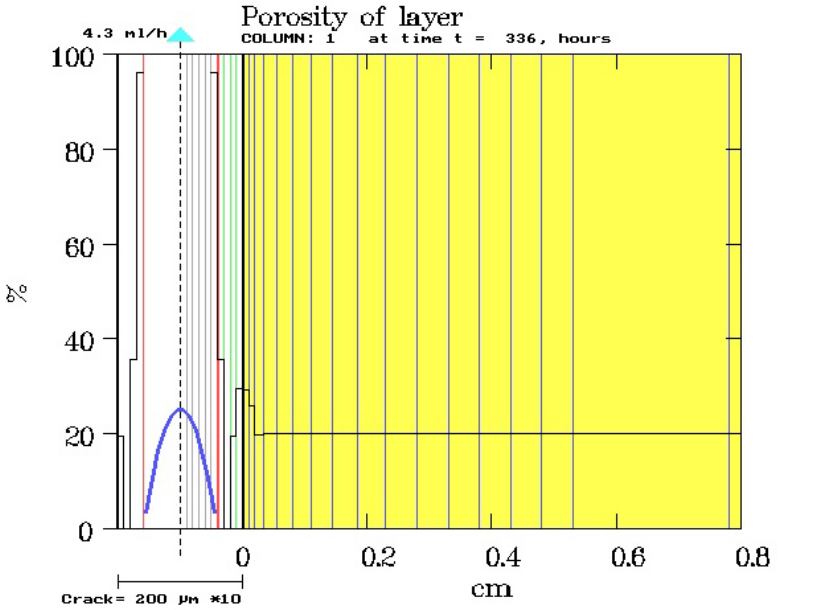

Fig. 26f **a_{2L}**

Cut through the five-column system showing the 6 upper layers in the mortar and 5 layers in the crack. The grey dots represents sand, red points are $Ca(OH)_2$, yellow is C-S-H etc, and green is calcite. White represents porosity. The grid layers on the last two columns are thin and have not reached low porosity.

Compare with Fig. 17o

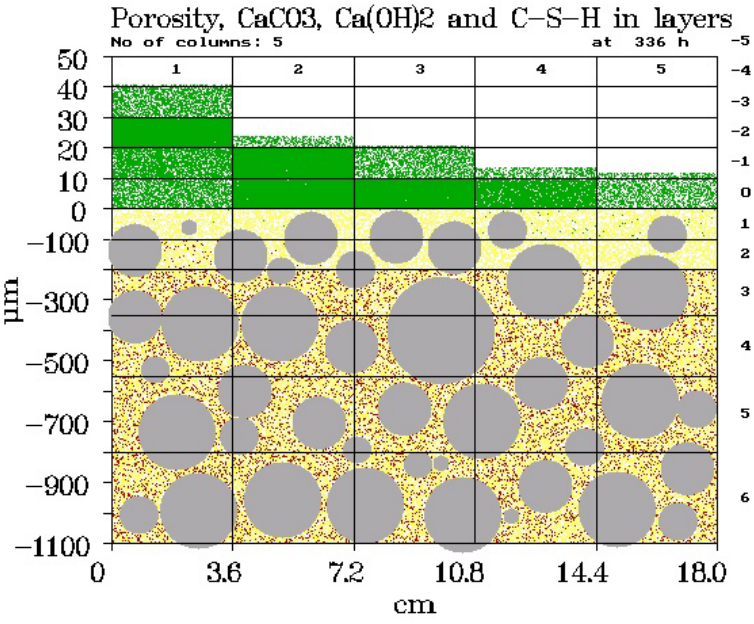

Case **a½m** with half the normal flow rate in a crack of the usual 9 cm length turned out to give calculation results practically identical to Case **a2L**. The concentration development in the outflowing solution was exactly the same (Fig. 26a) and the leach curves and apparent diffusivities for Na, R1 and R2 were also identical. (Fig. 26c). The amounts of precipitated and leached materials (Fig. 26b) were halved resulting in a distribution of precipitate exactly as in Fig. 26f although distributed over 9 cm in stead of 18.

It follows that doubling of the crack length or halving of the flow rate gives rise to rather similar reactions from the system. Separate figures for Case **a½m** were omitted.

7.8 Porous cementitious backfill

As a supplement to the examples with the type b mortar a single calculation has been performed for a cement mortar with especially high porosity. Such materials can be use as backfill in waste repositories where the filling of voids etc. is desirable to diminish liquid flow while possibilities for release of gases generated e.g. by metal corrosion must be maintained.

The product used in the Case **bf6ff** calculation has 50 % porosity. For simplicity and ease of comparison the contents of $Ca(OH)_2$ and alkali metal hydroxide are supposed to be the same as for the type b mortar used in the other examples. The increase in porosity from 20 to 50 % is obtained on the expense of a decreased content of sand in the mortar. In practice this is not a realistic possibility and if needed the model can also be set up for calculations on 'real' backfills e.g. of the three types used in experimental work described in [7].

One effect of the increased porosity is that the initial concentration of the alkali metal hydroxide in the pore solution is decreased because the same amount of NaOH is now dissolved in a larger volume of pore solution, compare the horizontal line in Fig. 27d with the corresponding lines for the type b mortar with 20 % porosity in e.g. Fig. 17g.

The effect of increased porosity should be a higher rate of diffusion of dissolved species in the pore solution in the backfill mortar. However, when the concentration (e.g. of sodium) is decreasing proportionally with the increasing porosity the amount of leached material and the apparent D_{leach} value are not directly influenced by the porosity. To match experimentally observed Na-diffusivities the form factor must increase with increasing porosity, see Section 5. For Case **bf6ff** ff = 0.3 was selected, i.e. considerably higher than the values between 0.1 and 0.025 used in the examples with varying pore diffusivities in type b mortar, see Section 7.4.

With ff = 0.3 the apparent diffusivities corresponding to the initial slope of the Na-leach curve in Fig. 27b is $1.0\ 10^{-6}$ cm^2/s in agreement with measurements on cementitious backfill materials, see Table 2 in Section 6.3. Only a slight decline in slope occurs at the end of the leach curves.

For comparison Fig. 27c shows the leach curves obtained in another calculation on 50 % porosity backfill using 0.05 as ff value. The initial slope of the Na-curve then corresponds to $1.65\ 10^{-7}$ cm^2/s, which is too low for this type of material and actually slightly lower than obtained for the Main Case **a** , see Fig. 17j.

For calcium and to some degree also hydroxyl the pore solution concentrations are determined by equilibrium with solid material. Both the larger volume of solution-filled pore

space available for diffusion and the increased ff value will the increase the amount of leached material.

The concentrations of cat- and anions in outflowing solution are shown in Fig. 27a and b. It is seen that the initial period with high leaching of $Ca(OH)_2$ is extended and that minimum and later increasing Ca-concentration was not reached within the 14 days calculation period. This is also partly due to the use of the same high ff value for the backfill mortar and the precipitated calcite layers permitting a higher release through the barrier.

The calcite porosity in one or two grid layers on the first four columns has reached the 0.001 minimum value, while this is not yet the case for the column at the outlet where the porosity is still about 40 %. The precipitation of calcite is especially large at the front end of the specimen where calcite fills 92 % of the crack, see Fig. 27f. The corresponding pressure loss is 1.8 cm H_2O, the highest value found in any of the example calculations. The leaching of the backfill mortar for $Ca(OH)_2$ is considerable as shown by the absence of red points in 3 or 4 of the outer mortar grid layers.

Figs. 27d and 27e shows the concentrations profiles in column 1 at the feed entrance after 3½, 7 10½ and 14 days. The sodium curves are more flat than usual reflecting the lower initial Na-concentration. The curves at 3½ days are before formation of a low porosity calcite layer. Consequently Na (and OH) concentrations are low and the Ca-concentrations high. Later the concentrations of Na and Ca is seen to drop over grid layer –7 where the porosity is low.

In general the calculation example confirms the experimental observation that formation of calcite layers preventing efficient contact between solution and the bulk material is also a possibility in coarse cracks in cement mortars of the backfill type.

Changing the program so that calculation with different ff-values in mortar and calcite layers is possible would be of interest.

Fig. 27a **bf_{6ff}**

Porous cement mortar (back fill)

$\varepsilon_{prod} = 0.5$ ff = 0.3

Concentrations of Ca, Na and OH in solution leaving the crack. Ca-concentration in the feed solution (horizontal line).

Compare with Fig. 17a.

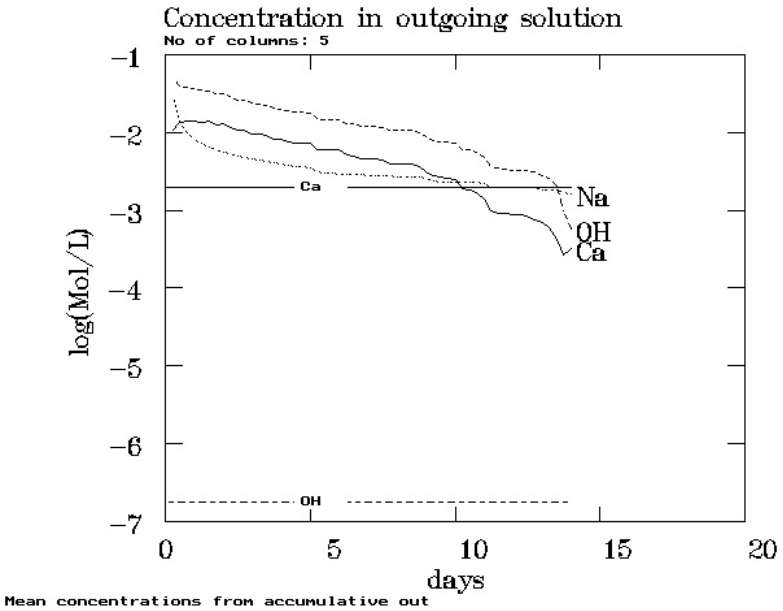

Fig. 27b **bf_{6ff}**

Leach curves for sodium and a radioisotope (Cs) calculated with and without correction for electrical interactions. The equivalent leached thickness is plotted versus the square root of time. Diffusivities corresponding to the slopes of the beginning and the end of the curves are indicated in the figure.

Compare with Figs. 17j and k.

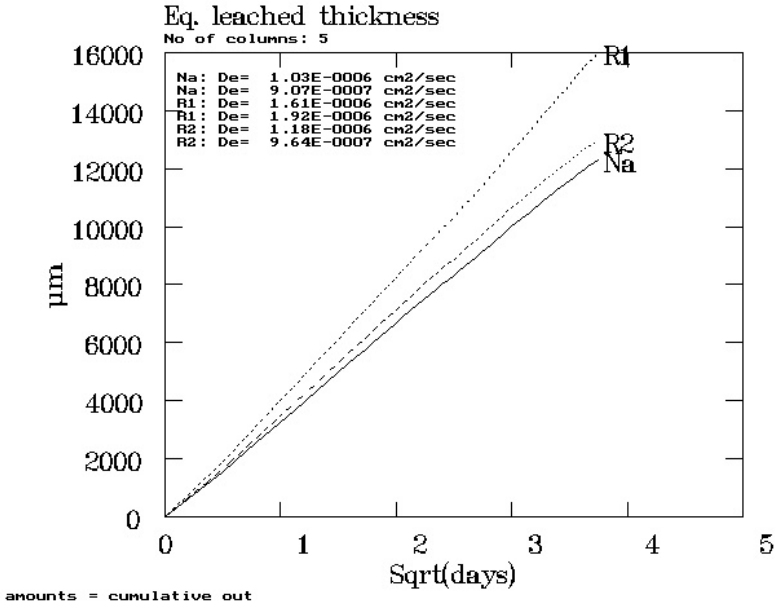

Fig. 27c **bf_{1ff}**

Porous cement mortar (with too low form factor)

$\varepsilon_{prod} = 0.5$ ff = 0.05

Leach curves for sodium and a radioisotope (Cs) as in Fig. 27b. Product porosity is the same but the form factor is as used in the Main Case for type b mortar. The diffusivities are then nearly unchanged.

Compare with Figs. 17j and k.

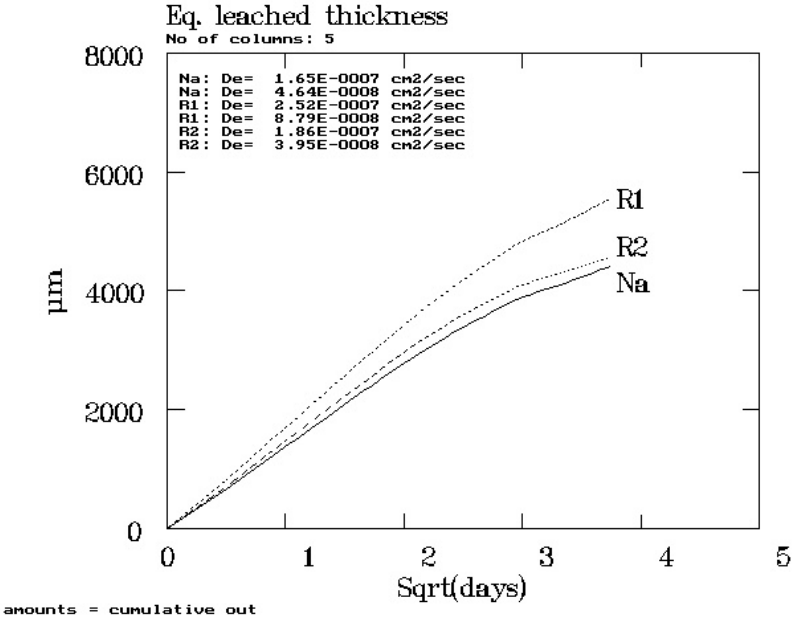

Fig. 27d **bf_{6ff}**

Porous cement mortar (back fill)

$\varepsilon_{prod} = 0.5$ ff=0.3

Concentration profiles for sodium in pore water in the backfill, the calcite layer and (not visible) the solution in the crack. Curves for column 1 (at the feed entrance) at t = 0 (horizontal) and after 3½, 7, 10½ and 14 days exposure.

Compare with Fig. 17g

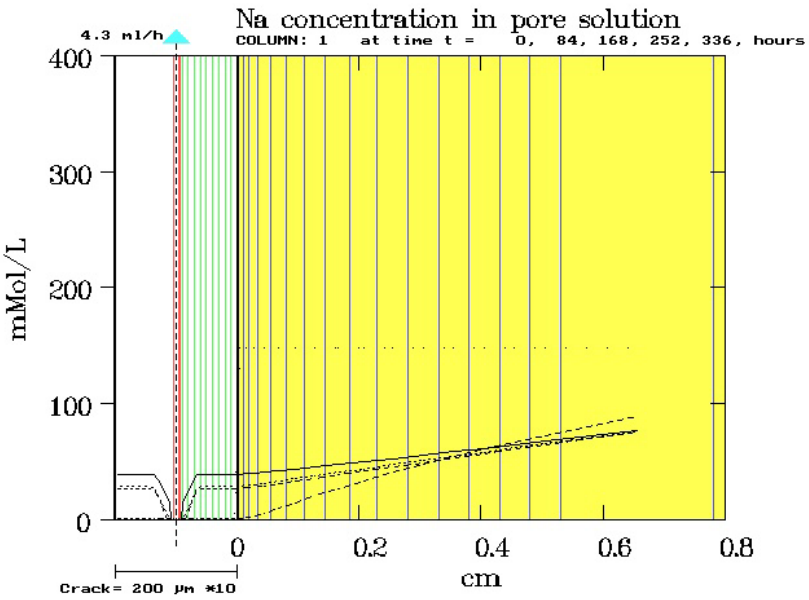

Fig. 27e **bf_{6ff}**

Concentration profiles for calcium in pore water in the backfill, the calcite layer and (not visible) the solution in the crack. Curves for the nearly closed column 1 (at the feed entrance) at t = 0 (horizontal) and after 3½, 7, 10½ and 14 days exposure.

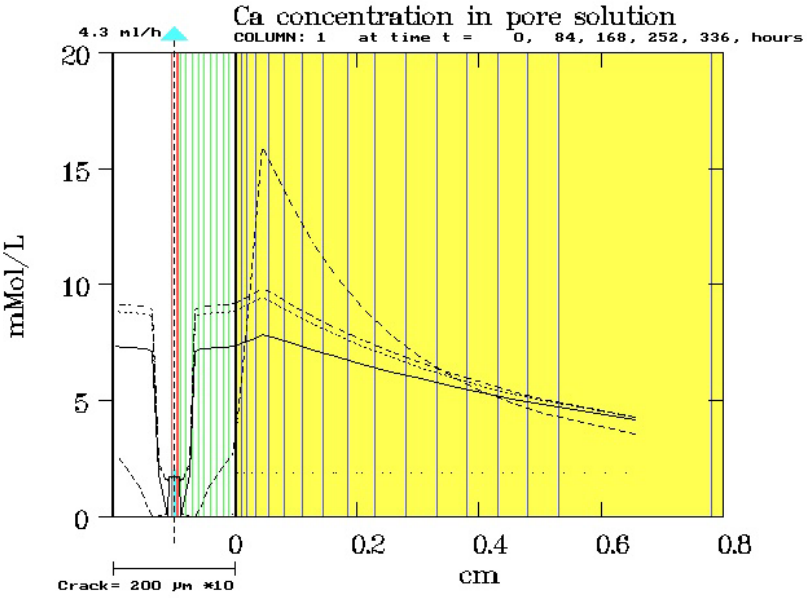

Fig. 27f **bf_{6ff}**

Cut through the five-column system showing the 6 upper layers in the mortar and 5 layers in the crack. The grey dots represents sand, red points are $Ca(OH)_2$, yellow is C-S-H etc, and green is calcite. White represents porosity.
The assumed increased mortar porosity is compensated by less sand in the product.

Compare with Fig. 17o

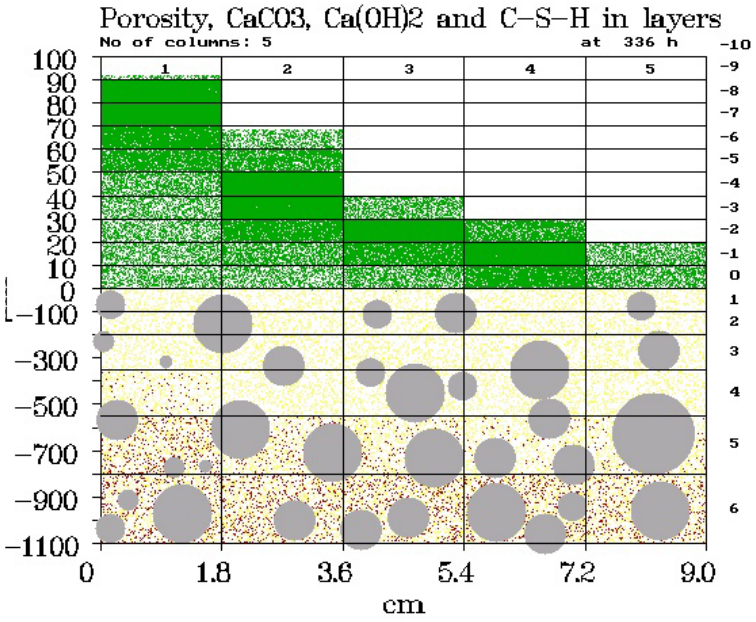

7.9. Summary

The series of example calculations demonstrate some effects of parameter variations and other assumptions about system set-up. Table 5 contains a summary of the calculated cumulative amounts of calcium, sodium and hydroxide diffused out from the cement mortar.

The amounts of calcium carbonate precipitated inside the crack over an initial 14 days period are also given together with the cumulative amount of carbonate species removed with the outflowing solution after passage of the crack.

Table 5. Summary of results from the calculation examples showing of the amount of materials diffused out from the cement mortar, the amount of precipitated calcite, and the amount of the carbonate species which entered with the feed but was not precipitated. To the left the apparent Na-diffusivities obtained from the slope of leach curves before and after formation of the covering calcite layer are compared with the pore-diffusivity for Na used in the calculations.

	Out-diffused from cement mortar			Precipitated	CO_2-species out from system	Na-diffusivities		
						D_{leach}		Dp_{Na}
	Ca	Na	OH	$CaCO_3$		initial	late	
Type b mortar $\varepsilon_{prod} = 0.20$	mMol after 14 days					10^{-7} cm^2/s		
b high final calcite porosity $\varepsilon_{min} = 0.2$ +	3.34	2.53	9.37	4.91	1.66	1.97	1.83	1.33
a Main case $\varepsilon_{prod} = 0.20$ $\varepsilon_{min} = 0.001$ $\varepsilon_{precip} = 0.50$ +	2.68	2.31	7.86	3.77	2.80	1.90	0.98	1.33
a_{35P} $\varepsilon_{precip} = 0.35$ +	2.52	2.26	7.62	3.63	2.94	1.87	0.88	1.33
a_{65P} $\varepsilon_{precip} = 0.65$ +	3.01	2.32	8.42	4.17	2.40	1.93	0.91	1.33
a_{80P} $\varepsilon_{precip} = 0.80$ +	3.60	2.48	9.78	5.10	1.47	1.97	1.46	1.33
$a_{½ff}$ decreased pore diffusivity ff = 0.025 +	1.86	1.62	5.43	3.35	3.22	0.94	0.43	0.67
a_{2ff} increased pore diffusivity ff = 0.100 +	3.78	3.27	11.02	4.23	2.34	3.65	2.11	2.67
a0 without NaOH +	2.78	-	5.58	2.81	3.76	-	-	-
aU aggressive feed solution +	2.06	2.21	6.55	2.61	5.10	1.57	1.08	1.33
aUU pure CO_2 solution	1.58?	2.27	6.06	2.50	5.31	1.95	1.53	1.33
a_{2a} double crack width 5	3.73	2.53	19.18	5.36	1.21	1.94	1.94	1.33
a_{2L} double crack length 4, 5	6.86	4.90	18.85	6.13	0.44	1.97	1.42	1.33
$a_{½m}$ reduced flow 4, 5	3.43	2.45	9.42	3.06	0.22	1.97	1.42	1.33
Backfill $\varepsilon_{prod} = 0.50$								
bf_{6ff} ff = 0.300 5	11.63	5.73	29.00	6.45	0.12	10.3	9.07	8.00
bf ff = 0.050 +	4.16	2.06	10.43	4.04	2.53	1.65	0.46	1.33

The cumulative amounts represent a snapshot of the status of the systems after the arbitrarily selected 14 days calculation period. They reflect assumptions about diffusivities etc. but also that the status of the systems can be different: In some cases a low porosity calcite layer covers the entire surface of the crack (indicated by + in the table), and in others the layer is still in a formative state with high porosity permitting increased leaching from one or more columns at the outlet from the crack (the column numbers are given in the table).

Calcium and OH-releases are increased with increasing values for the initial and final porosity of the calcite layer (ε_{precip} and ε_{min}), with increasing values for the form factor ff , and especially if formation of the covering layer is slow.

Sodium release is primarily determined by the selected ff value. To the right in the table the Na-diffusivities corresponding to the slopes of the sodium leach curves at the beginning and towards the end of the 14 days period are compared with the Na pore diffusivity $Dp = ff \cdot Dw$ used in the calculation. Formation of a low porosity ($\varepsilon_{min} = 0.001$) and completely covering layer decreases the D_{leach} value about a factor 2. The same ff-value is used for the mortar as well as the calcite layer and for high values of ff this may diminish the sealing effects of the calcite in an unrealistic manner.

The difference OH-2Ca-Na is a measure for the small amount of OH^- balanced by in-diffusion of carbonate species into the mortar. The value varies between 0.02 and 0.19 equivalents. In general only a few % of the total calcite is precipitated inside the mortar, the rest is present in the covering layer on the crack surface.

The sum of precipitated calcite and carbonate species removed with the outflowing solution is equal to the amount of carbonate species entering with the feed solution, in most of the examples 6.57 mMol.

The examples with changed chemical composition of the mortar (e.g. without NaOH) or with especially high porosity (backfills) illustrate that the model can handle various types of cement mortar.

The geometry of the crack, i.e. crack width and crack length relative to the flow rate of the feed solution has a strong influence on development of the system. However, the effect of increased grid layer thickness when the crack width is increase may introduce artefacts and should be investigated.

8. Discussion and conclusions

The numerical CRACK2 model presented in this report is of pseudo-two dimensional type combining advective transport of dissolved material through a crack in a cementitious material with diffusive transport of hydroxyl and other ions perpendicular to the crack. The transport equations are coupled with chemical equilibria for the dissolution/precipitation of calcium hydroxide and calcium carbonate and for the reactions between hydroxide ions and dissolved carbonate species. Together this has been sufficient to simulate characteristic features from experiments where a flow of calcium bicarbonate solution is passing slowly through a crack in cement mortar specimens.

The model simulates the formation of a covering layer of calcite crystals on the inner surfaces of the crack and demonstrates the effects such a layer can have on possibilities for chemical interaction between the flowing solution and the bulk of the cement mortar. This is important for understanding buffering behaviour and possibilities for transport of dissolved materials (such as radioisotopes) through a cracked concrete barrier.

Diffusive transport in the pore system in the mortar is modelled based on porosity development combined with pore diffusivities obtained from the readily available values for diffusivities of ions in dilute solution multiplied with a form factor (ff < 1) describing physical restrictions etc. of the pore system. The form factor can to be regarded as a calibration parameter usable for tuning of the model. In the model the form factor is considered constant although it probably is influenced by changes in porosity of the cement mortar and in particular of the calcite layer. The form factor may also be somewhat different for migrating species of different ionic size and charge.

The calculated concentration profiles for dissolved materials in the pore solution show large deviations from simple diffusion profiles as obtained e.g. from analytical solutions to Fick's laws. This is especially the case after a low-porosity covering layer has been formed. Apparent diffusivities obtained from experimental studies should therefore be used with caution. They represents complicated interactions between various features of the system, not simple bulk properties of the cementitious material.

Models simulating real systems always contain assumptions and simplifications. Some of the more important ones in the CRACK2 model are listed and discussed below.

Grid structure

The time development of the system is obtained from successive calculations using short time-steps and thin grid layers. The numerical structure and the employed mathematical expressions permit transport calculations for grid layers with different thickness, changing porosity and changing composition and diffusivities for the dissolved species in the pore solution. The calculation flexibility is important at interfaces between grid layers with significantly different properties, e.g. the solution in the crack and the outer layer with solid material.

The grid in itself is fixed and this may introduce discontinuities in the calculations, for example when a grid element is emptied for a solid phase such as calcium hydroxide.

The number of columns representing the successive sections of the crack is presently restricted to five, and this relatively coarse structure also gives rise to discontinuities.

Very steep concentration gradients over single grid layers occur and make it necessary to use very short time steps. To avoid mathematical instabilities some compromises have been necessary. The most important is the use of somewhat too low values for the diffusivities in the solution layers in the crack.

Calculation time

Short time steps give long calculation times, which in practise has limited the simulation periods to two weeks. As shown by the example calculation this in most cases includes the period with formation of the covering calcite layer. However, for further use of the model it would be desirable if the calculation time could be reduced e.g. by modification of the grid structure in the middle of the crack.

Chemical system

The major chemical species modelled are Na^+, Ca^{2+}, OH^-, CO_3^{2-}, HCO_3^- and H_2CO_3. Inside the alkaline systems H^+ is not important and is therefore omitted. K^+ is included as the equivalent amount of Na^+ and this is considered a permissible simplification although the diffusivities for the two ions are somewhat different.

The model and the calculation examples demonstrate that the alkali metal hydroxides present in the pore solution influence the calcite precipitation in an important manner. The effects may be transient but complete leaching of alkali metal hydroxide from specimens of reasonable dimensions can take years. They certainly cannot be disregarded in short-term experimental work.

The exclusion of silica chemistry is problematic. The omission of leaching (and precipitation) of C-S-H and other silica-containing hydrated cement minerals reduces the buffering capacity of the cement mortar and may also give a wrong impression of changes in transport properties of the porous materials, in particular the partly leached cementitious material.

Precipitation of small amounts of C-S-H in the layer of calcite crystals covering the inner surface of the crack could be important for diffusive transport through this layer. Magnesium present in the feed solution is known to precipitate together with the calcite and may have similar effects.

The modelling of radioisotopes has mainly been restricted to cesium assumed to behave like the other alkali metals. Strontium introduced with the feed solution was studied experimentally and can also be modelled, but comprehensive simulation would require facilities for modelling interaction with the quite large content of inactive strontium in cements.

Redox conditions are irrelevant for the chemical reactions considered in the model but in experiments with iron plates [7] constituting part of the crack more or less reducing conditions were established. This would decrease migration possibilities for the actinides.

Electrical interactions

The diffusing ions have different diffusivities but are not moving independently. This is treated in the model by calculating the diffusion potential and correcting the individual diffusion rates accordingly. Possible effects of electrical charges on the solids are disregarded. The high mobility of the OH^- ion will exercise a drag on cations increasing or decreasing their diffusion rate depending on the concentration gradient and the direction of diffusion. The effect is also demonstrated for radioisotopes e.g. the Cs^+ ions used in the example calculations.

Precipitation of calcite

The tendency to complete or nearly complete closure of thin (up to ~0.2 mm) cracks by precipitated calcite is less pronounced in the model than observed in reality. This may partly be due to the assumed uniform distribution of flow over the whole crack width. In real systems considerable decrease in flow rate will occur towards the edges of the crack or around trapped air bubbles resulting in local deposits of coarse crystals. The model cannot simulate this form for partial closure.

Besides the precipitation as uniform layers within the five column areas of the crack some further assumptions are made:

Precipitation is only possible in grid layers in contact with solid material, i.e. nucleation and formation of suspended crystallites in the central part of the crack are considered irrelevant. This is probably a quite realistic assumption.

When calcite is precipitated in contact with a solid surface this is supposed to occur as a material with a certain selected porosity ε_{precip} until the grid layer is filled. Example calculations show that this parameter has considerable influence on the build up of the layer. 50 % is probably a minimum value to be selected for ε_{precip}. Example calculations also show that the parameter has considerable influence on the tendency to crack closure.

After the grid layer is filled with loosely positioned crystals further calcite may be precipitated in the pore space until a preselected minimum porosity ε_{min} has been reached. If further precipitation occurs the model arbitrarily transfer this amount of calcite to the next outer layer. The low remaining porosity permits some out-diffusion of hydroxide ions at a rate depending on the build up of the alkali metal hydroxide concentration behind the nearly impermeable calcite layer. It has been found that a minimum porosity of about 0.1 % in the 10 μm thick grid layers gives an out-diffusion of alkali metals in reasonable agreement with experiments.

Membrane formation

The assumption about a minimum calcite porosity is only an approximation. What would happen in reality is that out-diffusing OH^- ions from the mortar somewhere in the pore system of calcite crystals filling a grid layer reacts with in-diffusing HCO_3^- ions producing CO_3^{2-} which together with Ca^{2+} (from the mortar or the feed solution) immediately would precipitate as $CaCO_3$. The result could be local blocking of this particular pore. Counter diffusion of ions producing a solid precipitate is well known to give rise to thin solid membranes with a strong tendency to self-repair, and this is probably what occurs in the pore channels between crystals in the initially precipitated relatively loose calcite. One effect is that a minor amount of additionally precipitated calcite could change a layer with considerable remaining porosity into a nearly impermeable barrier.

However, the barrier is not perfect and some alkali hydroxide seems to be able to penetrate. This could be due to diffusion in crystal seams where complete blockage may be difficult due to different orientation of the crystals. Defects due to precipitated C-S-H or magnesium minerals might also occur. Another possibility is mechanical breakage of thin crystal membranes in changing positions followed by immediate repair.

Barrier of this type with rather strong solutions of alkali metal hydroxide on one side (~0.05 M NaOH) and weak solution (0.005 M calcium bicarbonate) on the other is likely to produce osmotic phenomena with water diffusing from the crack into the mortar. This has not been investigated experimentally.

An attempt to measure electrical resistance over the calcite layer did not indicate development of any resistance [7]. This could be due to experimental problems, but thin solid membranes may not necessarily show significant high frequency impedance.

The general conclusions is that the CRACK2 model has made it possible to interpret a series of observations from experimental studies of deposition of calcium carbonate inside cracks in cementitious materials exposed to a slow flow of calcium bicarbonate solution.

The model supplies graphs of the concentrations profiles of dissolved materials inside the pores, information difficult to obtain experimentally but important for understanding the diffusion of alkali metal hydroxide and other ions through deposited calcite layers.

The model demonstrates that transient effects of leaching of alkali metal hydroxides influences leaching of e.g. calcium but also to some degree the release of radioisotopes one mechanism being the drag exerted by rapidly moving hydroxyl ions on the slower cations. .

The barrier effects of the formation of a nearly impermeable and self-repairing calcite membrane on the surface of the cementitious material are important.

In a repository for radioactive waste the calcium bicarbonate solution could be ground-water moving into the repository through a crack in an outer concrete barrier. After deposition of the calcite layer efficient buffering of the solution is prevented so that groundwater with nearly unchanged composition and pH can penetrate further into the facility. Concrete surfaces inside the facility may also be covered by calcite with similar effect. Eventually more or less unchanged groundwater could leave the repository through another crack in the outer barrier.

The presence of carbonate containing solution with near neutral pH inside the repository increases the possibilities for transport of some dissolved radioisotopes eventually resulting in releases outside the repository. However, this is by no means simple and actual behaviour will be very different for various types of radioisotopes.

On the other hand the formation of a covering calcite layer diminish possibilities for releases of radioactive substances (e.g. strontium) from inside cementitious material e.g. by leaching of cemented waste or by diffusive transport through the pore system in cement barriers.

On the positive side it should also be said that deposition of calcite inside cracks in concrete barriers may result in closure of (thin) cracks so that water flow is prevented or greatly decreased. This particular effect is not so well represented by the CRACK2 model but is well established in experimental work.

9. References

1) Reinhard, H.W. ed. “Penetration and Permeability of Concrete.” State-of-the-art report prepared by members of the RILEM Technical Committee 146-TCF, RILEM Report 16, E&FN Spon, London 1997.

2) Glasser, F.P, J. Cowie, J. ”The reaction between cement and natural waters containing dissolved carbon dioxide.” Advances in Cement Research, 1991/92, 4, No. 15, pp 119-134.

3) Edvardsen, Carola Katharina, geb. Eberweiser. “Wasserdurchlässigkeit und Selbstheilung von Trennrissen in Beton.” Dissertation, Reinisch-Westphalischen Technischen Hochschule Achen, October 1996.

4) Pfingsten, W. “ Experimental and modelling indications for self-healing of a cementitious medium level waste repository by calcite precipitation.”. Nuclear Technology, Vol. 140, pp 63-82, 2002.

5) Brodersen, K., Nilsson,K. "Mechanisms and Interaction Phenomena Influencing Releases in Low and Medium-Level Waste Disposal Systems." Final report 1986-1990 for CEC contract FI1W-0089-DK- (B) EUR 13662 EN, 1991.

6) Harris, A.W. (co-ordinator), Atkinson, A., Balek, V., Brodersen, K., Cole, G.B., Haworth, A., Malek, Z.Nickerson, A.K., Nilsson, K., and Smith, A.C. “The Performance of Cementitious Barriers in Repositories.” Final Report for CEC Contract FI2W-0040, EUR 16643 EN, 1998.

7) Glasser, F.P. (co-ordinator), Adenot, F., Bredy, P.J.C. Bloem, Fachinger, J., Sneyers, A., Marx, G., Brodersen, K., Cowper, M., Tyrer, M. et al. “Barrier performance of cements and concretes in nuclear waste management.” Final Report for CEC contract FI4W-CT96-0030, EUR 19780 EN, 2001.)

8) Brodersen,.K. “Transport properties of cracks and pores in concrete.” Nordic Concrete Research Meeting at Reykjavik, Island, August 1999, Proceedings pp. 119-121.

9) Glasser, F.P. et al “Medium Active Waste Form Characterisation, The Performance of Cement-Based Systems.” Annual report 1988 for CEC Contract F1 1W 00244 UK(H)

10) Staufer, D. “Introduction to Percolation Theory.” Taylor and Francis, London 1985.

11) Brandberg, F., Skagius, K. “Porosity, Sorption and Diffusivity Data Compiled for the SKB 91 Study.” SKB Technical Report 91-16, Stockholm 1991.

12) Newman, J.S. “Electrochemical Systems” Prentice-Hall Int. Series in the Phys. and Chem. Engi. Sciences, UK 1973.

13) Lide, D.R. ed. “CRC Handbook of Chemistry and Physics” 73ed. CRC Press 1992-1993.

Bibliographic data Sheet **Risø-R-1143(EN)**

Title and Authors

CRACK2 –
Modelling calcium carbonate deposition from bicarbonate solutions in cracks in concrete.

Knud Brodersen

ISBN

ISBN 87-550-2612-5
87-550-2613-3 (Internet)

ISSN

ISSN 0106-2840

Department or group

Risø Decommissioning

Date

18 March 2003

Group own reg, number(s)

Sponsorship

Pages	Table	Illustrations	References
99	5	88	13

Abstract

The numerical CRACK2 model simulates precipitation of calcite from calcium bicarbonate solution (e.g. groundwater) passing through cracks in concrete or other cementitious materials. A summary of experimental work is followed by a detailed description of the model.

Hydroxyl ions are transported by diffusion in pore systems in columns of cementitious materials. The hydroxyl is precipitating calcite from a flow of bicarbonate solution in a crack connecting the ends of a row of such columns. The cementitious material is simulated as calcium hydroxide mixed with inert material but with sodium hydroxide dissolved in the pore solution. Diffusive migration of cesium as radioactive isotope is also considered. Electrical interaction of the migrating ions is taken into account.

Example calculations demonstrate effects of parameter variations on distribution of precipitated calcite in the crack and on the composition of the outflowing solution, which can be compared directly with experimental results. Leaching behavior of sodium can be used to tune the model to experimental observations.

The calcite is mostly precipitated on top of the original crack surface and may under certain circumstances fill the crack. The produced thin layers of low porosity calcite act as a diffusion barrier limiting contact between cement and solution. Pore closure mechanisms in such layers are discussed.

Implications for safety assessment of radioactive waste disposal are shortly mentioned.
The model is also relevant for conventional uses of concrete.

Descriptors INIS/EDB

CALCITE, CALCIUM CARBONATE, CONCRETES, CRACKS, DIFFUSION, LEACHING, MATHEMATICAL MODELS; PRECIPITATION; RADIOACTIVE WASTE DISPOSAL